Attachment 6

Hope Creek Generating Station

Facility Operating License NPF-57
Docket No. 50-354

Final Stress Assessment of Hope Creek Unit 1 Steam Dryer at 115% CLTP Conditions
C.D.I. Report No. 08-21NP, Revision 1

This Document Does Not Contain Continuum Dynamics, Inc. Proprietary Information

CDI Report No. 08-21NP

Final Stress Assessment of Hope Creek Unit 1 Steam Dryer at 115% CLTP Conditions

Revision 1

Prepared by

Continuum Dynamics, Inc.
34 Lexington Avenue
Ewing, NJ 08618

Prepared under Purchase Order No. 4500413356 for

Nuclear Business Unit, PSEG Nuclear LLC
Materials Center, Alloway Creek Neck Road
Hancocks Bridge, NJ 08038

Approved by

Alan J. Bilanin

Reviewed by

Milton E. Teske

October 2008

This report complies with Continuum Dynamics, Inc. Nuclear Quality Assurance Program currently in effect.

Executive Summary

A harmonic finite element stress analysis method is used to assess stresses on the Hope Creek Unit 1 (HC1) steam dryer resulting from acoustic and hydrodynamic loads at 115% CLTP operating conditions. The analysis and the structural FEA model are both identical to the ones used previously to analyze the HC1 steam dryer at CLTP operation using main steam line strain gage measurements [1]. Stress estimates at EPU conditions were also produced in that report. In the present report the stresses at the 115% CLTP condition are developed using strain gage signals taken at this condition.

The analysis develops a series of unit stress solutions corresponding to the application of a unit pressure at a MSL at specified frequency, f. Each unit solution is obtained by first calculating the associated acoustic pressure field using a separate analysis that solves the damped Helmholtz equation within the steam dryer [2]. This pressure field is then applied to a finite element structural model of the steam dryer and the stress response at frequency, f, calculated using the commercial ANSYS 10.0 finite element analysis software. This stress response constitutes the unit solution and is stored as a file for subsequent processing. Once all unit solutions have been computed, the stress response for any combination of MSL pressure spectrums (obtained by Fast Fourier Transform of the pressure histories in the MSLs) is determined by a simple matrix multiplication of these spectrums with the unit solutions.

This report provides details of the ANSYS 10.0 finite element structural model of the HC1 steam dryer and reviews pertinent modeling considerations. It also summarizes the framework underlying the development and application of unit solutions in the frequency domain and shows how these solutions are used to develop stress histories for general load conditions. Next, it reviews the assessment of these stresses for compliance with the ASME B&PV Code [3], Section III, subsection NG, for the load combination corresponding to normal operation (the Level A Service Condition).

Results obtained from application of the methodology to the HC1 steam dryer using the Rev. 4 acoustic/hydrodynamic loads [4,5] show that at the nominal 115% CLTP case (no frequency shift) the smallest alternating stress intensity stress ratio (SR-a) is 2.74. The most limiting maximum stress ratio (SR-P) anywhere on the steam dryer is 1.51 at the weld joining the skirt to the upper support ring. These results account for all the end-to-end biases and uncertainties in the loads model [4] (see Table 4 below) and finite element analysis [6] (Table 5 below). They also reflect the elimination of plant and sensor noise in the 75-85 Hz frequency range, based on 1000# data [7]. To account for frequency uncertainties in the finite element model, the stresses are also computed for loads that are shifted in the frequency domain between ±10% in 2.5% increments. The lowest alternating stress ratio at any of these frequency shifts is SR-a=2.36 and occurs on the junction between the inner hood and hood support. The most limiting stress ratio associated with maximum stresses is SR-P = 1.50. These results are consistent with trends inferred from previous analyses at CLTP [1] and 111.5% CLTP [8] conditions using plant measurement data.

Table of Contents

Section	Page
Executive Summary	ii
Table of Contents	iii
1. Introduction and Purpose	1
2. Methodology	2
2.1 Overview	2
2.2 [[(3)]]	4
2.3 Computational Considerations	5
3. Finite Element Model Description	8
3.1 Steam Dryer Geometry	8
3.2 Material Properties	10
3.3 Model Simplifications	10
3.4 Perforated Plate Model	11
3.5 Vane Bank Model	12
3.6 Water Inertia Effect on Submerged Panels	13
3.7 Structural Damping	14
3.8 Mesh Details and Element Types	14
3.9 Connections Between Structural Components	15
3.10 Pressure Loading	22
3.11 Noise Filtering	24
3.12 Summary of Biases and Uncertainties	25
4. Structural Analysis	27
4.1 Static Analysis	27
4.2 Harmonic Analysis	27
4.3 Post-Processing	31
4.4 Computation of Stress Ratios for Structural Assessment	31
5. Results	35
5.1 General Stress Distribution and High Stress Locations	35
5.2 Load Combinations and Allowable Stress Intensities	49
5.3 Frequency Content and Sensitivity to Frequency Shift of the Stress Signals	63
6. Conclusions	71
7. References	72

1. Introduction and Purpose

In order to qualify the Hope Creek nuclear plant at 115% Current Licensed Thermal Power (CLTP) operating conditions a stress assessment of the steam dryer at this operating level using plant data is required. The purpose of the stress analysis discussed here is to calculate the maximum and alternating stresses generated at 115% CLTP and determine the margins that exist when compared to stresses that comply with the ASME Code [3]. This step establishes whether the modifications done prior to commercial operations are adequate for sustaining structural integrity and preventing future weld cracking at 115% CLTP operating conditions. The load combination considered here corresponds to normal operation (the Level A Service Condition) and includes fluctuating pressure loads developed from Hope Creek Unit 1 (HC1) main steam line data, and steam dryer weight. The fluctuating pressure loads, induced by the flowing steam, are predicted using a separate acoustic circuit analysis of the steam dome and main steam lines [5]. Level B service conditions, which include seismic loads, are not included in this evaluation since no physical modifications were made to the HC1 steam dryer for EPU operation.

[[

(3)]] This approach also affords a number of additional computational advantages over transient simulations including: [[(

3)]] This last advantage is realized through the use of "unit" solutions representing the stress distribution resulting from the application of a unit fluctuating pressure at one of the MSLs at a particular frequency. [[

(3)]]

This report describes the overall methodology used to obtain the unit solutions in the frequency domain and how to assemble them into a stress response for a given combination of pressure signals in the MSLs. This is followed by details of the HC1 steam dryer finite element model including the elements used and overall resolution, treatment of connections between elements, the hydrodynamic model, the implementation of structural damping and key idealizations/assumptions inherent to the model. Post-processing procedures are also reviewed including the computation of maximum and alternating stress intensities, identification of high stress locations, adjustments to stress intensities at welds, and evaluation of stress ratios used to establish compliance with the ASME Code.

The results for Rev. 4 acoustic/hydrodynamic loads [4] in terms of stress intensity distributions and stress ratios are presented next, together with accumulative PSDs of the dominant stress components. The latter show that the load and structural response are dominated by significant signals in the 41-49 Hz frequency range.

2. Methodology

2.1 Overview

Based on previous analysis undertaken at Quad Cities Units 1 and 2, the steam dryer can experience strong acoustic loads due to the fluctuating pressures in the MSLs connected to the steam dome containing the dryer. C.D.I. has developed an acoustic circuit model (ACM) that, given a collection of strain gauge measurements [9] of the fluctuating pressures in the MSLs, predicts the acoustic pressure field anywhere inside the steam dome and on the steam dryer [2,4,5]. The ACM is formulated in frequency space and contains two major components that are directly relevant to the ensuing stress analysis of concern here. [[

(1)

(2)

(3)]]

[[

(3)

(4)

(5)

(3)]]

[[

(6)

(3)]]

2.2 [[**(3)]]**
[[

(3)]]

[[

(3)]]

2.3 Computational Considerations

Focusing on the structural computational aspects of the overall approach, there are a number of numerical and computational considerations requiring attention. The first concerns the transfer of the acoustic forces onto the structure, particularly the spatial and frequency resolutions. The ANSYS finite element program inputs general distributed pressure differences using a table format. This consists of regular 3D rectangular (i.e., block) $n_x \times n_y \times n_z$ mesh where n_α is the number of mesh points in the α-th Cartesian direction and the pressure difference is provided at each mesh point (see Section 3.10). These tables are generated separately using a program that reads the loads provided from the ACM software, distributes these loads onto the finite element mesh using a combination of interpolation procedures on the surface and simple diffusion schemes off the surface (off-surface loads are required by ANSYS to ensure proper interpolation of forces), and written to ASCII files for input to ANSYS. A separate load file is written at each frequency for the real and imaginary component of the complex force.

The acoustic field is stored at 5 Hz intervals from 0 to 200 Hz. While a 5 Hz resolution is sufficient to capture frequency dependence of the acoustic field (i.e., the pressure at a point varies gradually with frequency), it is too coarse for representing the structural response especially at low frequencies. For 1% critical structural damping, one can show (as indicated in the design record file, DRF-CDI-174) that the frequency spacing needed to resolve a damped resonant peak at natural frequency, f_n, to within 5% accuracy is $\Delta f = 0.0064 \times f_n$ Thus for f_n=10 Hz where the lowest structural response modes occur, a frequency interval of 0.064 Hz or less is required. In our calculations we require that 5% maximum error be maintained over the range from f_n=5 Hz to 200 Hz resulting in a finest frequency interval of 0.0321 Hz at the low frequency end (this adequately resolves all structural modes up to 200 Hz). Since there are no structural modes between 0 to 5 Hz, a 0.5 Hz spacing is used over this range with minimal (less than 5%) error. The unit load, $\hat{\mathbf{f}}_n(\omega, \mathbf{R})$, at any frequency, ω_k, is obtained by linear interpolation of the acoustic solutions at the two nearest frequencies, ω_i and ω_{i+1}, spaced 5 Hz apart. Linear interpolation is sufficient since the pressure load varies slowly over each 5 Hz interval (linear interpolation of the structural response over these 5 Hz intervals would not be acceptable since it varies much more rapidly over these intervals).

Solution Management

[[

(3)]]

Upon completion of each frequency calculation, ANSYS is instructed to export the stresses which are stored in text files. There is one file per MSL per frequency per real/imaginary component, and each file contains the complete stress state over all nodes on the dryer. This format is convenient from a solution point of view. However, it makes it difficult to extract the stress response at a node since, in order to do so, thousands of files must be opened and searched through thousands of nodes until the node of interest is reached. [[

[(3)]]

Structural Damping

In harmonic analysis one has a broader selection of damping models than in transient simulations. A damping factor, z, of 1% critical damping is used in the structural analysis. In transient simulations, this damping can only be enforced exactly at two frequencies (where the damping model is "pinned"). Between these two frequencies the damping factor can by considerably smaller, for example 0.5% or less depending on the pinning frequencies. Outside the pinning frequencies, damping is higher. With harmonic analysis it is straightforward to enforce very close to 1% damping over the entire frequency range. In this damping model, the damping matrix, **D**, is set to

$$\mathbf{D} = \frac{2z}{\omega}\mathbf{K} \tag{7}$$

where **K** is the stiffness matrix and ω the forcing frequency. When comparing the response obtained with this model against that for a constant damping ratio, the maximum difference at any frequency is less than 0.5%, which is far smaller than the 100% or higher response variation obtained when using the pinned model required in transient simulation.

Load Frequency Rescaling

One way to evaluate the sensitivity of the stress results to approximations in the structural modeling and applied loads is to rescale the frequency content of the applied loads. In this procedure the nominal frequencies, ω_k, are shifted to $(1+\lambda)\omega_k$, where the frequency shift, λ, ranges between ±10%, and the response recomputed for the shifted loads. The objective of the frequency shifting can be explained by way of example. Suppose that in the actual dryer a strong structural-acoustic coupling exists at a particular frequency, ω^*. This means that the following conditions hold simultaneously: (i) the acoustic signal contains a significant signal at ω^*; (ii) the structural model contains a resonant mode of natural frequency, ω_n, that is near ω^*; and (iii) the associated structural mode shape is strongly coupled to the acoustic load (i.e., integrating the product of the mode shape and the surface pressure over the steam dryer surface produces a significant modal force). Suppose now that because of discretization errors and modeling idealizations that the predicted resonance frequency differs from ω^* by a small amount (e.g., 1.5%). Then condition (ii) will be violated and the response amplitude therefore significantly diminished. By shifting the load frequencies one re-establishes condition (ii) when $(1+\lambda)\omega^*$ is

near ω_n. The other two requirements also hold and a strong structural acoustic interaction is restored.

[[(6)

. [(3)]]

Evaluation of Maximum and Alternating Stress Intensities

Once the unit solutions have been obtained, the most intensive computational steps in the generation of stress intensities are: (i) the FFTs to evaluate stress time histories from (5); and (ii) the calculation of alternating stress intensities. [[

[(3)]]

The high computational penalty incurred in calculating the alternating stress intensities is due to the fact that this calculation involves comparing the stress tensors at every pair of points in the stress history. This comparison is necessary since in general the principal stress directions can vary during the response, thus for N samples in the stress history, there will be (N-1)N/2 such pairs or, for N=64K (the number required to accurately resolve the spectrum up to 200 Hz in 0.01 Hz intervals), 2.1×10^9 calculations per node each requiring the determination of the roots to a cubic polynomial. [[

[(3)]]

3. Finite Element Model Description

A description of the ANSYS model of the Hope Creek Unit 1 steam dryer follows. This model is virtually identical to one developed for previous investigations using time domain-based analysis methods [14]. It is also the exact same model used to analyze the HC1 dryer at CLTP operation and anticipated EPU conditions using the same frequency-based analysis [1].

3.1 Steam Dryer Geometry

A geometric representation of the Hope Creek steam dryer was developed from available drawings (provided by PSE&G and included in the design record files, DRF-PSEG-258 and DRF-175C) within the Workbench module of ANSYS. Field measurements taken by C.D.I. on an identical spare dryer for the cancelled Hope Creek Unit 2 were also used to develop this model (also contained in DRF-175C). The completed model is shown in Figure 1. This model includes modifications made to the HC1 steam dryer on-site, prior to commercial operation. These are:

- Tie bars, outer hoods, and center end plates were replaced on the original dryer (FDI-041-79450).
- Reinforcement bars were added to the middle and inner hoods (HCI-KTI-415-7)
- Back-welding of the middle and inner hoods weld joint to their end plates (HCI-KTI-415-3 and -5)

The modified areas are shown in Figure 2.

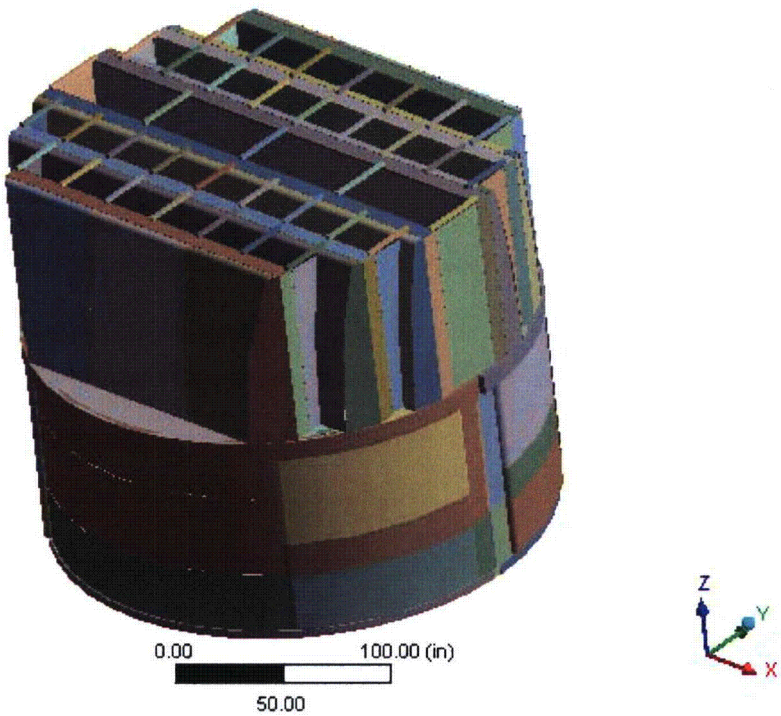

Figure 1. Overall geometry of the HC1 steam dryer model.

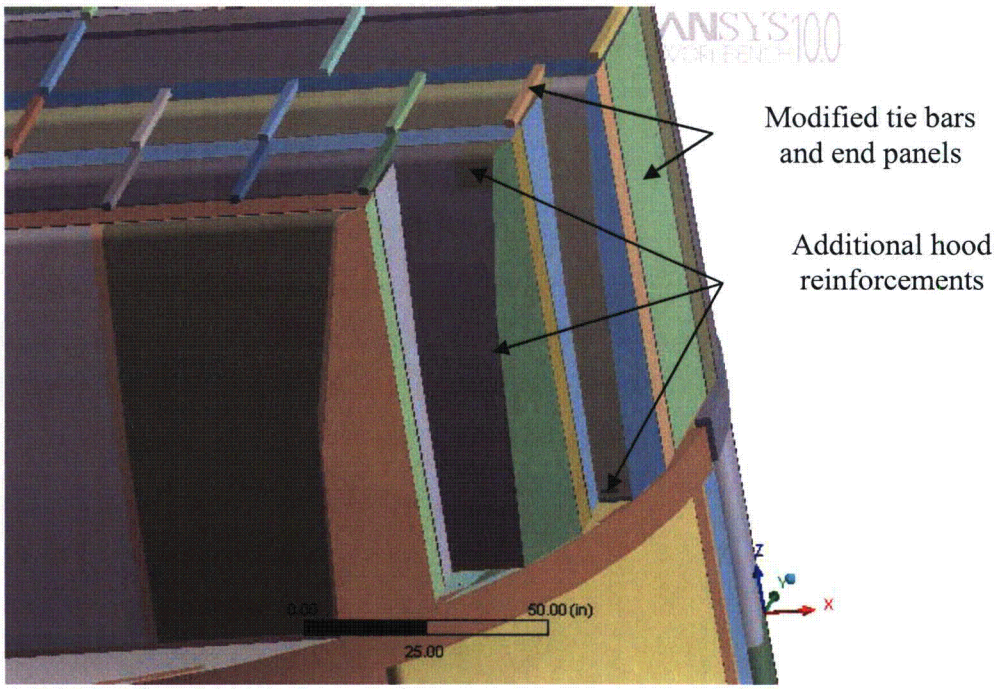

Figure 2. On-site modifications accounted for in the model and associated geometrical details.

3.2 Material Properties

The steam dryer is constructed from Type 304 stainless steel and has an operating temperature of 550°F. Properties used in the analysis are summarized below in Table 1.

Table 1. Material properties.

	Young's Modulus (10^6 psi)	Density (lbm/in^3)	Poisson's Ratio
structural steel	25.55	0.284	0.3
structural steel for perforated plates	15.33	0.227	0.3
structural steel with added water inertia	25.55	1.183	0.3

The structural steel modulus is taken from Appendix A of the ASME Code for Type 304 Stainless Steel at an operating temperature 550°F. The effective properties of perforated plates and submerged parts are discussed in Sections 3.4 and 3.6. Note that the increased effective density for submerged components is only used in the harmonic analysis. When calculating the stress distribution due to the static dead weight load, the unmodified density of steel (0.284 lbm/in^3) is used throughout.

3.3 Model Simplifications

The following simplifications were made to achieve reasonable model size while maintaining good modeling fidelity for key structural properties:

- Perforated plates were approximated as continuous plates using modified elastic properties designed to match the static and modal behaviors of the perforated plates. The perforated plate structural modeling is summarized in Section 3.4 and Appendix C of [1].

- The drying vanes were replaced by point masses attached to the corresponding trough bottom plates and vane bank top covers. The bounding perforated plates, vane bank end plates, and vane bank top covers were explicitly modeled (see Section 3.5).

- The added mass properties of the lower part of the skirt below the reactor water level were obtained using a separate hydrodynamic analysis (see Section 3.6).

- Fixed constraints were imposed at the underside of the steam dryer upper support ring where it makes contact with the four steam dryer support brackets that are located on the reactor vessel and spaced at 90° intervals (Figure 3). No credit was taken for the constraints from the reactor vessel lift lugs.

- Most welds were replaced by node-to-node connections; interconnected parts share common nodes along the welds. In other locations the constraint equations between nodal degrees of freedom were introduced as described in Section 3.9.

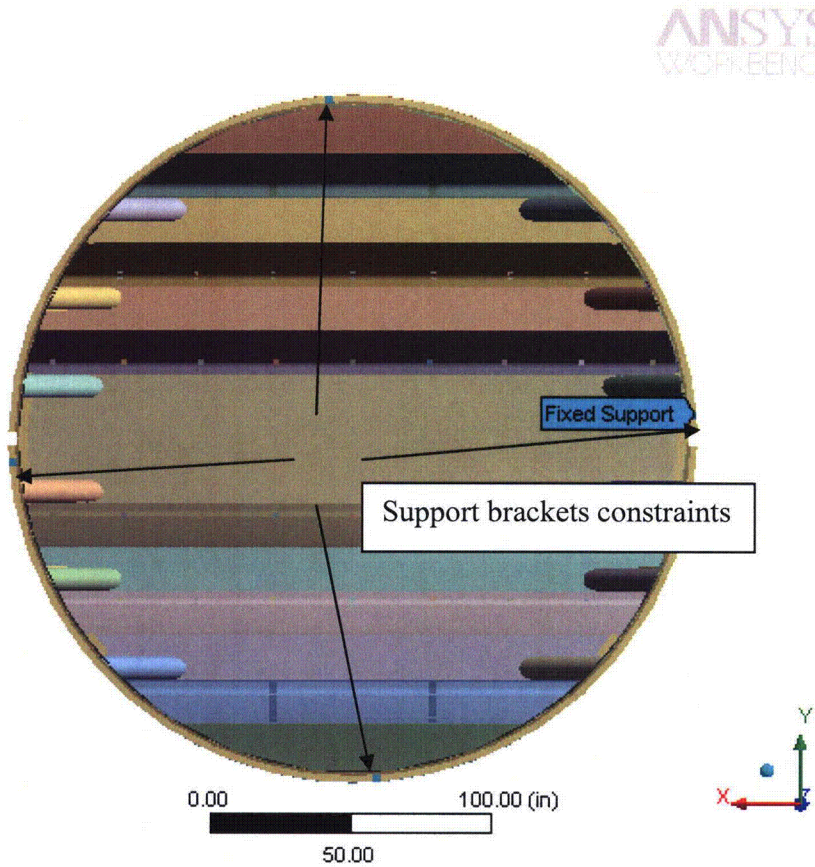

Figure 3. Fixed support constraints.

3.4 Perforated Plate Model

The perforated plates were modeled as solid plates with adjusted elastic and dynamic properties. Properties of the perforated plates were assigned according to the type and size of perforation. Based on [15], for an equilateral triangular pattern with given hole size and spacing, the effective moduli of elasticity were found. The hole pattern and thickness of the perforated plates was based on conservative estimates and field measurements of accessible plates. Subsequent more recent detailed measurements have confirmed that the actual plates are at least 50% thicker. Therefore, since maximum and alternating stresses scale as $1/(\text{thickness})^2$, the current analysis is conservative.

Tests were carried out to verify that this representation of perforated plates by continuous ones with modified elastic properties preserves the modal properties of the structure. These tests are summarized in Appendix C of [1] and compare the predicted first modal frequency for a cantilevered perforated plate against an experimentally measured value. The prediction was obtained using the analytical formula for a cantilevered plate and the modified Young's modulus and Poisson's ratio given by O'Donnell [15]. The measured and predicted frequencies are in close agreement, differing by less than 2%.

3.5 Vane Bank Model

The vane bank assemblies consist of many vertical angled plates that are computationally expensive to model explicitly, since a prohibitive number of elements would be required. These parts have significant weight which is transmitted through the surrounding structure, so it is important to capture their gross inertial properties. Here the vane banks are modeled as a collection of point masses located at the center of mass for each vane bank section (see Figure 4). The following masses were used for the vane bank sections, based on data found on provided drawings:

inner banks:	6,545 lbm
middle banks:	5,970 lbm; and
outer banks:	4,685 lbm.

These masses were applied to the base plates and vane top covers using the standard ANSYS point mass modeling option, element MASS21. ANSYS automatically distributes the point mass inertial loads to the nodes of the selected structure. The distribution algorithm minimizes the sum of the squares of the nodal inertial forces, while ensuring that the net forces and moments are conserved. Vane banks are not exposed to main steam lines directly, but rather shielded by the hoods.

The collective stiffness of the vane banks is expected to be small compared to the surrounding support structure and is neglected in the model. In the static case it is reasonable to expect that this constitutes a conservative approach, since neglecting the stiffness of the vane banks implies that the entire weight is transmitted through the adjacent vane bank walls and supports. In the dynamic case the vane banks exhibit only a weak response since (i) they have large inertia so that the characteristic acoustically-induced forces divided by the vane masses and inertias yield small amplitude motions, velocities and accelerations; and (ii) they are shielded from acoustic loads by the hoods, which transfer dynamic loads to the rest of the structure. Thus, compared to the hoods, less motion is anticipated on the vane banks so that approximating their inertial properties with equivalent point masses is justified. Nevertheless, the bounding parts, such as perforated plates, side panels, and top covers, are retained in the model since they can individually exhibit a strong modal response. Errors associated with the point mass representation of the vane banks are compensated for by frequency shifting of the applied loads.

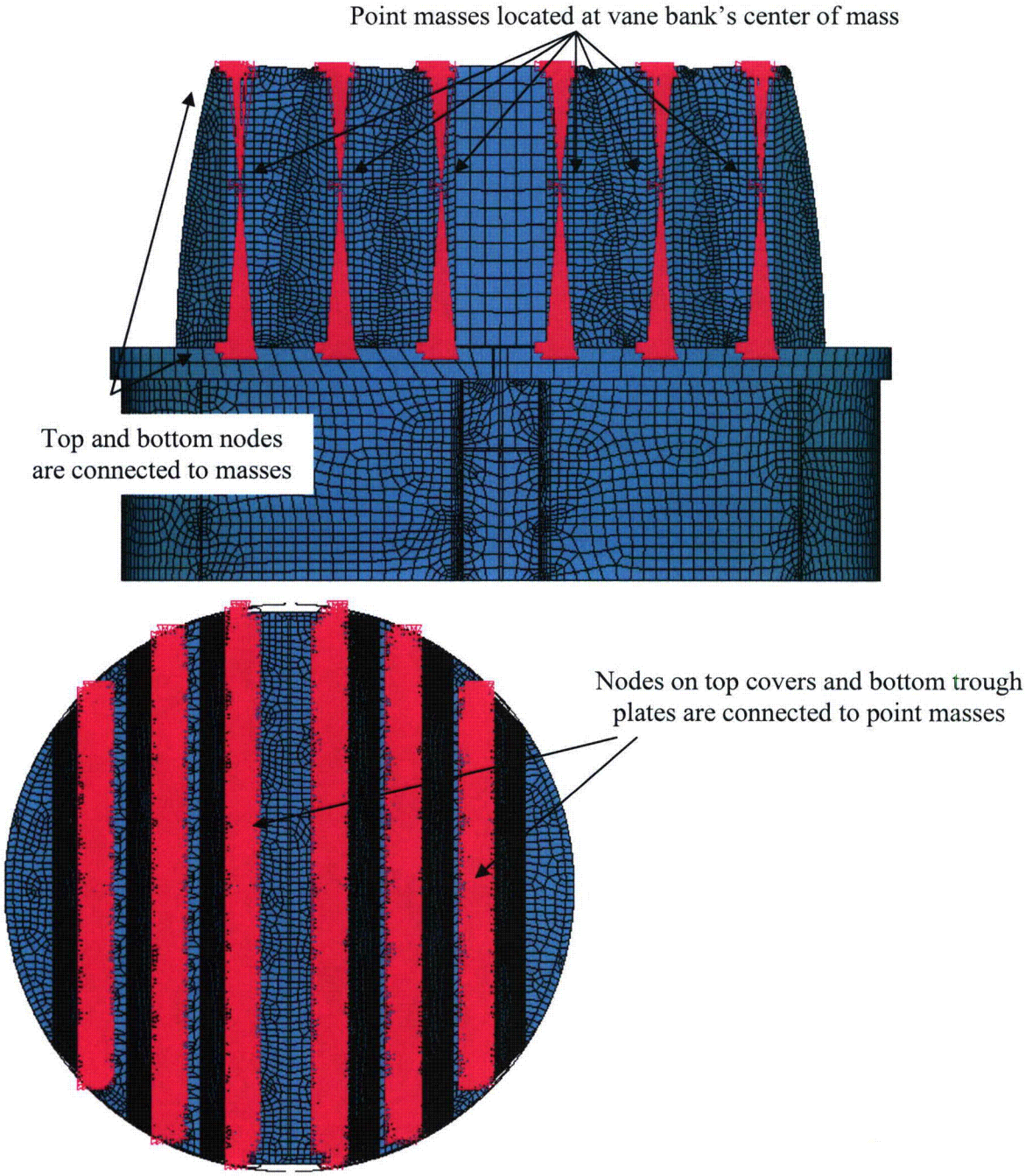

Figure 4. Point masses representing the vanes. The pink shading represents where constraint equations between nodes are applied in the point mass implementation.

3.6 Water Inertia Effect on Submerged Panels

Water inertia was modeled by an increase in density of the submerged structure to account for the added hydrodynamic mass. This added mass was found by a separate hydrodynamic analysis (included in DRF-175C supporting this report) to be 0.225 lbm/in^2 on the submerged

skirt area. This is modeled by effectively increasing the material density for the submerged portions of the skirt. Since the skirt is 0.25 inches thick, the added mass is equivalent to a density increase of 1.183 lbm/in^3. This added water mass was included in the ANSYS model by appropriately modifying the density of the submerged structural elements when computing harmonic response. For the static stresses, the unmodified density of steel is used throughout.

3.7 Structural Damping

Structural damping was defined as 1% of critical damping for all frequencies. This damping is consistent with guidance given on pg. 10 of NRC RG-1.20 [16].

3.8 Mesh Details and Element Types

Shell elements were employed to model the skirt, hoods, perforated plates, side and end plates, trough bottom plates, reinforcements, base plates and cover plates. Specifically, the four-node, Shell Element SHELL63, was selected to model these structural components. This element models bending and membrane stresses, but omits transverse shear. The use of shell elements is appropriate for most of the structure where the characteristic thickness is small compared to the other plate dimensions. For thicker structures, such as the upper and lower support rings, solid brick elements were used to provide the full 3D stress. The elements SURF154 are used to assure proper application of pressure loading to the structure. Mesh details and element types are shown in Table 2 and Table 3.

Table 2. FE Model Summary.

Description	Quantity
Total Nodes	93,951
Total Elements	126,322
Element Types	5
Materials	3

Table 3. Listing of Element Types.

Generic Element Type Name	Element Name	ANSYS Name
20-Node Quadratic Hexahedron	SOLID186	20-Node Hexahedral Structural Solid
4-Node Elastic Shell	SHELL63	4-Node Elastic Shell
4-Node Linear Quadrilateral Shell	SHELL181	4-Node Finite Strain Shell
Mass Element	MASS21	Structural Mass
Pressure Surface Definition	SURF154	3D Structural Surface Effect

The mesh is generated automatically by ANSYS with adaptive refinement near edges. The maximum allowable mesh spacing is specified by the user. Here a 3 inch maximum allowable spacing is specified everywhere except in the following areas: drain pipes (2 inch maximum spacing); base plates (2.75 inches); perforated plates (2 inches); top tie rods (0.75 inches); and the curved portions of the drain channels (1.5 inches). Details of the finite element mesh are shown in Figure 5. Numerical experiments carried out using the ANSYS code applied to simple

analytically tractable plate structures with dimensions and mesh spacings similar to the ones used for the steam dryer, confirm that the natural frequencies are accurately recovered (less than 1% errors for the first modes). These errors are compensated for by the use of frequency shifting.

3.9 Connections Between Structural Components

Most connections between parts are modeled as node-to-node connections. This is the correct manner (i.e., within the finite element framework) of joining elements away from discontinuities. At joints between shells, this approach omits the additional stiffness provided by the extra weld material. Also, locally 3D effects are more pronounced. The latter effect is accounted for using weld factors. The deviation in stiffness due to weld material is negligible, since weld dimensions are on the order of the shell thickness. The consequences upon modal frequencies and amplitude are, to first order, proportional to t/L where t is the thickness and L a characteristic shell length. The errors committed by ignoring additional weld stiffness are thus small and readily compensated for by performing frequency shifts.

When joining shell and solid elements, however, the problem arises of properly constraining the rotations, since shell element nodes contain both displacement and rotational degrees of freedom at every node whereas solid elements model only the translations. A node-to-node connection would effectively appear to the shell element as a simply supported, rather than (the correct) cantilevered restraint and significantly alter the dynamic response of the shell structure.

To address this problem, constraint equations are used to properly connect adjacent shell- and solid-element modeled structures. Basically, all such constraints express the deflection (and rotation for shell elements) of a node, $\mathbf{R}_1$, on one structural component in terms of the deflections/rotations of the corresponding point, $\mathbf{P}_2$, on the other connected component. Specifically, the element containing $\mathbf{P}_2$ is identified and the deformations at $\mathbf{P}_2$ determined by interpolation between the element nodes. The following types of shell-solid element connections are used in the steam dryer model including the following:

1. Shell edge to shell edge connections with dissimilar meshes.
2. Connections of shell faces to solid faces (Figure 6a). While only displacement degrees of freedom are explicitly constrained, this approach also implicitly constrains the rotational degrees of freedom when multiple shell nodes on a sufficiently dense grid are connected to the same solid face.
3. Connections of shell edges to solids (e.g., connection of the bottom of closure plates with the upper ring). Since solid elements do not have rotational degrees of freedom, the coupling approach consists of having the shell penetrate into the solid by one shell thickness and then constraining both the embedded shell element nodes (inside the solid) and the ones located on the surface of the solid structure (see Figure 6b). Numerical tests involving simple structures show that this approach and penetration depth reproduce both the deflections and stresses of the same structure modeled using only solid elements or ANSYS' bonded contact technology. Continuity of rotations and displacements is achieved.
4. Connections of solid elements to shells, e.g., connections of the tie bars to the vane covers.

The use of constraint conditions rather than the bonded contacts advocated by ANSYS for connecting independently meshed structural components confers better accuracy and useful numerical advantages to the structural analysis of the steam dryer including better conditioned and smaller matrices. The smaller size results from the fact that equations and degrees of freedom are eliminated rather than augmented (in Lagrange multiplier-based methods) by additional degrees of freedom. Also, the implementation of contact elements relies on the use of very high stiffness elements (in penalty function-based implementations) or results in indefinite matrices (Lagrange multiplier implementations) with poorer convergence behavior compared to positive definite matrices.

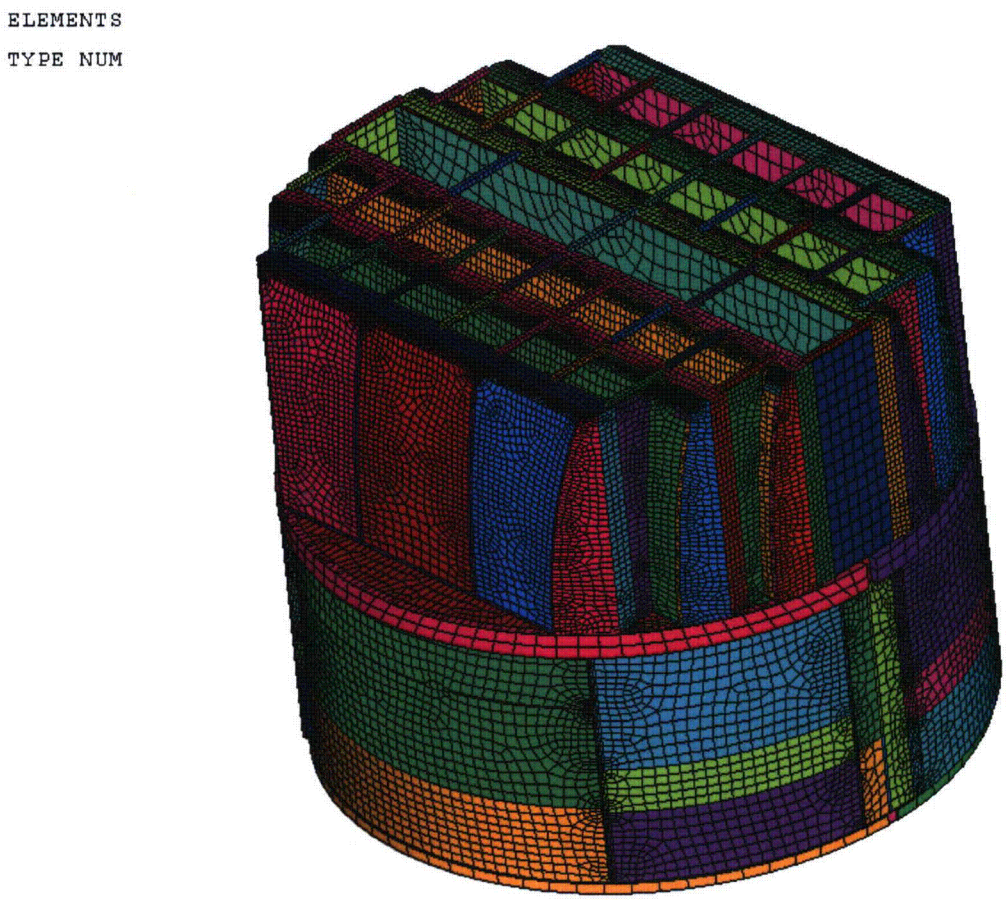

Figure 5a. Mesh overview. The colors emphasize element type.

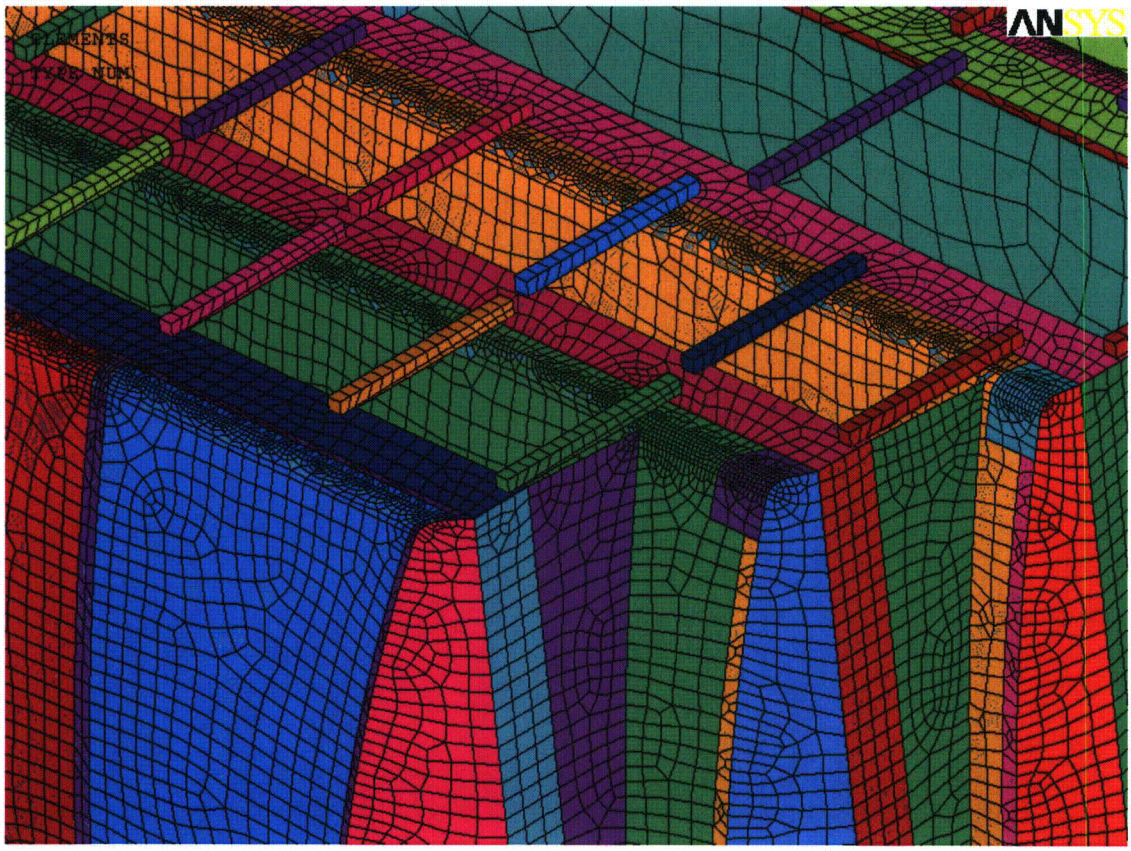

Figure 5b. Close up of mesh showing hoods, reinforcement panels and tie bars. The colors emphasize element type.

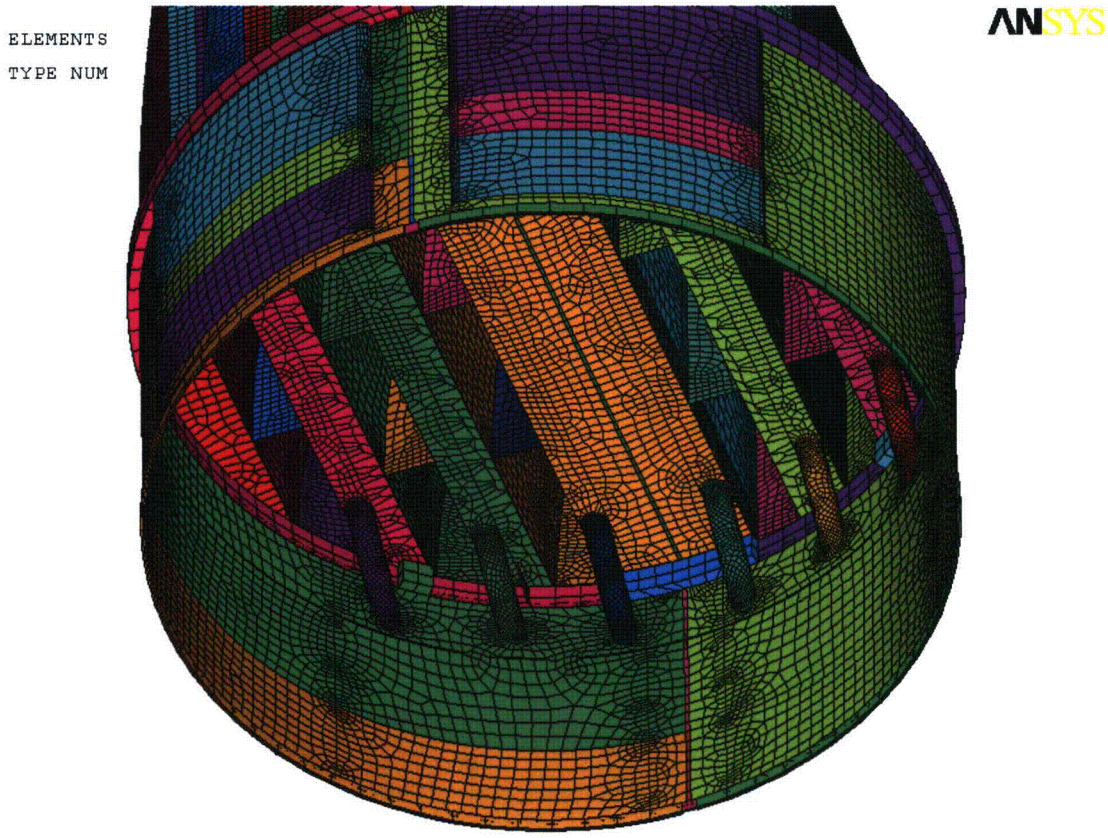

Figure 5c. Close up of mesh showing drain pipes and hood supports. The colors emphasize element type.

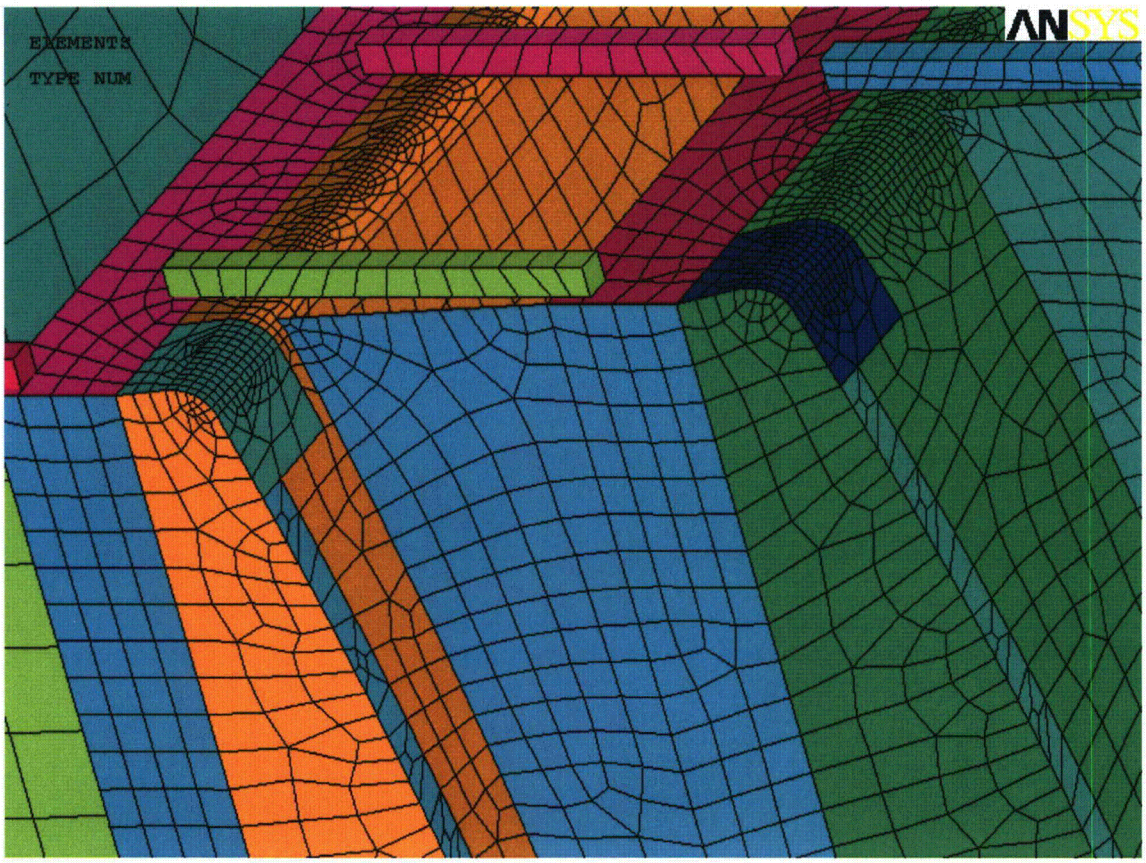

Figure 5d. Close up of mesh showing node-to-node connections between closure panels, end plates, and hoods. The colors emphasize element types.

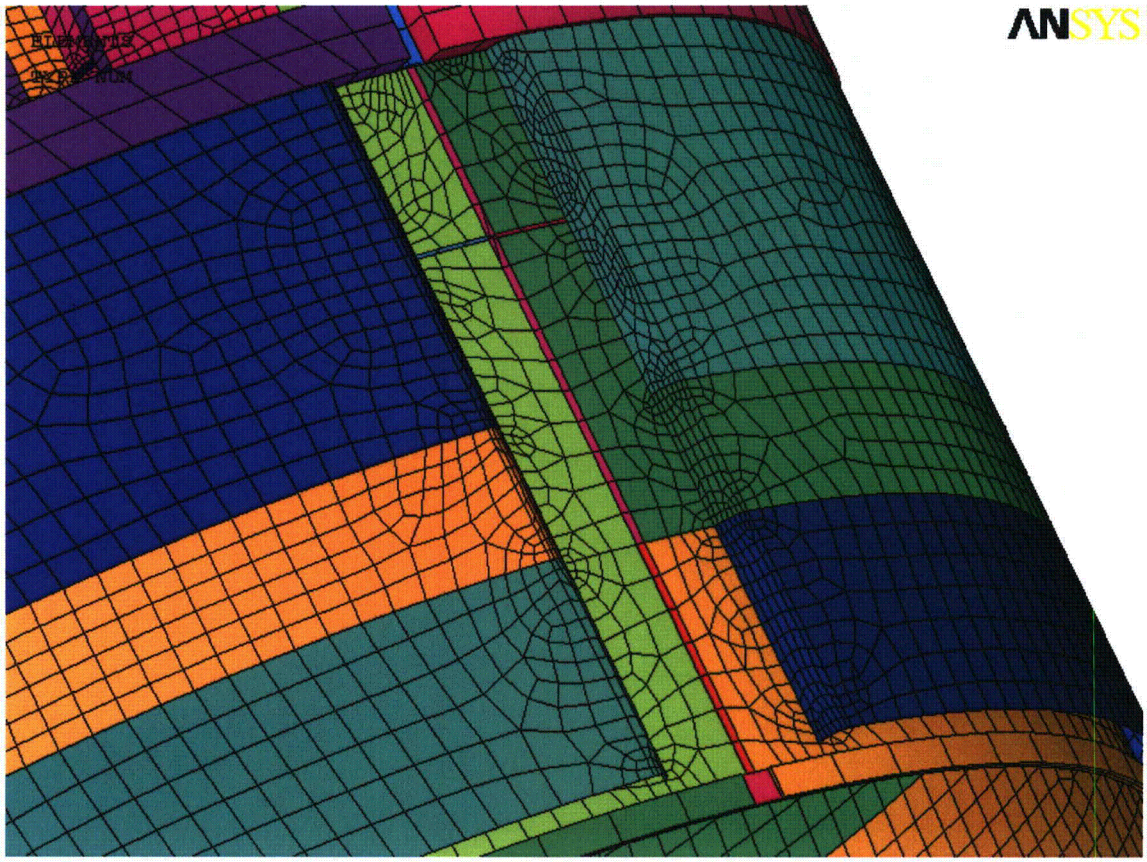

Figure 5e. Close up of mesh showing node-to-node connections between the skirt and drain channels. The colors emphasize element type.

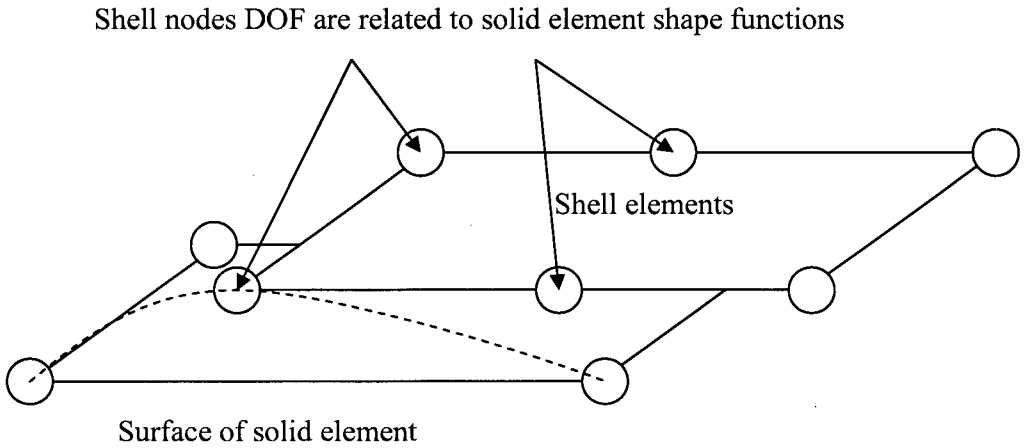

Figure 6a. Face-to-face shell to solid connection.

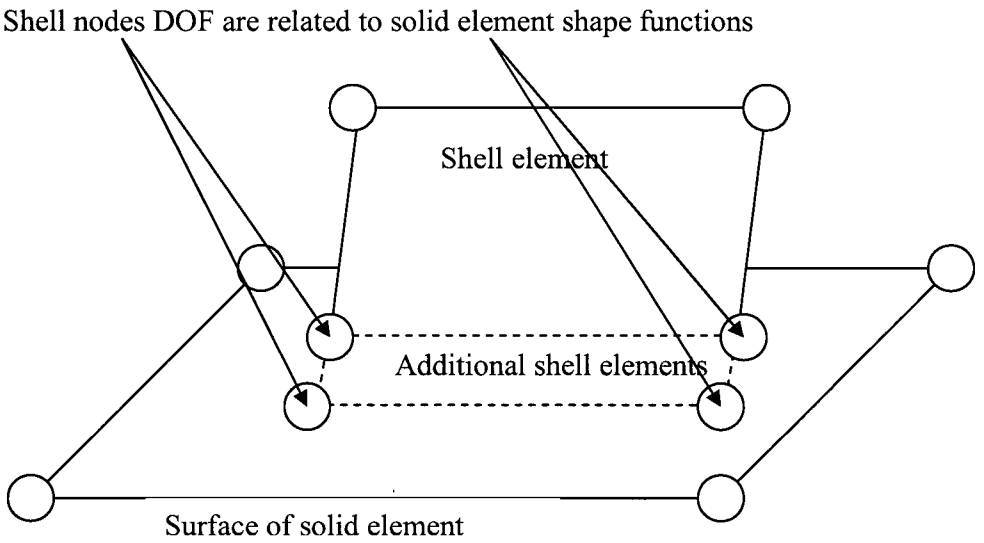

Figure 6b. Shell edge-to-solid face connection.

3.10 Pressure Loading

The harmonic loads are produced by the pressures acting on the exposed surfaces of the steam dryer. At every frequency and for each MSL, the pressure distribution corresponding to a unit pressure at the MSL inlet is represented on a three-inch grid lattice grid (i.e., a mesh whose lines are aligned with the x-, y- and z-directions) that is superimposed over the steam dryer surface. This grid is compatible with the "Table" format used by ANSYS to "paint" general pressure distributions upon structural surfaces. The pressures are obtained from the Helmholtz solver routine in the acoustic analysis [2].

In general, the lattice nodes do not lie on the surface, so that to obtain the pressure differences at the surface, it is necessary to interpolate the pressure differences stored at the lattice nodes. This is done using simple linear interpolation between the eight forming nodes of the lattice cell containing the surface point of interest. Inspection of the resulting pressures at selected nodes shows that these pressures vary in a well-behaved manner between the nodes with prescribed pressures. Graphical depictions of the resulting pressures and comparisons between the peak pressures in the original nodal histories and those in the final surface load distributions produced in ANSYS, all confirm that the load data are interpolated accurately and transferred correctly to ANSYS.

The harmonic pressure loads are only applied to surfaces above the water level, as indicated in Figure 7. In addition to the pressure load, the static loading induced by the weight of the steam dryer is analyzed separately. The resulting static and harmonic stresses are linearly combined to obtain total values which are then processed to calculate maximum and alternating stress intensities for assessment in Section 5.

[[

[3]]] This is useful since revisions in the loads model do not necessitate recalculation of the unit stresses.

The results produced here utilize the Rev. 4 acoustic/hydrodynamic loads model described in [4,5] to calculate the MSL pressure signals $P_n(\omega)$ and associated biases and uncertainties.

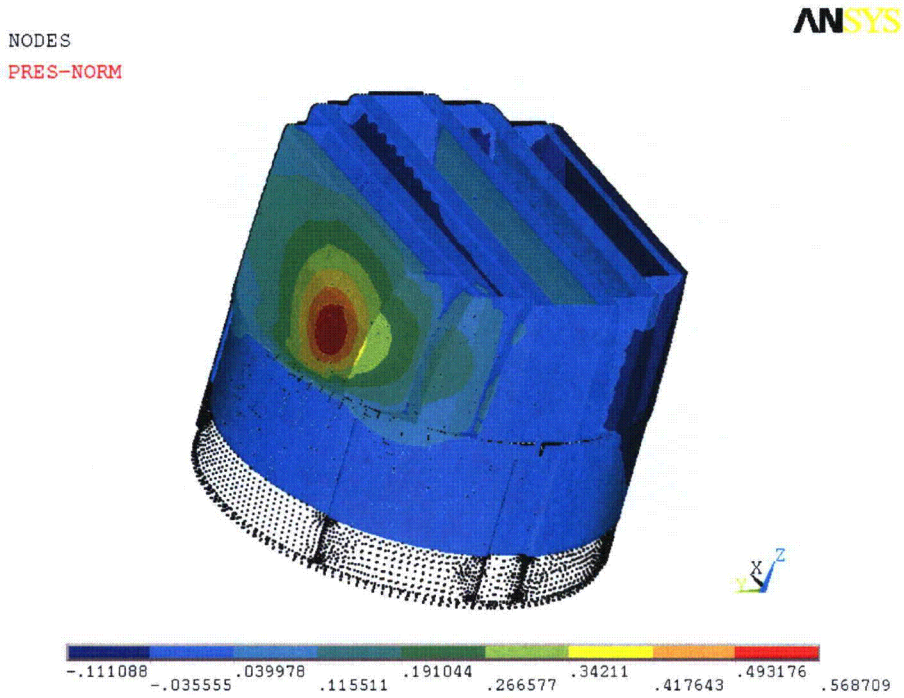

Frequency no. 372: 50.2 Hz

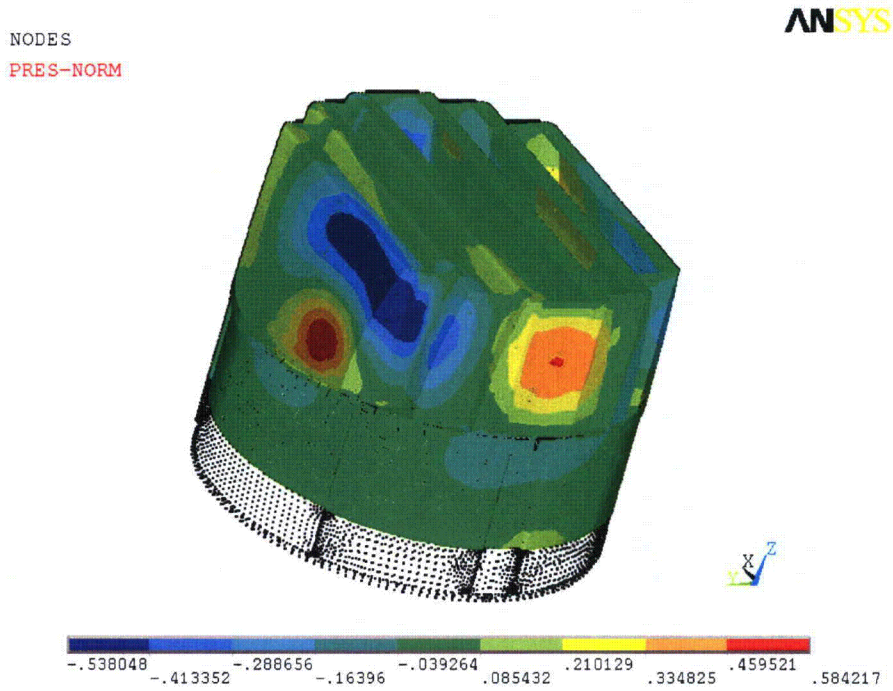

Frequency no. 544: 150.7 Hz

Figure 7. Real part of unit pressure loading MSL C (in psid) on the steam dryer at different frequencies. No loading is applied to submerged parts (nodes at the bottom).

3.11 Noise Filtering

The presence of sensor noise and MSL turbulence is found to produce a strong 80 Hz signal in the ACM model. This amplification can be identified with a 'sloshing' mode at this frequency where the acoustic pressure varies from negative minimum at one pair of MSL exits to a maximum value at the opposite pair with a zero value near the top of the steam dome. This mode experiences comparatively little damping because it does not produce significant motion at the steam/water interface. Since neither sensor noise nor the non-coherent turbulence constitute acoustic sources, they should not be included in the ACM and associated acoustic loads. The ACM analysis however, does not distinguish between the acoustic and non-acoustic fluctuations in the MSL signals that could lead to sizeable, but fictitious 80 Hz acoustic loads and resulting stresses on the dryer that dominate the response.

To remove these fictitious loads, data were collected [7] with the system maintained at operating pressure (1000 psi) and temperature, but little (5-8% of CLTP) flow. The recirculation pumps were in operation so that the background plant noise and vibrations were present. At these conditions the acoustic loads are negligible so that these data, referred to as the 1000# data, originates entirely from non-acoustic sources such as sensor noise and mechanical vibrations. This information is valuable since it allows one to distinguish between the acoustic and non-acoustic content in the full power signal and therefore modify the full power loads so that only the acoustic component is retained. The 1000# strain gage signals are filtered in the same manner as the 115% CLTP data and are fed into the ACM model to obtain the monopole and dipole signals at the MSL inlets. Since there is negligible flow, these signals are fictitious, i.e., the hoop strains measured by the strain gages are not due to pressure fluctuations, but rather due to noise. However, under the supposition that these signals are acoustic in origin the hypothetical stresses due to these signals can nevertheless be computed. This was done in [1] which confirmed that the noise represented by the 1000# data induces a strong response at 80 Hz. The corresponding artificial stress response at the limiting nodes was determined to be approximately one half the total stress response.

To compensate for the non-acoustic noise source represented in the 1000# data, the 115% CLTP MSL inlet pressure signals are modified on the 75-85 Hz frequency range according to:

$$P(f) = P_0(f) * \max\left[0, 1 - \frac{\bar{N}(f)}{\bar{P}_0(f)}\right] \tag{8}$$

where f is the frequency (in Hz), $P_0(f)$ is the MSL inlet pressure (monopole or dipole) at 115% CLTP conditions before correction, P(f) is the corresponding post-correction pressure and $\bar{N}(f)$ and $\bar{P}_0(f)$ are averaged pressure amplitudes associated with the 1000# data and 115% CLTP data respectively. Specifically,

$$\bar{P}_0(f) = \frac{1}{2}\int_{f-1}^{f+1} |P_0(f)|\, df \tag{9}$$

where $|P_0(f)|$ denotes the absolute value of the complex quantity. Hence $\overline{P}_0(f)$ is the average amplitude of the 115% CLTP pressure in the ±1 Hz interval about frequency, f. The same definition, but using the 1000# pressure signal, is used for $\overline{N}(f)$. Note that this modification leaves the phase information in the original full power signal unchanged.

3.12 Summary of Biases and Uncertainties

The biases and uncertainties associated with the ACM Rev. 4 and modeling approximations were recomputed are summarized in Table 4 and Table 5 respectively. The HCGS SRV acoustic resonance range is 116-120 Hz. This subset of the 100-150 Hz interval has a different bias and uncertainty as reflected in Table 4. The biases and uncertainties for the ACM model are obtained from [4]. For the finite element model the biases and uncertainties are as follows:

(i) A general finite element modeling uncertainty (25.26%) accounting for simplifications, approximations and idealizations (e.g., omission of weld material, vane bank mass modeling, etc.) made in the model, discrepancies between actual and as-modeled dimensions or tolerances and the effects of pre-stress. This error was derived from an extensive vibration test [6] that was performed on the spare Hope Creek Unit 2 steam dryer. The dryer was subjected to shaker excitation at eight different locations and the dryer responses measured using accelerometers at various points on the dryer for peak forcing frequencies in the range 0-250 Hz. The 25.26% value was obtained by comparing the measured response data against response predictions obtained with the ANSYS finite element model.

(ii) A 9.53% bias error in the stresses due to the use of a finite mesh spacing in the FE model. This value was determined by examining the convergence of stress with mesh spacing on a multi-component structure representative of the hood and hood supports when subjected to the complex spatially and temporally varying load [17].

(iii) A bias error due to the use of a discrete frequency schedule. This schedule is chosen to ensure a maximum error in the response peak estimation of 5% which translates into a 5% non-conservative bias error. Note that as explained in [12], this maximum error corresponds to a 1.72% bias error when averaged over a discrete frequency interval.

These biases and uncertainties are applied to the MSL inlet pressure signals (i.e., by appropriate adjustment of the Fourier coefficients).

Table 4. ACM Rev. 4 bias and uncertainty for specified frequency intervals (from CDI Report No. 07-09P, Table 6.1).

[[

(3)]]

Table 5. Bias and uncertainty contributions to total uncertainty for HC1 plant data.

[[

(3)]]

4. Structural Analysis

The solution is decomposed into static and harmonic parts, where the static solution produces the stress field induced by the supported structure subjected to its own weight and the harmonic solution accounts for the harmonic stress field due to the unit pressure of given frequency in one of the main steam lines. All solutions are linearly combined, with amplitudes provided by signal measurements in each steam line, to obtain the final displacement and stress time histories. This decomposition facilitates the prescription of the added mass model accounting for hydrodynamic interaction and allows one to compare the stress contributions arising from static and harmonic loads separately. Proper evaluation of the maximum membrane and membrane+bending stresses requires that the static loads due to weight be accounted for. Hence both static and harmonic analyses are carried out.

4.1 Static Analysis

The results of the static analysis are shown in Figure 8. Only a few locations exhibited high stress intensity levels. These locations include the skirt/upper support ring connection with stress intensity 8,775 psi, the trough thin section/vane bank end plate/thick closure plate junction with stress intensity 5,416 psi and the thin closure plate/inner hood junction with stress intensity 8,133 psi. All locations are near the steam dryer support brackets. Close up views of these locations are shown in Figure 9. Note that these locations have high stress intensity also when static and transient runs are combined, primarily due to static loading.

4.2 Harmonic Analysis

The harmonic pressure loads were applied to the structural model at all surface nodes described in Section 3.10. Typical stress intensity distributions over the structure are shown in Figure 10. Stresses were calculated for each frequency, and results from static and harmonic calculations were combined.

To evaluate maximum stresses, the stress harmonics including the static component are transformed into a time history using FFT, and the maximum and alternating stress intensities for the response, evaluated. According to ASME B&PV Code, Section III, Subsection NG-3216.2 the following procedure was established to calculate alternating stresses. For every node, the stress difference tensors, $\boldsymbol{\sigma}'_{nm} = \boldsymbol{\sigma}_n - \boldsymbol{\sigma}_m$, are considered for all possible pairs of the stresses $\boldsymbol{\sigma}_n$ and $\boldsymbol{\sigma}_m$ at different time levels, t_n and t_m. Note that all possible pairs require consideration, since there are no "obvious" extrema in the stress responses. However, in order to contain computational cost, extensive screening of the pairs takes place (see Section 2.3), so that pairs known to produce alternating stress intensities less than 1,500 psi are rejected. For each remaining stress difference tensor, the principal stresses S_1, S_2, S_3 are computed and the maximum absolute value among principal stress differences, $S_{nm} = \max\{|S_1 - S_2|, |S_1 - S_3|, |S_2 - S_3|\}$, obtained. The alternating stress at the node is then one-half the maximum value of S_{nm} taken over all combinations (n,m), i.e., $S_{alt} = \frac{1}{2}\max_{n,m}\{S_{nm}\}$. This alternating stress is compared against allowable values, depending on the node location with respect to welds.

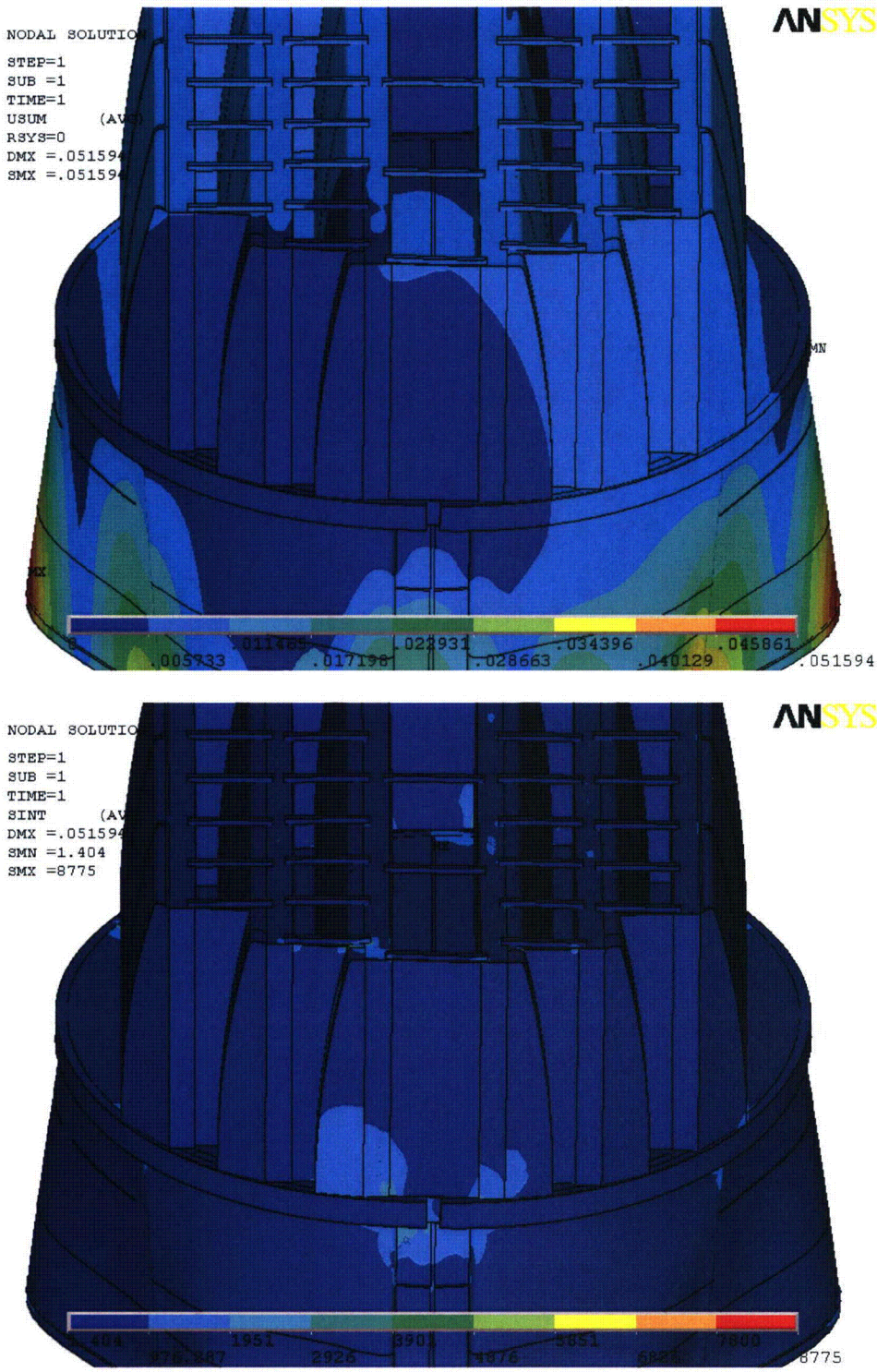

Figure 8. Overview of static calculations showing displacements (top, in inches) and stress intensities (bottom, in psi). Maximum displacement (DMX) is 0.052"; maximum stress intensity (SMX) is 8,775 psi. Note that displacements are amplified for visualization.

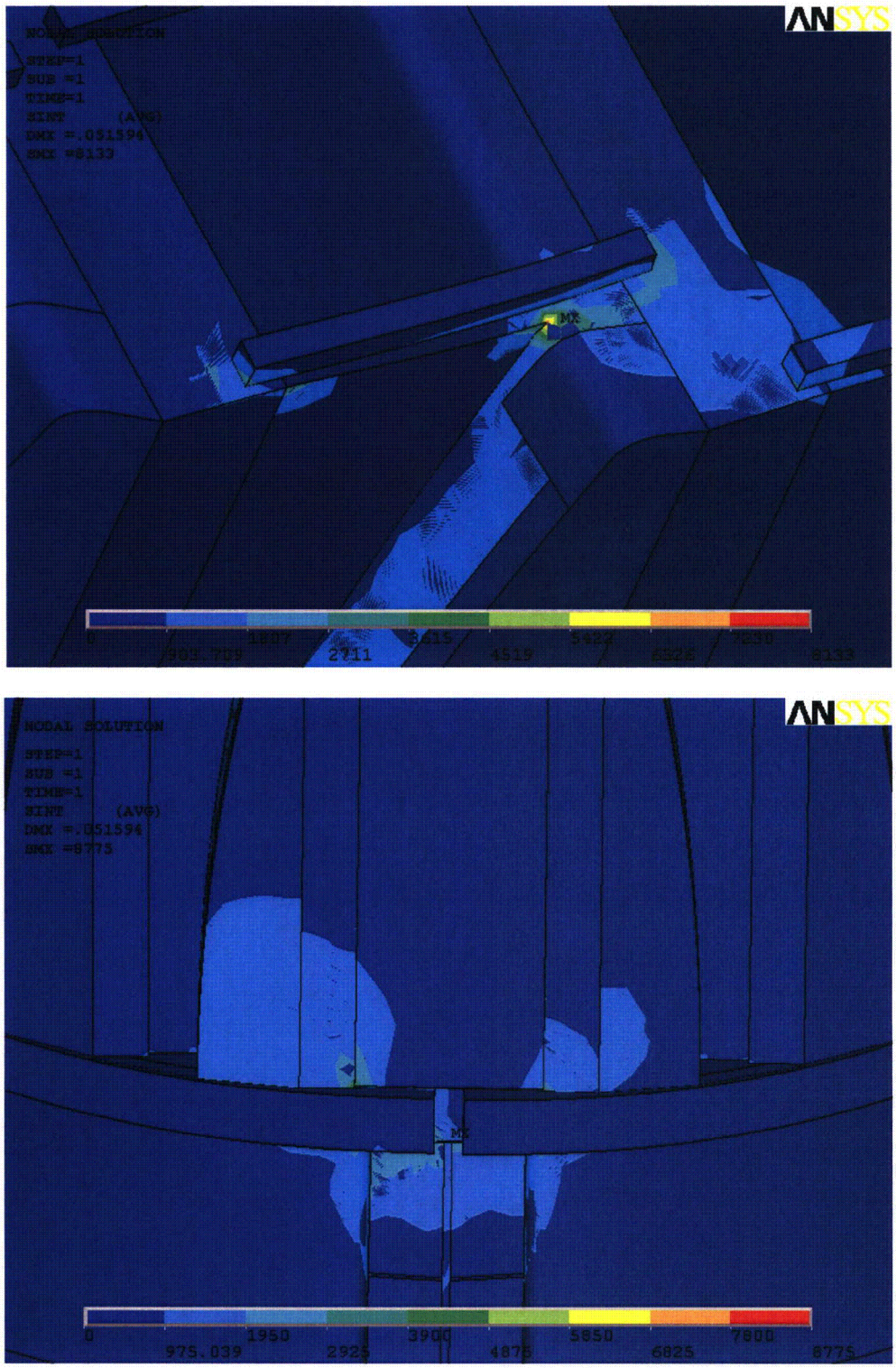

Figure 9. Close up of high static stress intensity (in psi) locations at closure plates and near support brackets.

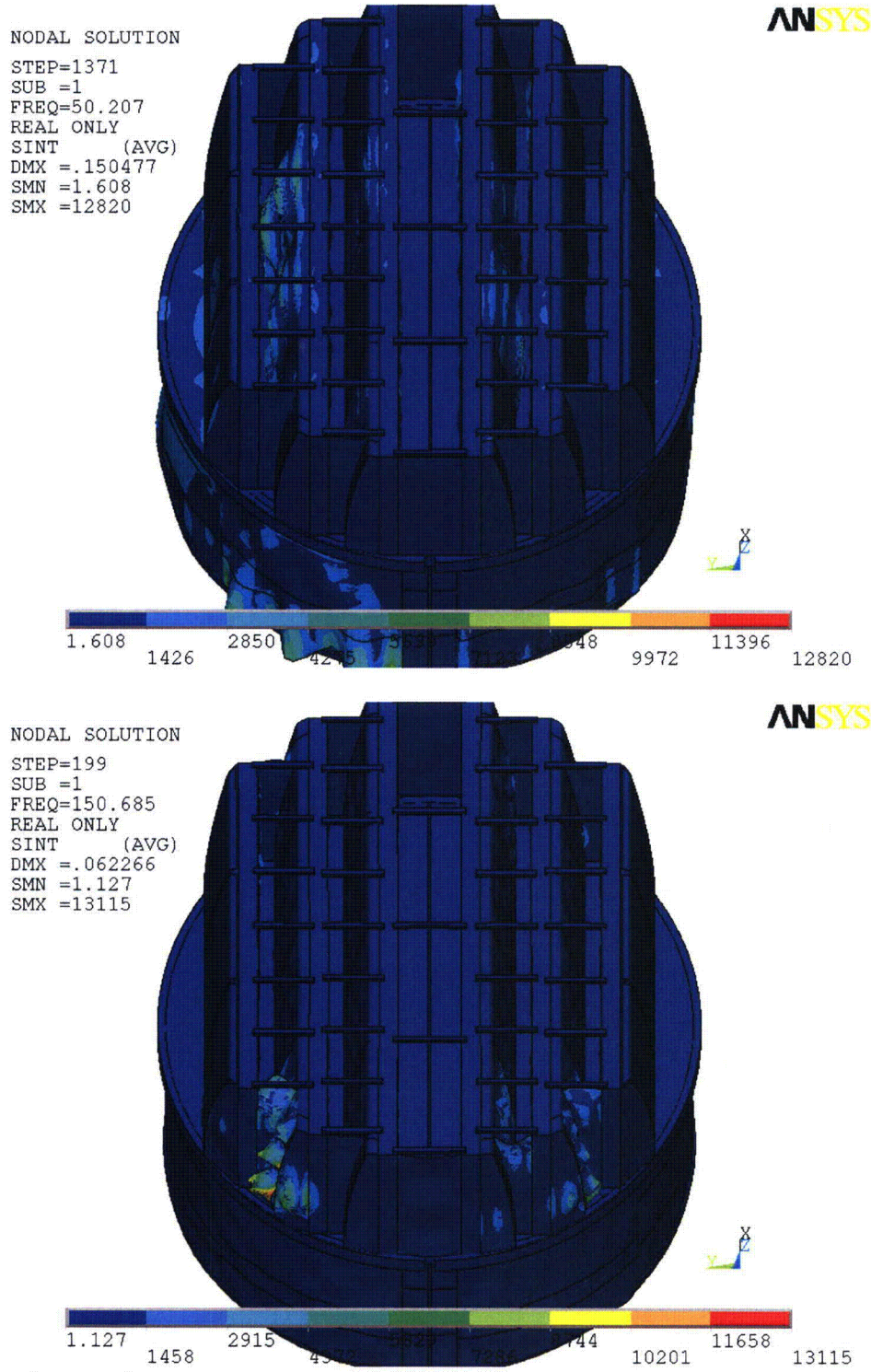

Figure 10. Overview of harmonic calculations showing real part of stress intensities (in psi) along with displacements. Unit loading MSL C for frequencies 50.2 Hz (top) and 150.7 Hz (bottom).

4.3 Post-Processing

The static and unsteady stresses computed at every node with ANSYS were exported into files for subsequent post-processing. These files were then read into separate customized software to compute the maximum and alternating stresses at every node. The maximum stress was defined for each node as the largest stress intensity occurring during the time history. Alternating stresses were calculated according to the ASME standard described above. For shell elements the maximum stresses were calculated separately at the mid-plane, where only membrane stress is present, and at top/bottom of the shell, where bending stresses are also present.

For nodes that are shared between several structural components or lie on junctions, the maximum and alternating stress intensities are calculated as follows. First, the nodal stress tensor is computed separately for each individual component by averaging over all finite elements meeting at the node and belonging to the same structural component. The time histories of these stress tensors are then processed to deduce the maximum and alternating stress intensities for each structural component. Finally, for nodes shared across multiple components, the highest of the component-wise maximum and alternating stresses is recorded as the "nodal" stress. This approach prevents averaging of stresses across components and thus yields conservative estimates for nodal stresses at the weld locations where several components are joined together.

The maximum stresses are compared against allowable values which depend upon the stress type (membrane, membrane+bending, alternating – Pm, Pm+Pb, S_{alt}) and location (at a weld or away from welds). These allowables are specified in the following section. For solid elements the most conservative allowable for membrane stress, Pm, is used, although bending stresses are nearly always present also. The structure is then assessed in terms of stress ratios formed by dividing allowables by the computed stresses at every node. Stress ratios less than unity imply that the associated maximum and/or alternating stress intensities exceed the allowable levels. Post-processing tools calculate the stress ratios, identifying the nodes with low stress ratios and generating files formatted for input to the 3D graphics program, TecPlot, which provides more general and sophisticated plotting options than currently available in ANSYS.

4.4 Computation of Stress Ratios for Structural Assessment

The ASME B&PV Code, Section III, subsection NG provides different allowable stresses for different load combinations and plant conditions. The stress levels of interest in this analysis are for the normal operating condition, which is the Level A service condition. The load combination for this condition is:

Normal Operating Load Combination = Weight + Pressure + Thermal

The weight and fluctuating pressure contributions have been calculated in this analysis and are included in the stress results. The static pressure differences and thermal expansion stresses are small, since the entire steam dryer is suspended inside the reactor vessel and all surfaces are exposed to the same conditions. Seismic loads only occur in Level B and C cases, and are not

considered in this analysis. No physical modifications were made to the HC1 steam dryer since commercial operation; therefore, seismic loading would not change.

Allowable Stress Intensities

The ASME B&PV Code, Section III, subsection NG shows the following (Table 6) for the maximum allowable stress intensity (Sm) and alternating stress intensity (Sa) for the Level A service condition. The allowable stress intensity values for type 304 stainless steel at operating temperature 550°F are taken from Table I-1.2 and Fig. I-9.2.2 of Appendix I of Section III, in the ASME B&PV Code. The calculation for different stress categories is performed in accordance with Fig. NG-3221-1 of Division I, Section III, subsection NG.

Table 6. Maximum allowable stress intensity and alternating stress intensity for all areas other than welds. The notation Pm represents membrane stress; Pb represents stress due to bending; Q represents secondary stresses (from thermal effects and gross structural discontinuities, for example); and F represents additional stress increments (due to local structural discontinuities, for example).

Type	Notation	Service Limit	Allowable Value (psi)
Maximum Stress Allowables:			
General Membrane	Pm	Sm	16,900
Membrane + Bending	Pm + Pb	1.5 Sm	25,350
Primary + Secondary	Pm + Pb + Q	3.0 Sm	50,700
Alternating Stress Allowable:			
Peak = Primary + Secondary + F	S_{alt}	Sa	13,600

When evaluating welds, either the calculated or allowable stress was adjusted, to account for stress concentration factor and weld quality. Specifically:

- For maximum allowable stress intensity, the allowable value is decreased by multiplying its value in Table 6 by 0.55.

- For alternating stress intensity, the calculated weld stress intensity is multiplied by a weld stress intensity (fatigue) factor of 1.8, before comparison to the Sa value given above.

The weld factors of 0.55 and 1.8 were selected based on the observable quality of the shop welds and liquid penetrant NDE testing of all welds (excluding tack and intermittent welds, which were subject to 5X visual inspection) during fabrication. These factors are consistent with fatigue strength reduction factors recommended by the Welding Research Council, [22], and stress concentration factors at welds, provided in [23] and [24]. GE Purchase Specification for the HCGS Steam Dryer (21A9355 Section 9.2) called for liquid penetrant testing of all welds (excluding tack and intermittent welds) along the entire length or circumference, using the guidance of ASME Boiler and Pressure Code, Paragraph N-6127.3. In addition, critical welds are subject to periodical visual inspections in accordance with the requirements of GE SIL 644 SIL and BWR VIP-139 [25]. Therefore, for weld stress intensities, the allowable values are shown in Table 7.

These factors (0.55 and 1.8) also conservatively presume that the structure is joined using fillet welds unless specified otherwise. Since fillet welds correspond to larger stress concentration factors than other types of welds, this assumption is a conservative one.

Table 7. Weld Stress Intensities.

Type	Notation	Service Limit	Allowable Value (psi)
Maximum Stress Allowables:			
General Membrane	Pm	0.55 Sm	10,065
Membrane + Bending	Pm + Pb	0.825 Sm	15,098
Primary + Secondary	Pm + Pb + Q	1.65 Sm	30,195
Alternating Stress Allowables:			
Peak = Primary + Secondary + F	S_{alt}	Sa	13,600

Comparison of Calculated and Allowable Stress Intensities

The classification of stresses into general membrane or membrane + bending types was made according to the exact location, where the stress intensity was calculated; namely, general membrane, Pm, for middle surface of shell element, and membrane + bending, Pm + Pb, for other locations. For solid elements the most conservative, general membrane, Pm, allowable is used.

The structural assessment is carried out by computing stress ratios between the computed maximum and alternating stress intensities, and the allowable levels. Locations where any of the stresses exceed allowable levels will have stress ratios less than unity. Since computation of stress ratios and related quantities within ANSYS is time-consuming and awkward, a separate FORTRAN code was developed to compute the necessary maximum and alternating stress intensities, Pm, Pm+Pb, and S_{alt}, and then compare it to allowables. Specifically, the following quantities were computed at every node:

1. The maximum membrane stress intensity, Pm (evaluated at the mid-thickness location for shells),
2. The maximum membrane+bending stress intensity, Pm+Pb, (taken as the largest of the maximum stress intensity values at the bottom, top, and mid thickness locations, for shells),
3. The alternating stress, S_{alt}, (the maximum value over the three thickness locations is taken).
4. The stress ratio due to a maximum stress intensity assuming the node lies at a non-weld location (note that this is the minimum ratio obtained considering both membrane stresses and membrane+bending stresses):
   SR-P(nw) = min{ Sm/Pm, 1.5 * Sm/(Pm+Pb) }.
5. The alternating stress ratio assuming the node lies at a non-weld location,
   SR-a(nw) = Sa / (1.1 * S_{alt}),
6. The same as 4, but assuming the node lies on a weld,
   SR-P(w)=SR-P(nw) * f_{sw} * 0.55

7. The same as 5, but assuming the node lies on a weld,
   SR-a(w)=SR-a(nw) * f_{sw} / 1.8.

where f_{sw}=1 at all welds (when justified, f_{sw} can be adjusted to reflect different weld types). Note that in steps 4 and 6, the minimum of the stress ratios based on Pm and Pm+Pb, is taken. The allowables listed in Table 6, Sm=16,900 psi and Sa=13,600 psi. The factors, 0.55 and 1.8, are the weld factors discussed above. The factor of 1.1 accounts for the differences in Young's moduli for the steel used in the steam dryer and the values assumed in alternating stress allowable. According to NG-3222.4 in subsection NG of Section III of the ASME Code, the effect of elastic modulus upon alternating stresses is taken into account by multiplying alternating stress S_{alt} at all locations by the ratio, E/E_{model}=1.1, where:

$E = 28.3\ 10^6$ psi, as shown on Fig. I-9.2.2. ASME BP&V Code
$E_{model} = 25.55\ 10^6$ psi (Table 1)

The appropriate maximum and alternating stress ratios, SR-P and SR-a, are thus determined and a final listing of nodes having the smallest stress ratios is generated. The nodes with stress ratios lower than 4 are plotted in TecPlot (a 3D graphics plotting program widely used in engineering communities [26]). These nodes are tabulated and depicted in the following Results Section.

5. Results

The stress intensities and associated stress ratios resulting from the Rev. 4 acoustic/hydrodynamic loads [4] at 115% CLTP with associated biases and uncertainties factored in, are presented below. The biases and uncertainties for both the ACM model and finite element analysis are fully accounted for as summarized in Section 3.12. Also, noise is removed in the 75-85 Hz frequency range as explained in Section 3.11. Section 5.1 tabulates the highest maximum and alternating stress intensities and presents contour plots of these stresses to indicate which points on the dryer experience significant stress concentration and/or modal response. Section 5.2 compares the stresses against allowable values, accounting for stress type (maximum and alternating) and location (on or away from a weld). The results are presented in terms of stress ratios and the locations with the lowest stress ratios are identified. Section 5.3 examines the spectral content of select nodes.

In each section results are presented both at nominal conditions (no frequency shift) and with frequency shift included. Unless specified otherwise, frequency shifts are generally performed at 2.5% increments. The tabulated stresses and stress ratios are obtained using a 'blanking' procedure that is designed to prevent reporting a large number of high stress nodes from essentially the same location on the structure. In the case of stress intensities (section 5.1) this procedure is as follows. The relevant stress intensities are first computed at every node and then nodes sorted according to stress level. The highest stress node is noted and all neighboring nodes within 10 inches of the highest stress node and its symmetric images (i.e., reflections across the x=0 and y=0 planes) are "blanked" (i.e., excluded from the search for subsequent high stress locations). Of the remaining nodes, the next highest stress node is identified and its neighbors (closer than 10 inches) blanked. The third highest stress node is similarly located and the search continued in this fashion until all nodes are either blanked or have stresses less than half the highest value on the structure. In Section 5.2, a similar blanking procedure is applied to the stress ratios rather than stresses. Thus the lowest stress ratio of a particular type in a 10" neighborhood and its symmetric images is identified and all other nodes in these regions excluded from listing in the table. Of the remaining nodes, the one with the lowest stress ratio is reported and its neighboring points similarly excluded, and so on until all nodes are either blanked or have a stress ratio higher than 4.

5.1 General Stress Distribution and High Stress Locations

The maximum stress intensities obtained by post-processing the ANSYS stress histories for 115% CLTP at nominal frequency and with frequency shift operating conditions are listed in Table 8. Contour plots of the stress intensities over the steam dryer structure are shown on Figure 11 (nominal frequency) and Figure 12 (maximum stress over all nine frequency shifts including nominal). The figures are oriented to emphasize the high stress regions. Note that these stress intensities *do not* account for weld factors but do include end-to-end bias and uncertainty. Further, it should be noted that since the allowable stresses vary with location, stress intensities do not necessarily correspond to regions of primary structural concern. Instead, structural evaluation is more accurately made in terms of the stress ratios which compare the computed stresses to allowable levels with due account made for stress type and weld factors. Comparisons on the basis of stress ratios are made in Section 5.2.

The general stress state in terms of stress intensities and low stress ratio locations is very similar to the ones reported previously for 111.5% CLTP [8]. For the peak stresses, Pm and Pm+Pb, most of the nodes that were in the Table 8 of [8] reappear here either directly or as a reflected image (i.e., reflected across the x=0 or y=0 planes). The values show little change since they are dominated by the static component. As at 111.5% CLTP, all of the nodes with highest alternating stress intensities occur on the inner and middle hoods. Given the similarity between the results at 111.5% and 115% CLTP, the associated discussion and observations essentially the same.

The maximum stress intensities in most areas are low (less than 500 psi, or 5% of the most conservative critical stress). For the membrane stresses (Pm) the high stress regions tend to occur at: (i) the outermost portion of the inner hood near the connection to the closure plate; (ii) the weld joining the skirt and the upper support ring near the supports; and (iii) the central base plate/vane bank junction. In all cases the stress is dominated by static stresses as evidenced by the small alternating stresses (less than 700 psi) in the rightmost columns in the table. The closure plates and regions in the vicinity of where they connect to adjacent hoods or vane banks, experience high stresses since they restrain any deflection of the adjacent vane banks.

The membrane + bending stress (Pm+Pb) distributions evidence a pronounced modal response over the inner and middle hoods. However, the highest stress locations are still dominated by the static component as is confirmed by the low alternating stress values in the right hand column of Table 8. Stress concentrations are visible near the hood supports, at the bottoms of the hoods, near the tops of the closure plates and along the skirt/drain channel welds.

The alternating stresses are generally small at nominal operation with the highest reported value (2,072 psi) occurring on the inner hood and the highest value on a weld being 2,507 psi at the inner hood/hood support junction. With frequency shifting this is also the limiting alternating stress node and its highest alternating stress intensity increases to 2,910 psi at the +7.5% frequency shift. This is 16% higher than without frequency shifting. It is also 14% higher than the highest alternating stress intensity found on the dryer at any frequency shift at 111.5% CLTP. The alternating stress intensity contour plots essentially record the modes excited by this signal, which here are seen to be confined to inner and middle hoods which, though not directly exposed to the main MSL pressure fluctuations (like the outer hoods are) are of thinner construction and therefore exhibit a significant response.

Table 8a. Locations with highest predicted stress intensities for 115% CLTP conditions with no frequency shift. Noise is filtered between 75-85 Hz. Alternating stresses are only computed at nodes where stresses can exceed 500 psi.

Stress Category	Location		Location (in)				Stress Intensities (psi)		
		Weld	x	y	z	node	Pm	Pm+Pb	S_{alt}
Pm	outer portion of inner hood (top near closure plate)	No	109	-27.6	95.3	44886	6152	8763	620
"	central base plate/inner vane bank/side panel	Yes	-118.8	14.4	7.5	85994	4138	5696	<500
"	skirt/upper support ring	Yes	118.7	-5.9	-2	91960	3971	5743	<500
"	closure plate/middle side panel/top cover plate/ top perforated plate	Yes	108.4	-45.9	95.9	91627	3761	4534	552
"	inner hood backing bar/closure plate	Yes	-108.4	38.4	8.1	87035	3479	3670	<500
Pm+Pb	skirt/upper support ring	Yes	118.8	0.6	-2	88325	2299	9200	0
"	outer portion of inner hood (top near closure plate)	No	109	-27.6	95.3	44886	6152	8763	620
"	central base plate/inner vane bank/side panel	Yes	-118.8	14.4	7.5	85994	4138	5696	0
"	drain pipe/skirt	Yes	88.2	79.6	-20.5	91083	1934	5466	0
"	cover plate/outer hood	Yes	59.1	101.4	7.5	93493	1455	4936	557
S_{alt}	inner hood/hood support	Yes	0	-36.1	49.6	80664	1107	2560	2507
"	inner hood/backing bar	Yes	-30	-38.4	8.5	79668	385	2423	2261
"	inner hood/hood support	Yes	0	-34.7	60.8	80662	1043	2234	2216
"	inner hood/hood support	Yes	0	37.2	38.4	88025	955	2208	2144
"	inner hood	No	-30.4	-37.5	34.7	44920	481	2098	2072

Node numbers are retained for further reference.
Spatial coordinate are in the coordinate system, defined by the origin at the centerline of steam dryer 7.5" below bottom plates. The x-axis is parallel to the hoods, y-axis is normal to the hoods pointing from MSL AB to MSL CD, z-axis is vertical, positive up.

Table 8b. Locations with highest predicted stress intensities taken over all frequency shifts at 115% CLTP. Noise is filtered between 75-85 Hz. Alternating stresses are only computed at nodes where stresses can exceed 500 psi.

Stress Category	Location	Weld	% Freq. Shift	Location (in)				Stress Intensities (psi)		
				x	y	z	node	Pm	Pm+Pb	S_{alt}
Pm	outer portion of inner hood (top near closure plate)	No	10	109	-27.6	95.3	44886	6215	8823	721
"	central base plate/inner vane bank/side panel	Yes	10	-118.8	14.4	7.5	85994	4209	5775	<500
"	skirt/upper support ring	Yes	7.5	118.7	-5.9	-2	91960	4044	5821	<500
"	closure plate/middle side panel/top cover plate/ top perforated plate	Yes	5	-108.4	45.9	95.9	85891	3820	4813	834
"	inner hood backing bar/closure plate	Yes	5	-108.4	38.4	8.1	87035	3594	3833	538
Pm+Pb	skirt/upper support ring	Yes	7.5	118.8	0.6	-2	88325	2305	9318	526
"	outer portion of inner hood (top near closure plate)	No	10	109	-27.6	95.3	44886	6215	8823	721
"	central base plate/inner vane bank/side panel	Yes	10	-118.8	14.4	7.5	85994	4209	5775	<500
"	drain pipe/skirt	Yes	10	88.2	79.6	-20.5	91083	2032	5724	623
"	cover plate/old outer hood remnant	Yes	10	59.1	101.4	7.5	93493	1455	5088	696
S_{alt}	inner hood/hood support	Yes	7.5	0	-36.1	49.6	80664	1284	2991	2910
"	inner hood/hood support	Yes	7.5	0	-34.7	60.8	80662	1229	2751	2745
"	inner hood/hood support	Yes	7.5	0	-37.2	38.4	80716	1138	2771	2732
"	middle hood/hood support	Yes	-5	0	-68.3	42.2	90114	1031	2518	2335
"	inner hood/backing bar	Yes	0	-30	-38.4	8.5	79668	444	2423	2261

See Table 8a for coordinates description.

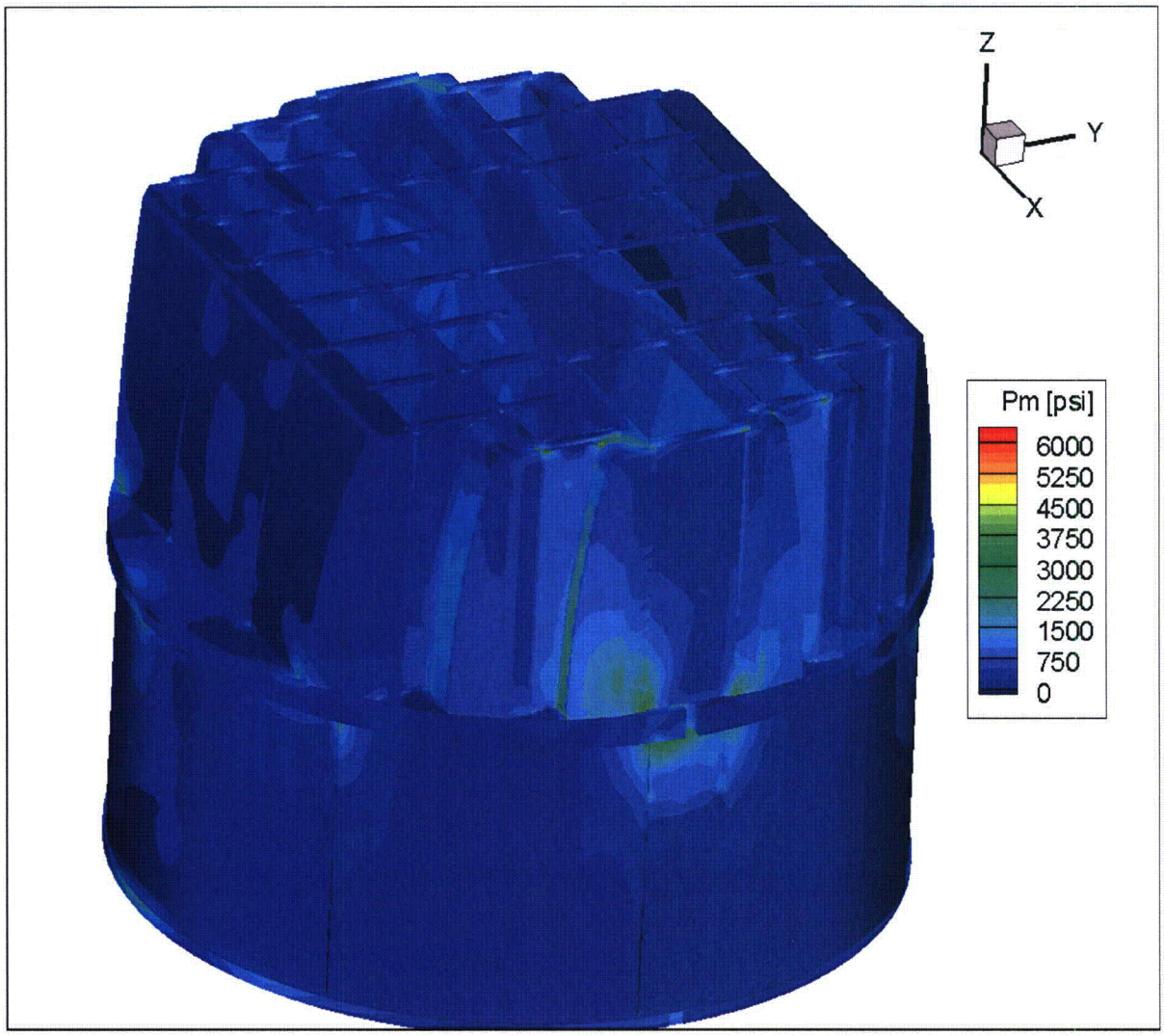

Figure 11a. Contour plot of maximum membrane stress intensity, Pm, for 115% CLTP load. The maximum stress intensity is 6,152 psi.

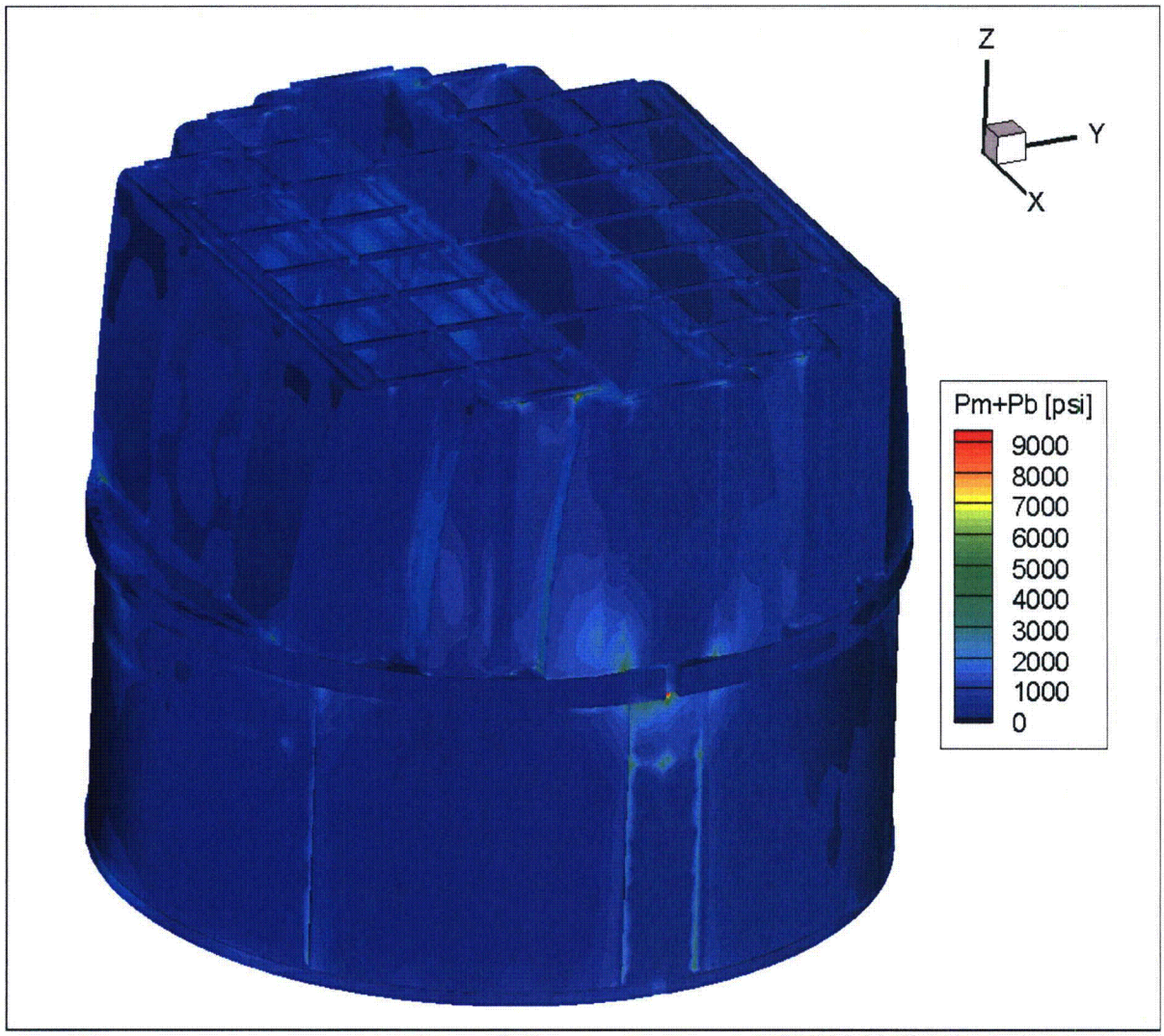

Figure 11b. Contour plot of maximum membrane+bending stress intensity, Pm+Pb, for 115% CLTP load. The maximum stress intensity is 9,200 psi. First view.

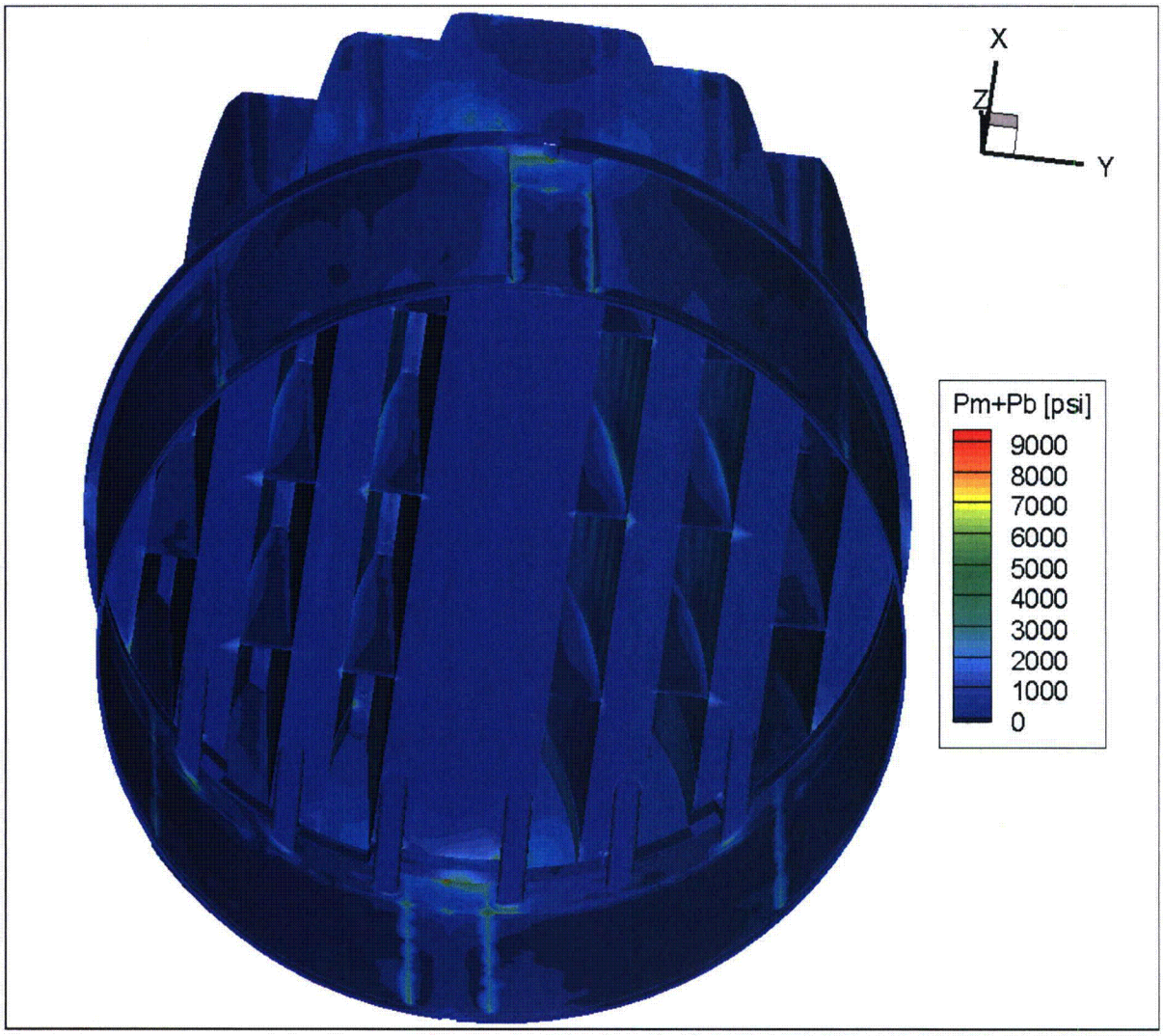

Figure 11c. Contour plot of maximum membrane+bending stress intensity, Pm+Pb, for 115% CLTP load. Second view from below.

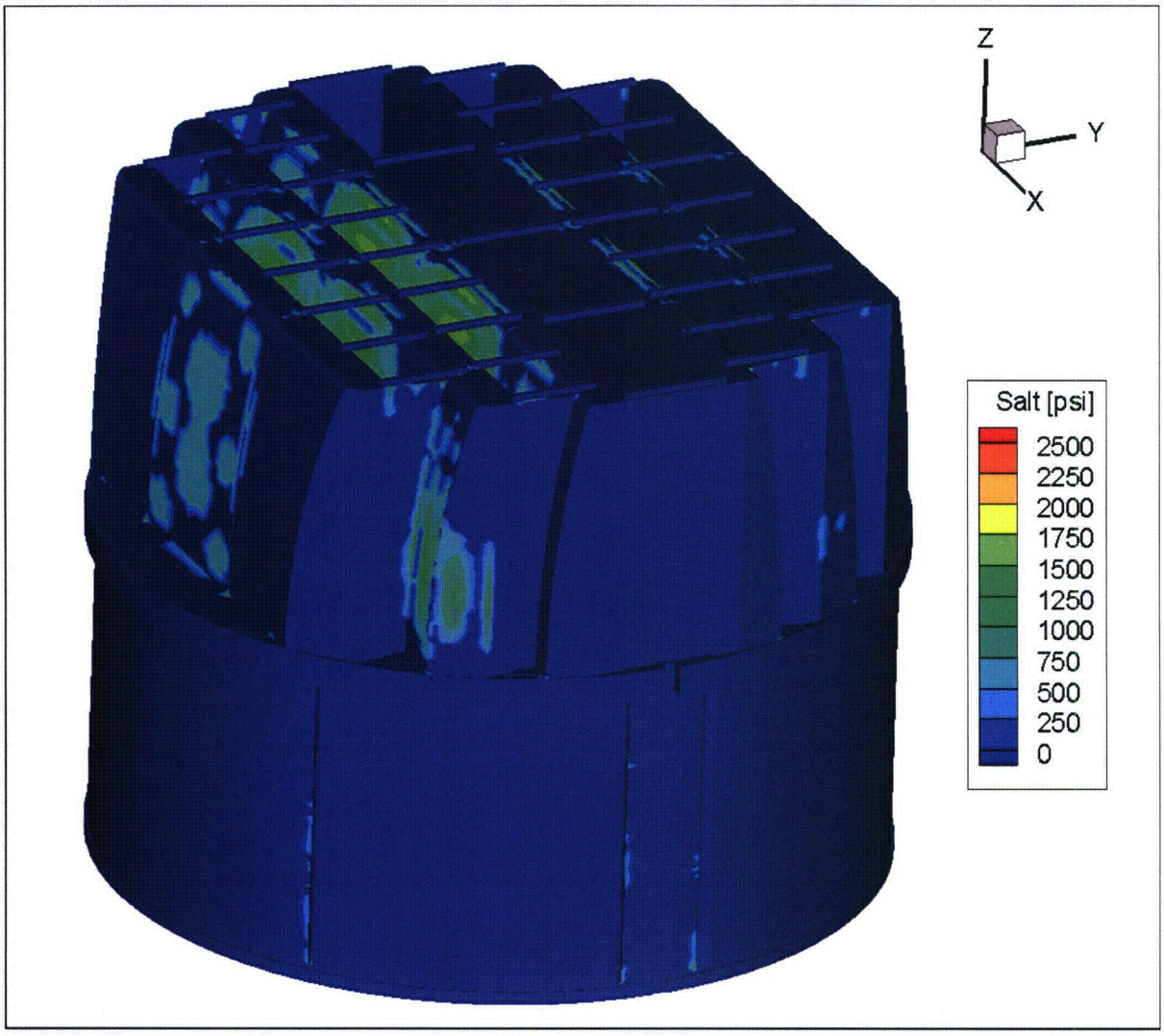

Figure 11d. Contour plot of alternating stress intensity, S_{alt}, for 115% CLTP load. The highest alternating stress intensity is 2,507 psi. First view.

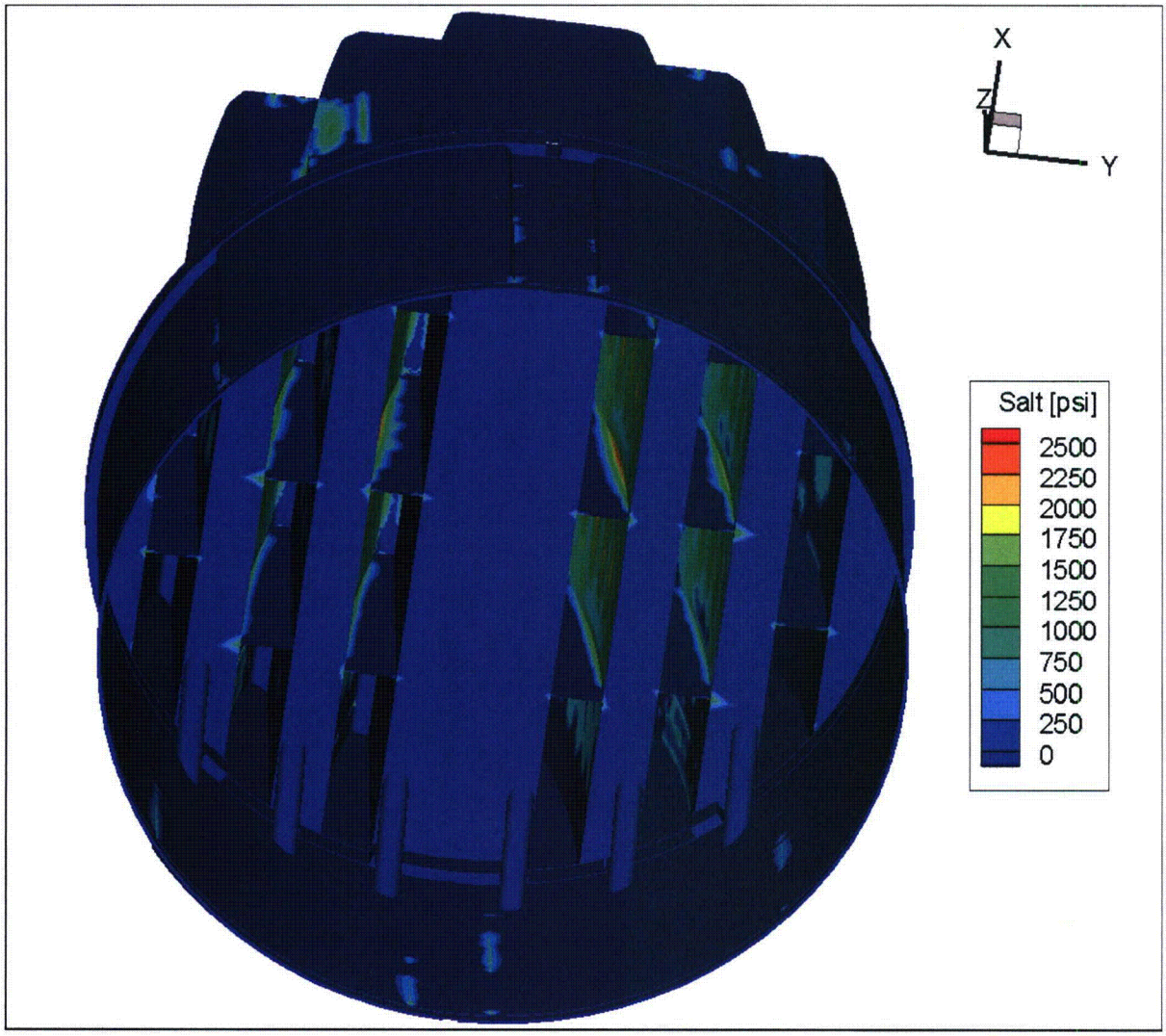

Figure 11e. Contour plot of alternating stress intensity, S_{alt}, for 115% CLTP load. This second view from below shows the high alternating stress intensity on the hoods and the hood/hood support junctions.

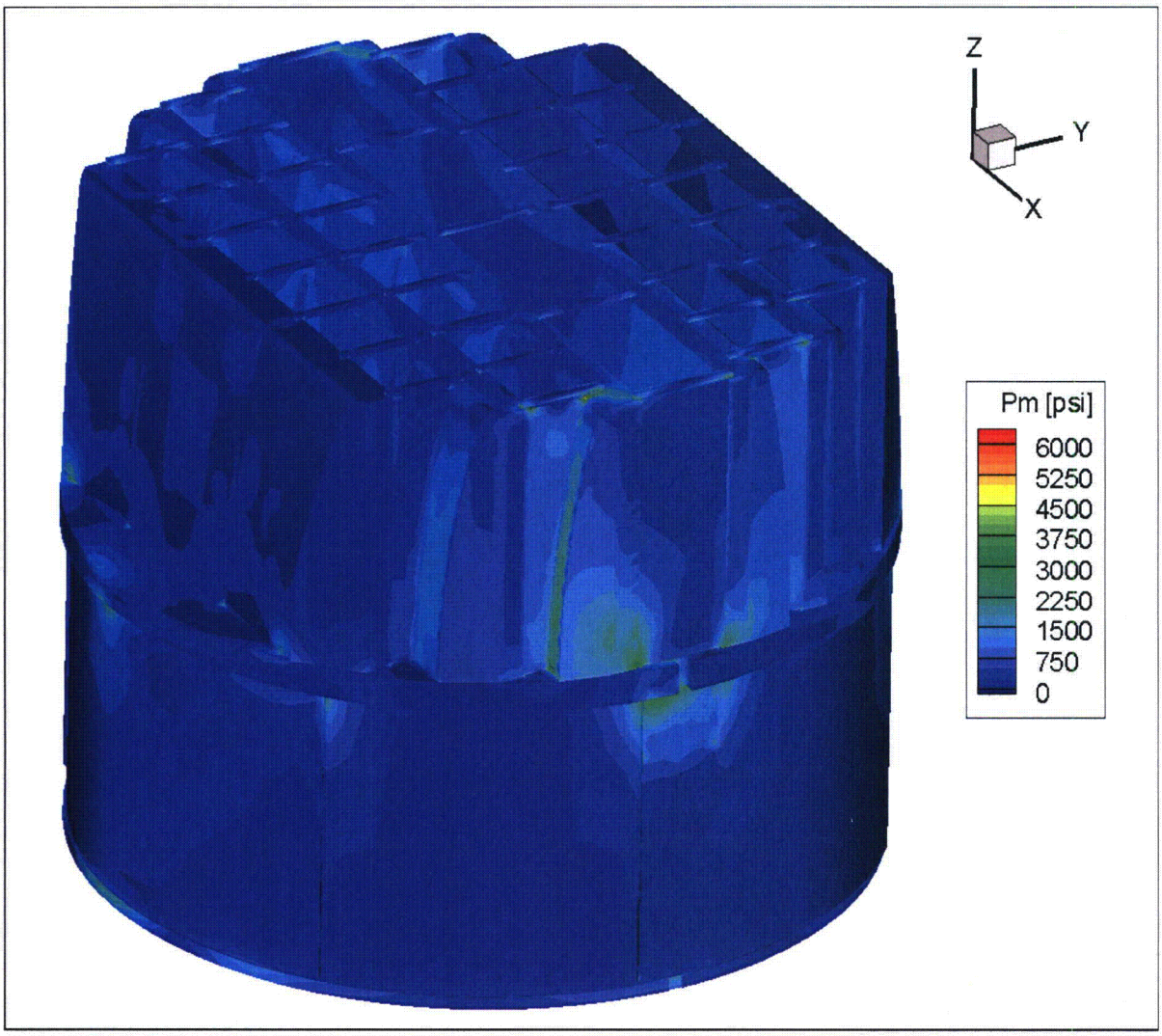

Figure 12a. Contour plot of maximum membrane stress intensity, Pm, for 115% CLTP operation with frequency shifts. The recorded stress at a node is the maximum value taken over all frequency shifts. The maximum stress intensity is 6,215 psi.

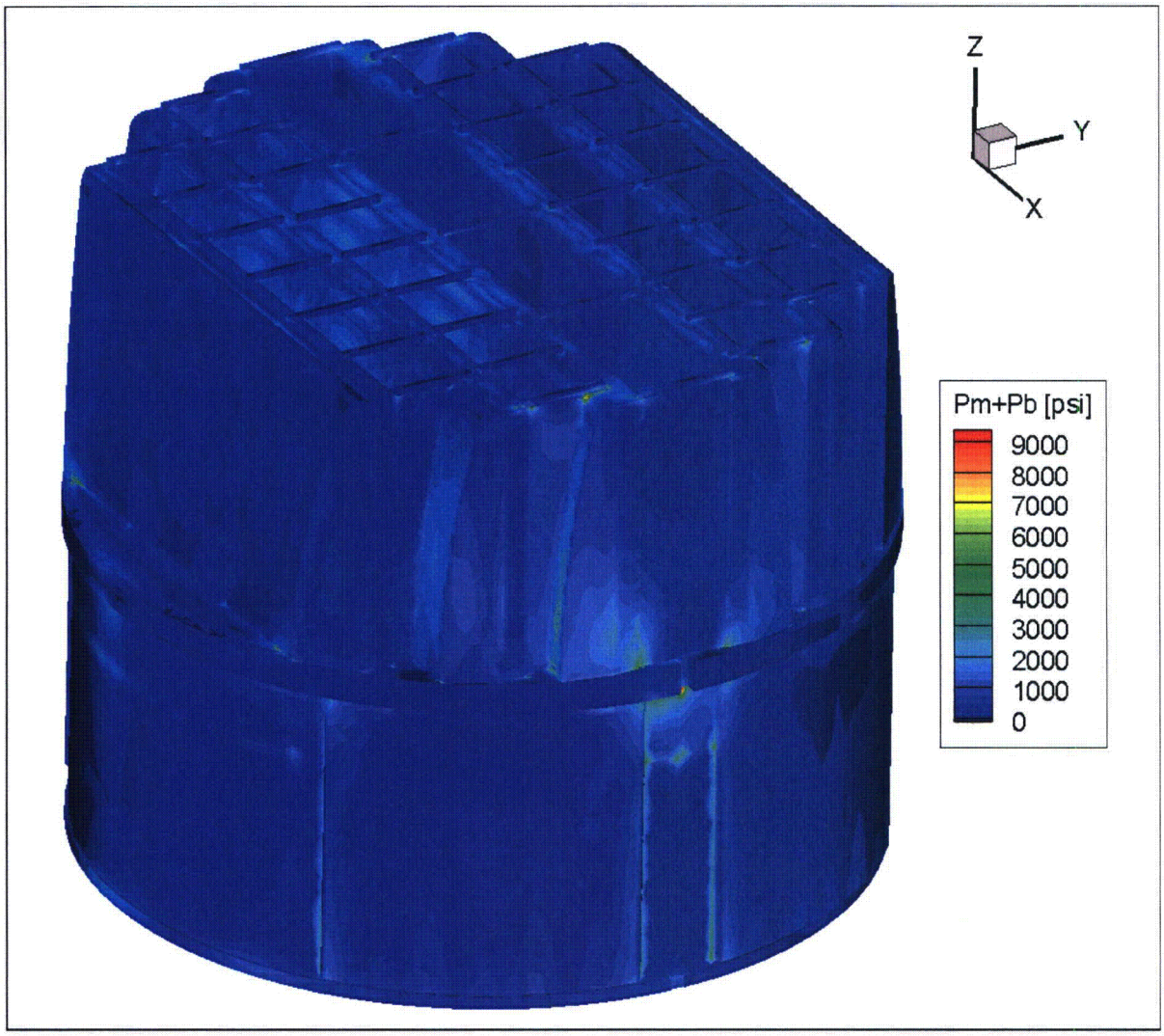

Figure 12b. Contour plot of maximum membrane+bending stress intensity, Pm+Pb, for 115% CLTP operation with frequency shifts. The recorded stress at a node is the maximum value taken over all frequency shifts. The maximum stress intensity is 9,318 psi. First view.

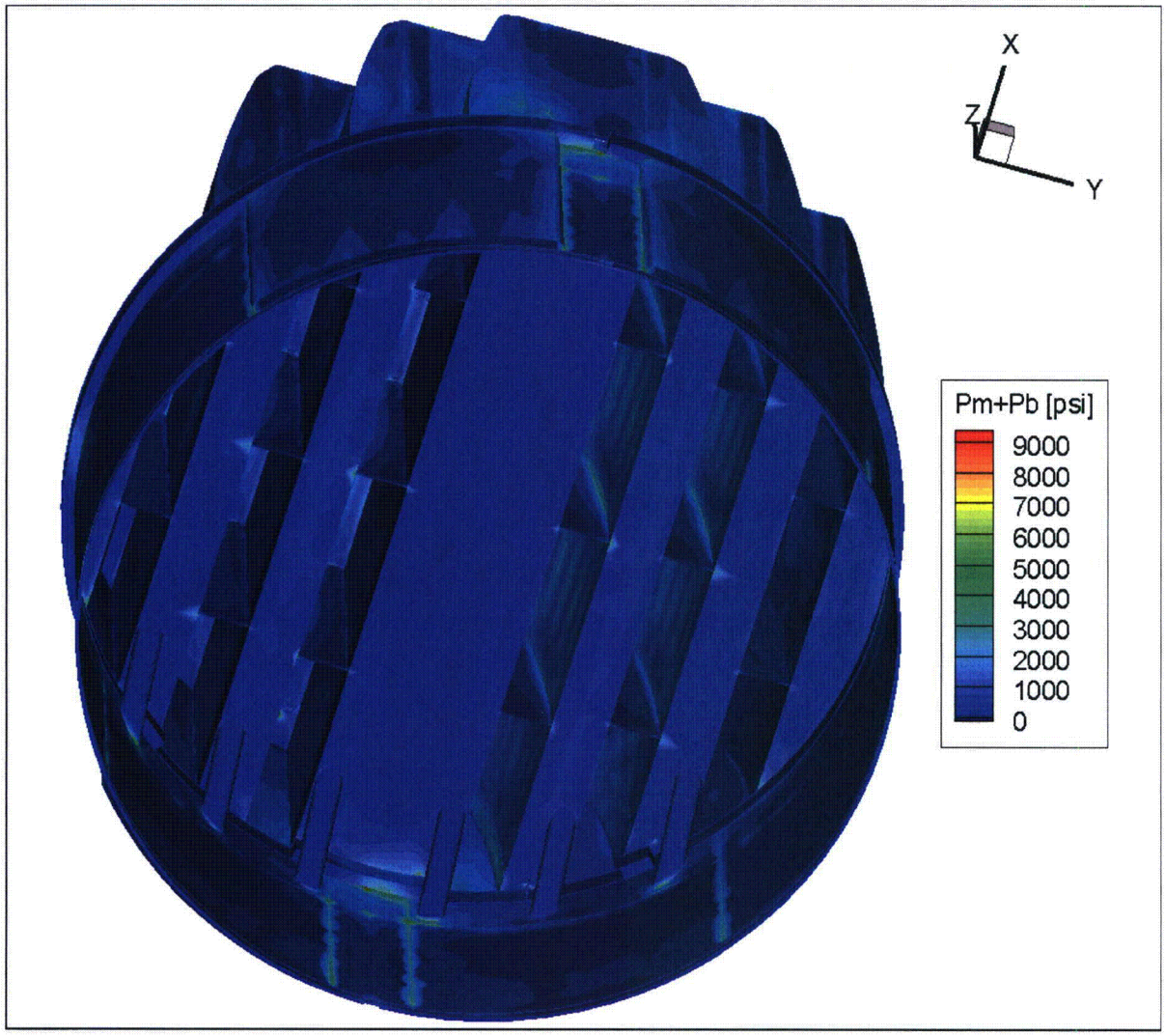

Figure 12c. Contour plot of maximum membrane+bending stress intensity, Pm+Pb, for 115% CLTP operation with frequency shifts. This second view from beneath reveals high stress and modal response of the hood/hood support junctions.

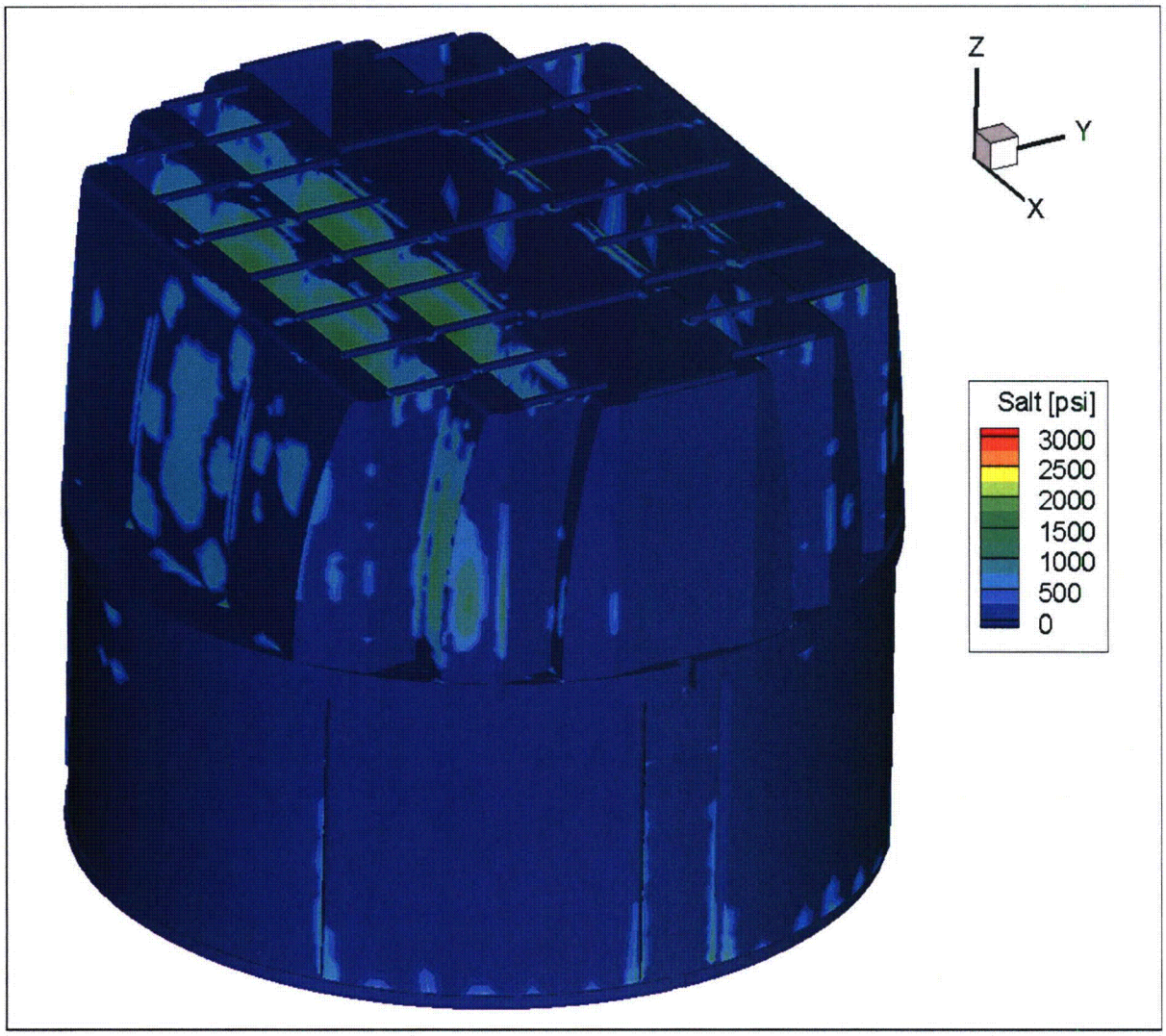

Figure 12d. Contour plot of alternating stress intensity, S_{alt}, for 115% CLTP operation with frequency shifts. The recorded stress at a node is the maximum value taken over all frequency shifts. The maximum alternating stress intensity is 2,910 psi. First view.

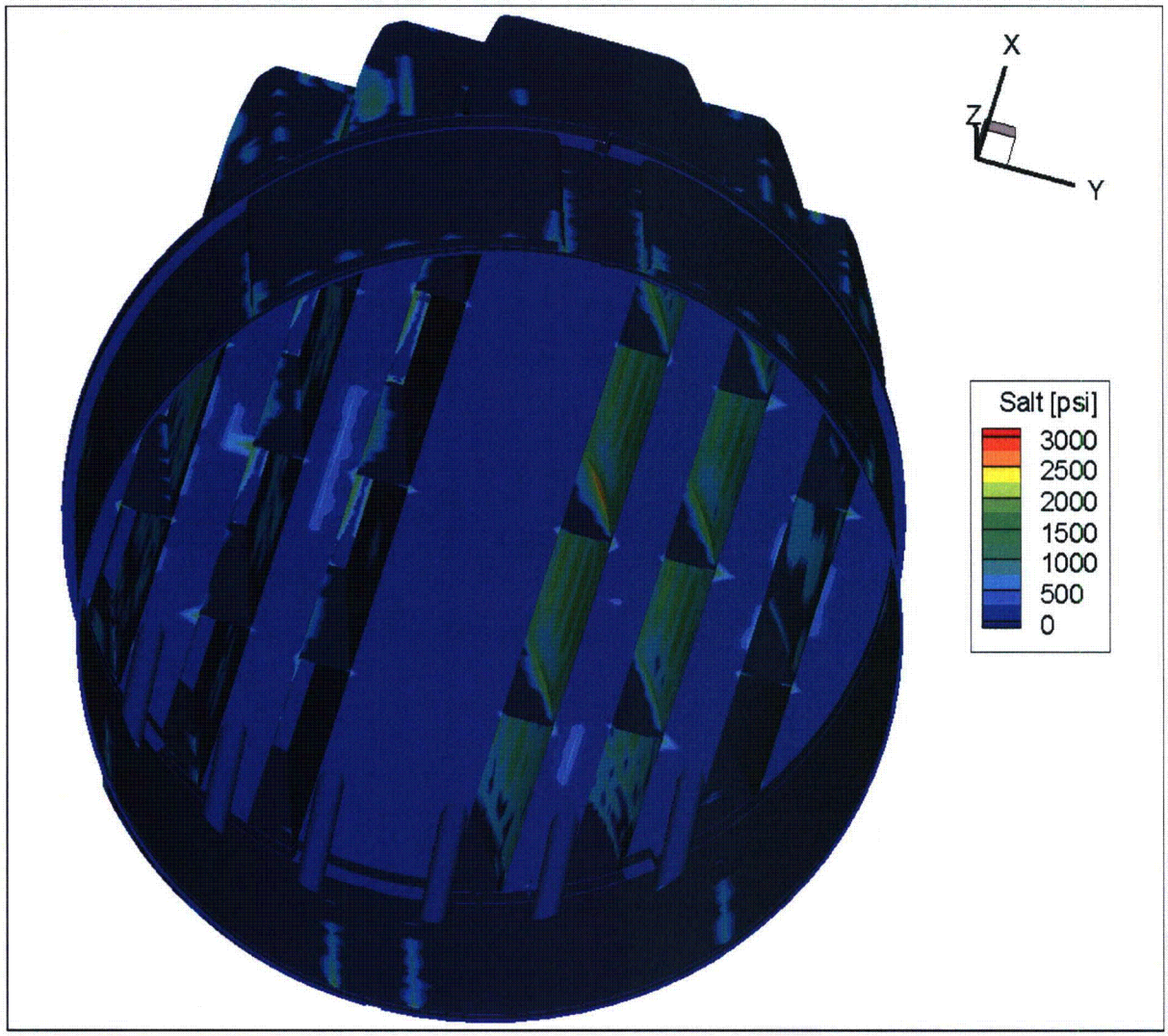

Figure 12e. Contour plot of alternating stress intensity, S_{alt}, for 115% CLTP operation with frequency shifts. This second view from beneath reveals more of the high stress regions on the hood/hood support junctions.

5.2 Load Combinations and Allowable Stress Intensities

The stress ratios computed for 115% CLTP at nominal frequency and with frequency shifting are listed in Table 9. The stress ratios are grouped according to type (SR-P for maximum membrane and membrane+bending stress, SR-a for alternating stress) and location (away from welds or on a weld).

For 115% CLTP operation at nominal frequency the minimum stress ratio is identified as a maximum stress, SR-P=1.51, and occurs at the junction of the skirt and upper support ring. At this condition, the dryer stress state is effectively governed by maximum stresses and, more specifically, by the weight-induced static stress field. This is clear from Table 9a where all entries in the right hand column for the list of maximum stress intensities show negligible alternating stress ratios, SR-a>5. All remaining locations for maximum stresses with SR-P less than 3 are listed in Table 9a. These locations, together with all nodes having stress ratios below 4.0 are depicted in the accompanying Figure 13.

The effects of frequency shifts can be conservatively accounted for by identifying the minimum stress ratio at every node, where the minimum is taken over all the frequency shifts considered (including the nominal or 0% shift case). The resulting stress ratios are then processed as before to identify the smallest stress ratios anywhere on the structure, categorized by stress type (maximum or alternating) and location (on or away from a weld). The results are summarized in Table 9b and show that the minimum stress ratio, SR-P=1.50, is virtually the same as before and is still identified with a maximum stress. This is the smallest stress ratio encountered anywhere on the structure for any frequency shift at the 115% CLTP condition. Because the alternating stress ratio at this location exceeds 13.0, the minimum stress ratio does not change appreciably with frequency shift. For the same reason these stress ratios are essentially unchanged from the ones at 111.5% CLTP [8].

The minimum alternating stress ratio at any frequency shift, SR-a=2.36, occurs on the weld joining the inner hood and hood support. In fact, the first three nodes with the smallest alternating stress ratios lie on this weld. The next lowest alternating stress ratio occurs on the middle hood/hood support junction and all nodes with SR-a<4 involve the inner and middle hoods. These are depicted in Figure 14e which identifies the 13 limiting nodes listed in Table 9b and also displays all nodes with SR-a<4 without blanking. The limiting alternating stress ratios with and without frequency shifts (SR-a=2.74 and 2.36 respectively) differ by less than 14%. However, the variations in stress intensity with frequency shift in the ±10% range are considerably higher than this as shown in Section 5.3.

In summary, the lowest stress ratio on the dryer is due to a deadweight dominated maximum stress, SR-P=1.50. This ratio shows negligible variation with frequency shift as shown further in Section 5.3. The lowest alternating stress ratio anywhere on the dryer is SR-a=2.36 and occurs at the +7.5% frequency shift. These values are well above allowable and account for all end-to-end biases and correspond to CLTP loads adjusted to eliminate non-acoustic content in the 75-85 Hz range using the 1000# data.

Table 9a. Locations with minimum stress ratios for 115% CLTP conditions with no frequency shift. Noise is filtered between 75-85 Hz. Stress ratios are grouped according to stress type (maximum – SR-P; or alternating – SR-a) and location (away from a weld or at a weld). Bold text indicates minimum stress ratio of any type on the structure. Locations are depicted in Figure 13. Alternating stress ratios at non-welds are all greater than 4.0.

Stress Ratio	Weld	Location	Location (in.)				Stress Intensity (psi)			Stress Ratio	
			x	y	z	node	Pm	Pm+Pb	S_{alt}	SR-P	SR-a
SR-P	No	1. outer portion of inner hood (top near closure plate)	109	-27.6	95.3	44886	6152	8763	620	2.74	20.42
SR-a	No	NONE (All SR-a > 4)									
SR-P	**Yes**	**1. skirt/upper support ring**	**118.8**	**0.6**	**-2**	**88325**	**2299**	**9200**	**<500**	**1.51**	**>13**
"	"	2. closure plate/inner hood	108.4	27.9	94.9	85409	5156	7561	1295	1.80	5.31
"	"	3. central base plate/inner vane bank/side panel	-118.8	14.4	7.5	85994	4138	5696	<500	2.24	>13
"	"	4. closure plate/middle side panel/top cover plate/ top perforated plate	108.4	-45.9	95.9	91627	3761	4534	552	2.47	12.44
"	"	5. drain pipe/skirt	88.2	79.6	-20.5	91083	1934	5466	<500	2.55	>13
"	"	6. backing bar/closure plate	-108.4	38.4	8.1	87035	3479	3670	<500	2.67	>13
"	"	7. cover plate/old outer hood remnant	59.1	101.4	7.5	93493	1455	4936	557	2.83	12.34
										0.00	
SR-a	Yes	1. inner hood/hood support	0	-36.1	49.6	80664	1107	2560	2507	5.45	2.74
"	"	2. backing bar/inner hood	-30	-38.4	8.5	79668	385	2423	2261	5.75	3.04
"	"	3. inner hood/hood support	0	-34.7	60.8	80662	1043	2234	2216	6.24	3.10
"	"	4. inner hood/hood support	0	37.2	38.4	88025	955	2208	2144	6.32	3.20
"	"	5. backing bar/middle hood	29.1	-69.9	8.5	89651	465	2026	1939	6.88	3.54
"	"	6. middle hood/hood support	0	67.6	49.6	87901	862	2020	1849	6.90	3.72
"	"	7. middle hood/hood support	0	-68.7	38.4	90115	764	1883	1685	7.41	4.08

See Table 8a for coordinates description.

Table 9b. Locations with minimum stress ratios for 115% CLTP conditions with frequency shifts. Noise is filtered between 75-85 Hz. Stress ratios at every node are recorded as the lowest stress ratio identified during the frequency shifts. Stress ratios are grouped according to stress type (maximum – SR-P; or alternating – SR-a) and location (away from a weld or at a weld). Bold text indicates minimum stress ratio of any type on the structure. Locations are depicted in Figure 14.

Stress Ratio	Weld	Location	% Freq. Shift	Location (in.)				Stress Intensity (psi)			Stress Ratio	
				x	y	z	node	Pm	Pm+Pb	S_{alt}	SR-P	SR-a
SR-P	No	1. outer portion of inner hood (top near closure plate)	10	109	-27.6	95.3	44886	6215	8823	721	2.72	17.15
SR-a	No	NONE (All SR-a > 4)										
SR-P	**Yes**	**1. skirt/upper support ring**	**7.5**	**118.8**	**0.6**	**-2**	**88325**	**2305**	**9318**	**526**	**1.50**	**13.05**
"	"	2. closure plate/inner hood	5	108.4	27.9	94.9	85409	5271	7724	1295	1.76	5.31
"	"	3. central base plate/inner vane bank/side panel	10	-118.8	14.4	7.5	85994	4209	5775	0	2.21	>13
"	"	4. closure plate/middle side panel/top cover plate/ top perforated plate	5	-108.4	45.9	95.9	85891	3820	4813	834	2.44	8.23
"	"	5. drain pipe/skirt	10	88.2	79.6	-20.5	91083	2032	5724	623	2.44	11.03
"	"	6. backing bar/closure plate	5	-108.4	38.4	8.1	87035	3594	3833	538	2.59	12.76
"	"	7. cover plate/old outer hood remnant	10	59.1	101.4	7.5	93493	1455	5088	696	2.74	9.86
											0.00	
SR-a	Yes	1. inner hood/hood support	7.5	0	-36.1	49.6	80664	1284	2991	2910	4.66	2.36
"	"	2. inner hood/hood support	7.5	0	-34.7	60.8	80662	1229	2751	2745	5.07	2.50
"	"	3. inner hood/hood support	7.5	0	-37.2	38.4	80716	1138	2771	2732	5.03	2.51
"	"	4. middle hood/hood support	-5	0	-68.3	42.2	90114	1031	2518	2335	5.53	2.94
"	"	5. inner hood/backing bar	0	-30	-38.4	8.5	79668	444	2423	2261	5.75	3.04

See Table 8a for coordinates description.

Table 9b (continued). Locations with minimum stress ratios for 115% CLTP conditions with frequency shifts. Noise is filtered between 75-85 Hz. Stress ratios at every node are recorded as the lowest stress ratio identified during the frequency shifts. Stress ratios are grouped according to stress type (maximum – SR-P; or alternating – SR-a) and location (away from a weld or at a weld).

Stress Ratio	Weld	Location	% Freq. Shift	Location (in.)				Stress Intensity (psi)			Stress Ratio	
				x	y	z	node	Pm	Pm+Pb	S_{alt}	SR-P	SR-a
SR-a	Yes	6. middle hood/hood support	-5	0	-65.6	64.4	90096	1010	2528	2251	5.51	3.05
"	"	7. middle hood/hood support	-7.5	0	-67.1	53.3	90095	1068	2310	2133	6.04	3.22
"	"	8. inner hood/hood support	7.5	0	-32.9	71.9	80704	962	2251	2028	6.20	3.39
"	"	9. middle hood/backing bar	0	29.1	-69.9	8.5	89651	471	2026	1939	6.88	3.54
		10. inner hood/hood support	7.5	0	-37.9	27.2	80667	861	1919	1873	7.27	3.67
		11. middle hood/hood support	-5	0	-69.2	31	90100	827	1995	1827	6.99	3.76
		12. inner hood/hood support	5	-59.5	-36.8	42.2	80650	791	1859	1809	7.50	3.80
		13. inner hood/hood support	5	-59.5	-35.6	53.4	80594	822	1827	1786	7.63	3.85

See Table 8a for coordinates description.

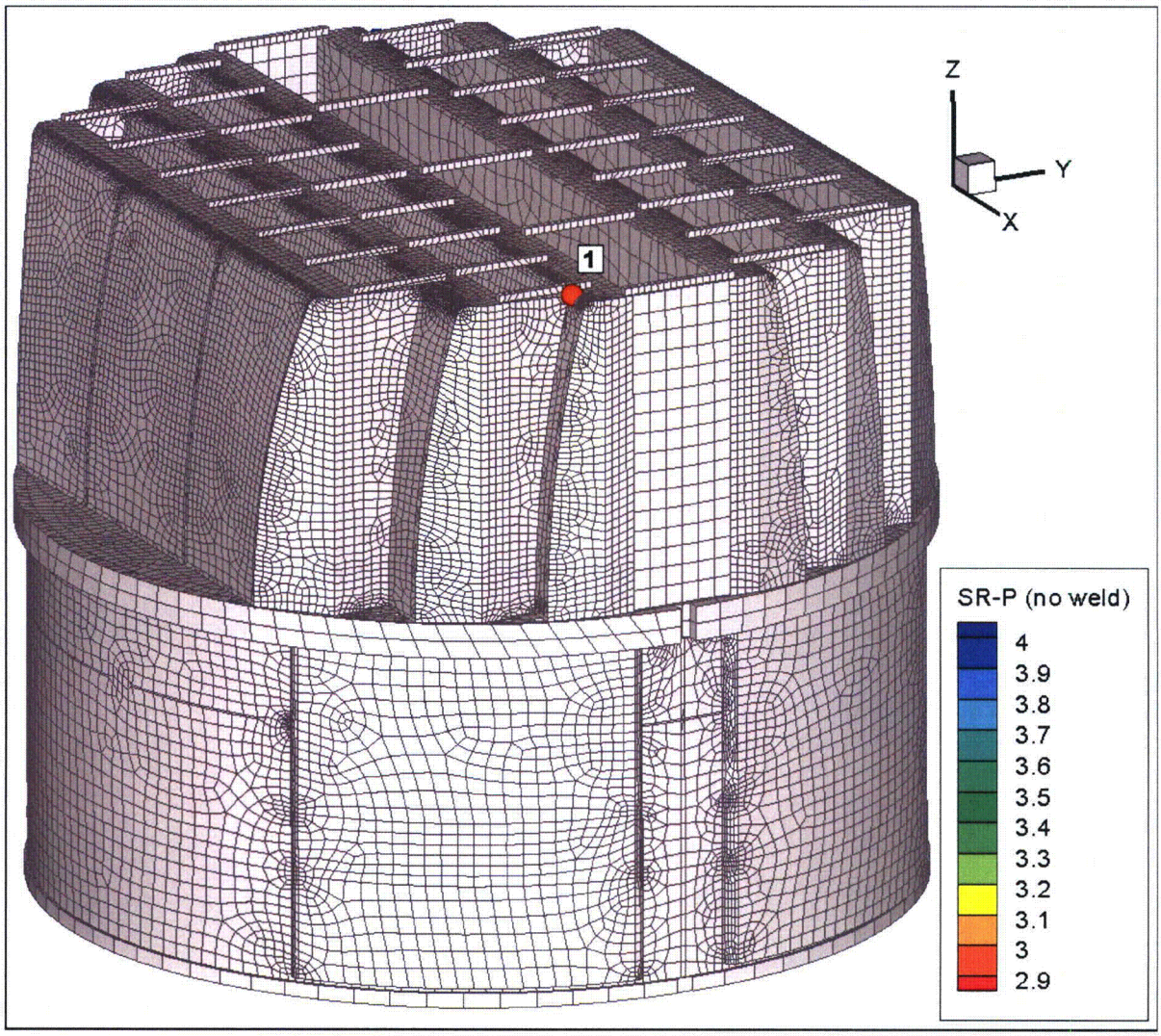

Figure 13a. Location of smallest maximum stress ratio, SR-P≤4, at non-welds for nominal 115% CLTP operation. Number refers to the enumerated locations for SR-P values at non-welds in Table 9a.

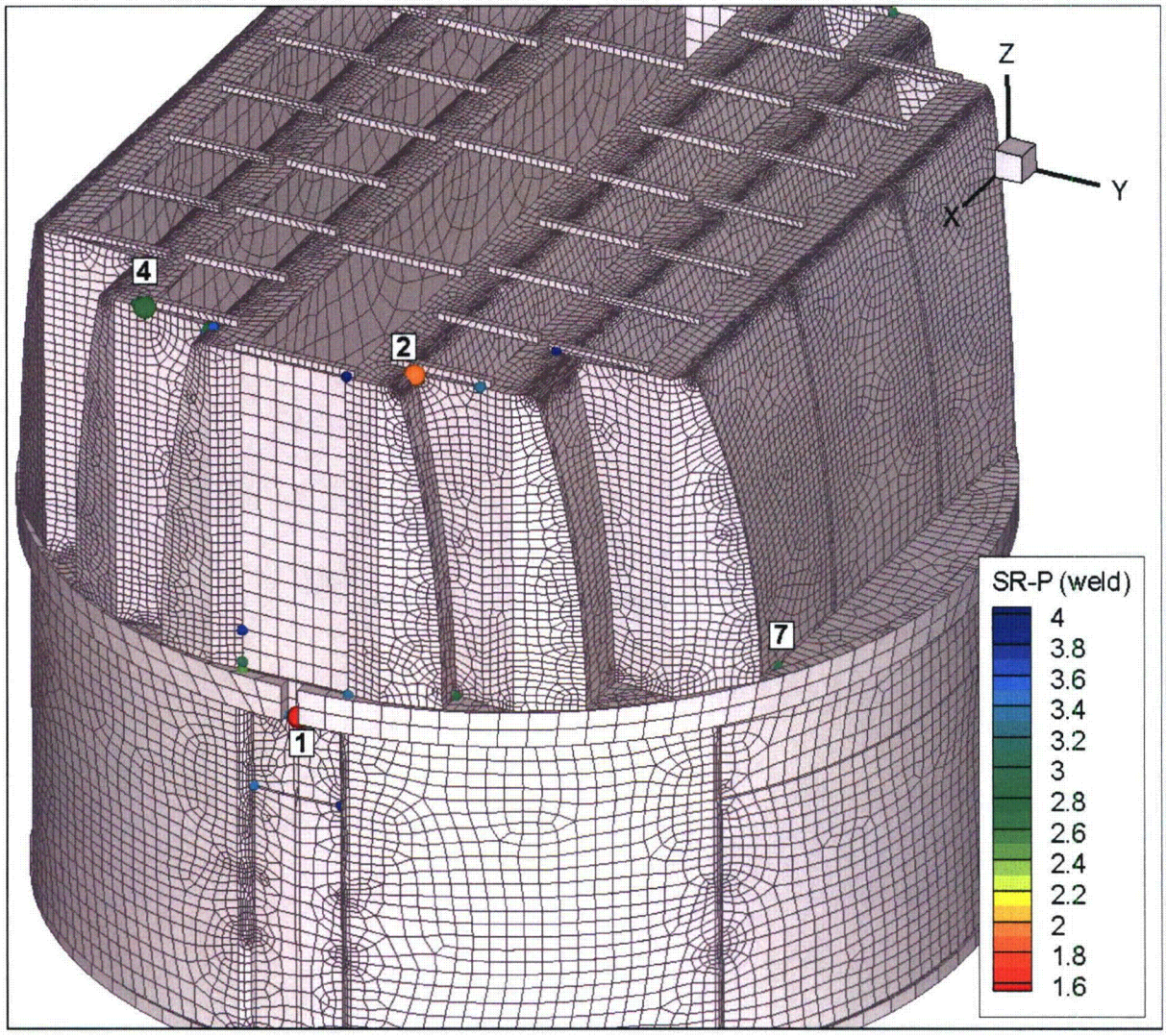

Figure 13b. Locations of smallest maximum stress ratios, SR-P≤4, at welds for nominal 115% CLTP operation. Numbers refer to the enumerated locations for SR-P values at welds in Table 9a. First view showing locations 1, 2, 4 and 7.

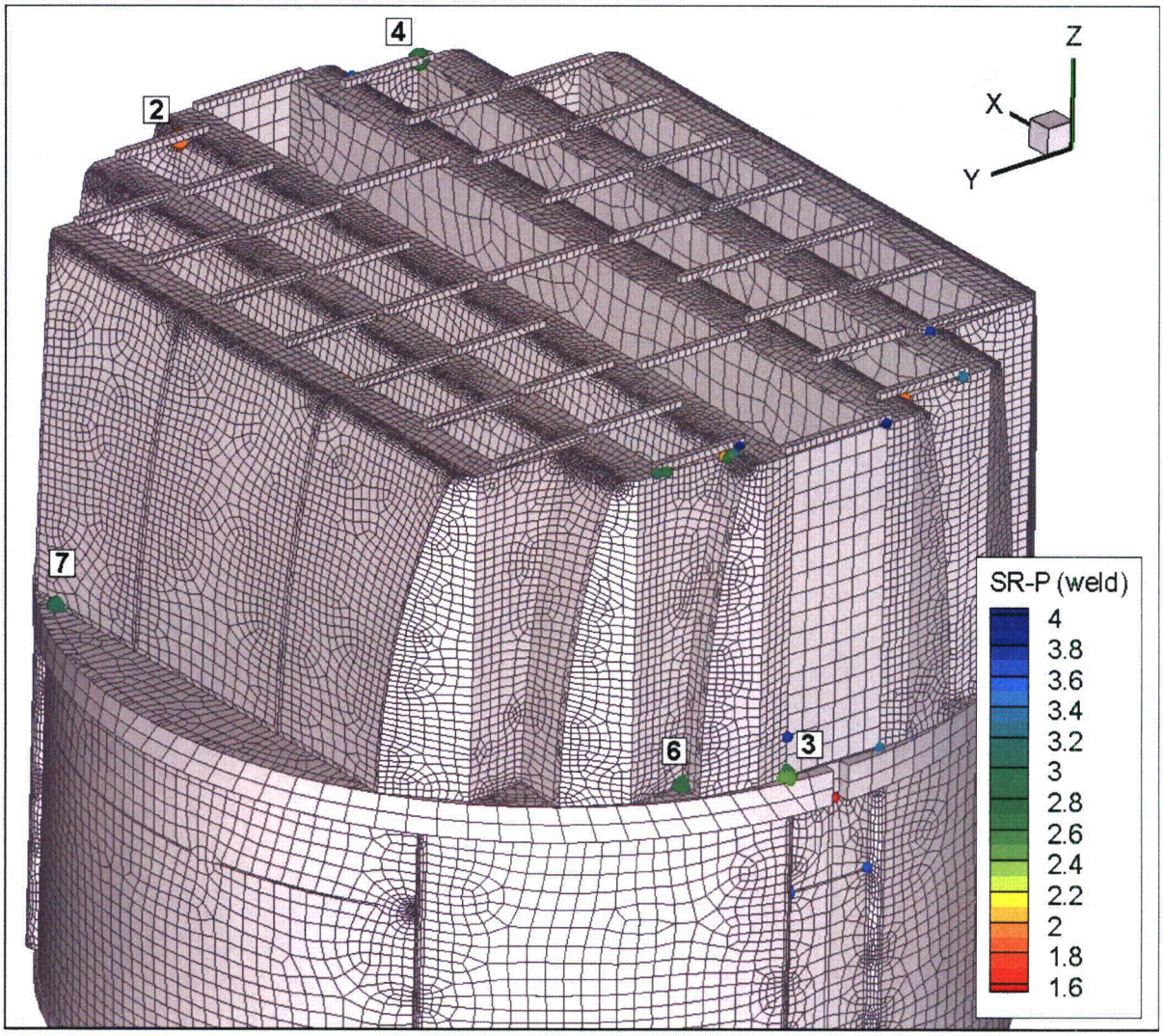

Figure 13c. Locations of smallest maximum stress ratios, SR-P≤4, at welds for nominal 115% CLTP operation. Numbers refer to the enumerated locations for SR-P values at welds in Table 9a. Second view showing locations 2-4, 6 and 7.

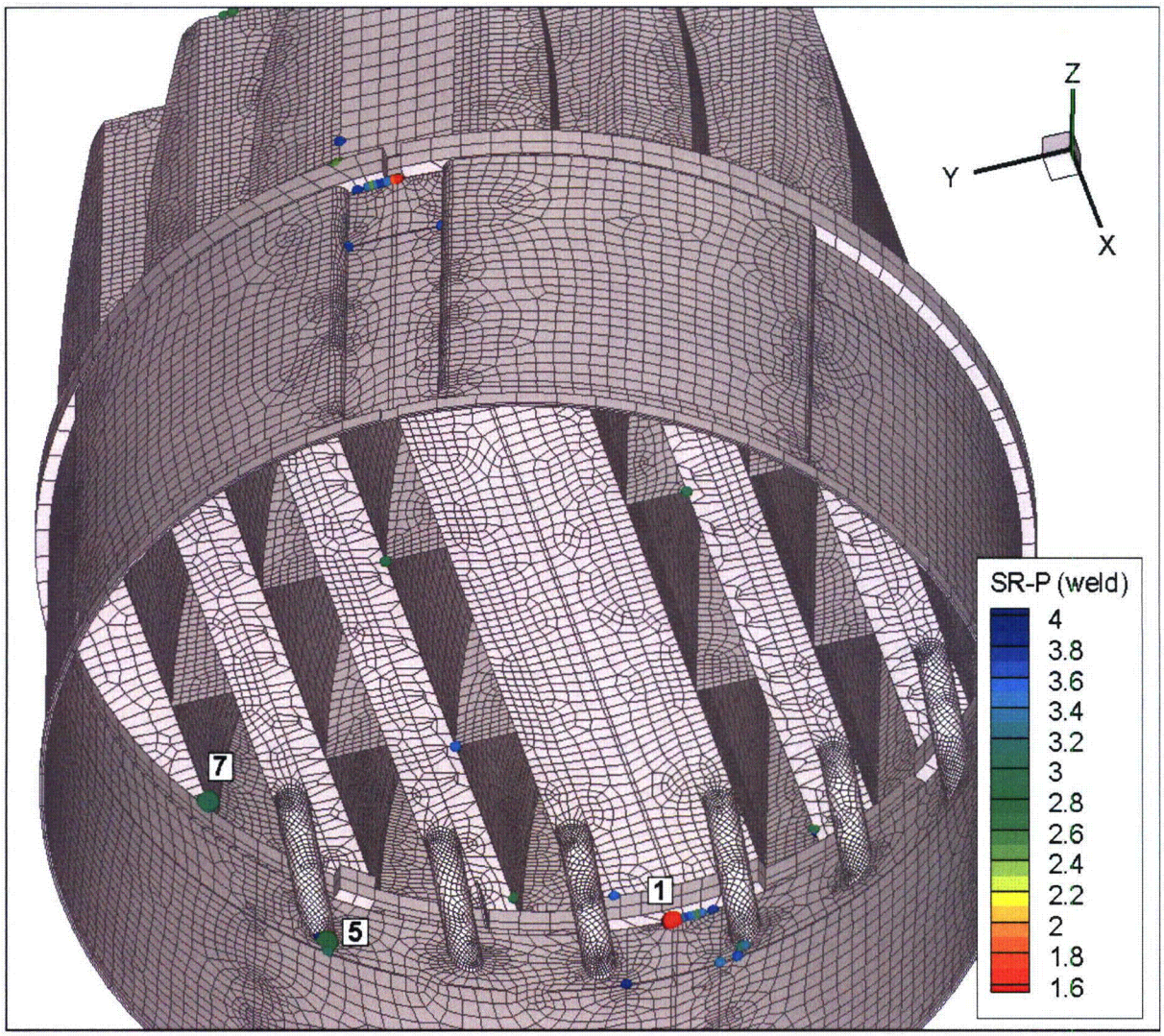

Figure 13d. Locations of smallest maximum stress ratios, SR-P≤4, at welds for nominal 115% CLTP operation. Numbers refer to the enumerated locations for SR-P values at welds in Table 9a. Third view showing locations 1, 5 and 7.

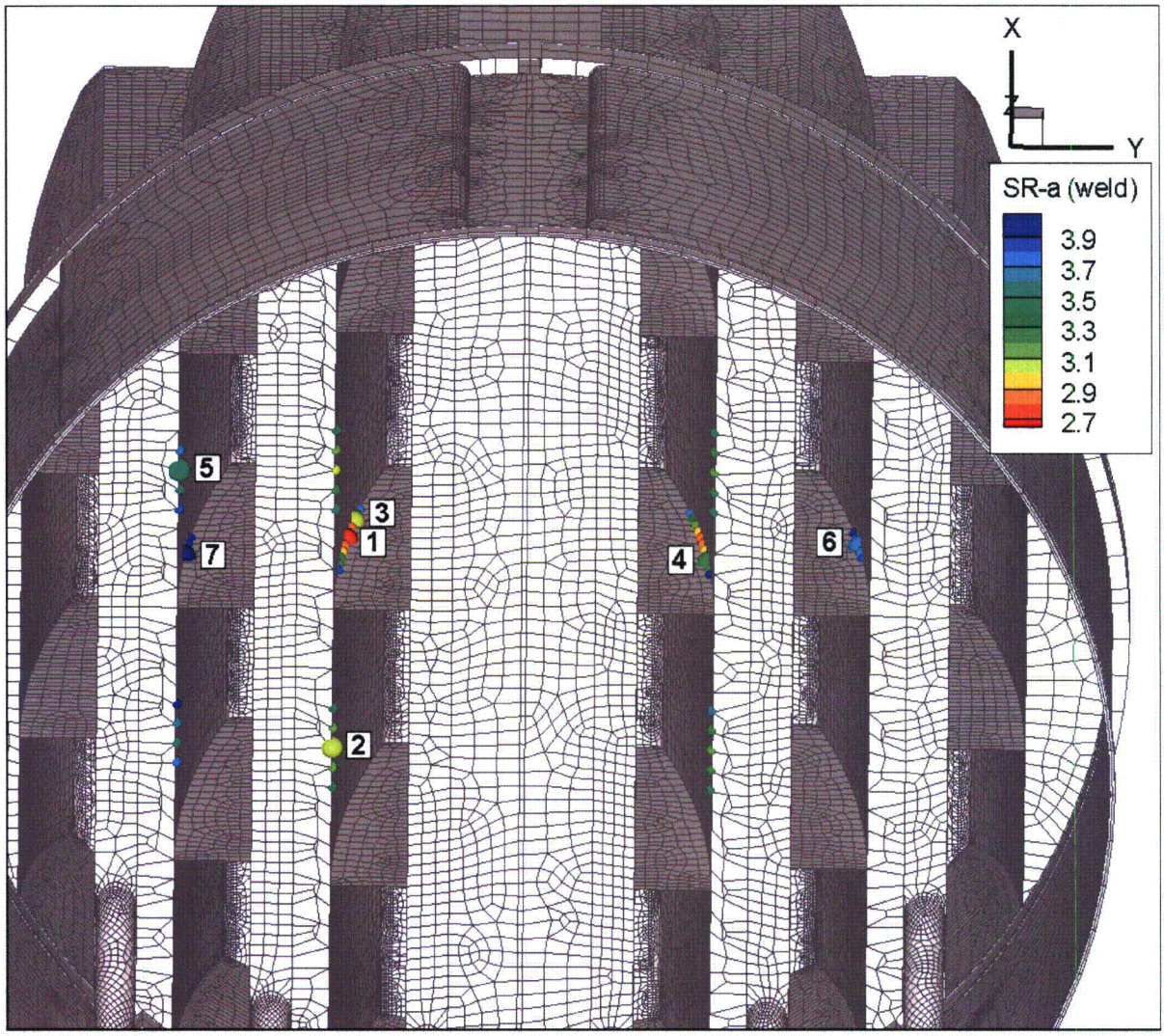

Figure 13e. Locations of smallest alternating stress ratios, SR-a≤4, at welds for nominal 115% CLTP operation. Numbers refer to the enumerated locations for SR-a values at welds in Table 9a. All locations 1-7 are shown.

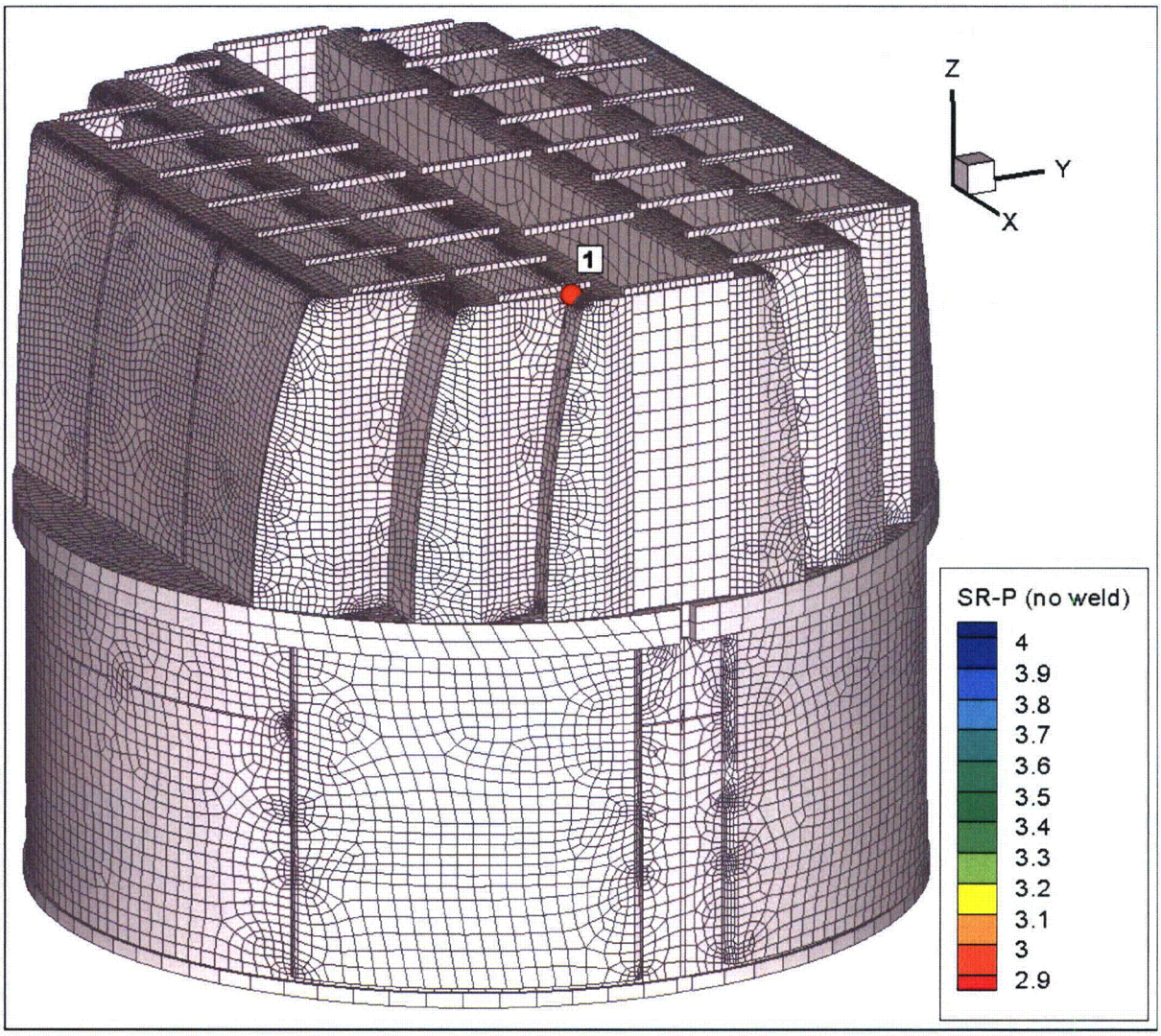

Figure 14a. Location of minimum stress ratio, SR-P≤4, associated with maximum stress intensities at non-welds for 115% CLTP operation with frequency shifts. The recorded stress ratio is the minimum value taken over all frequency shifts. The number refers to the enumerated location for SR-P values at non-welds in Table 9b.

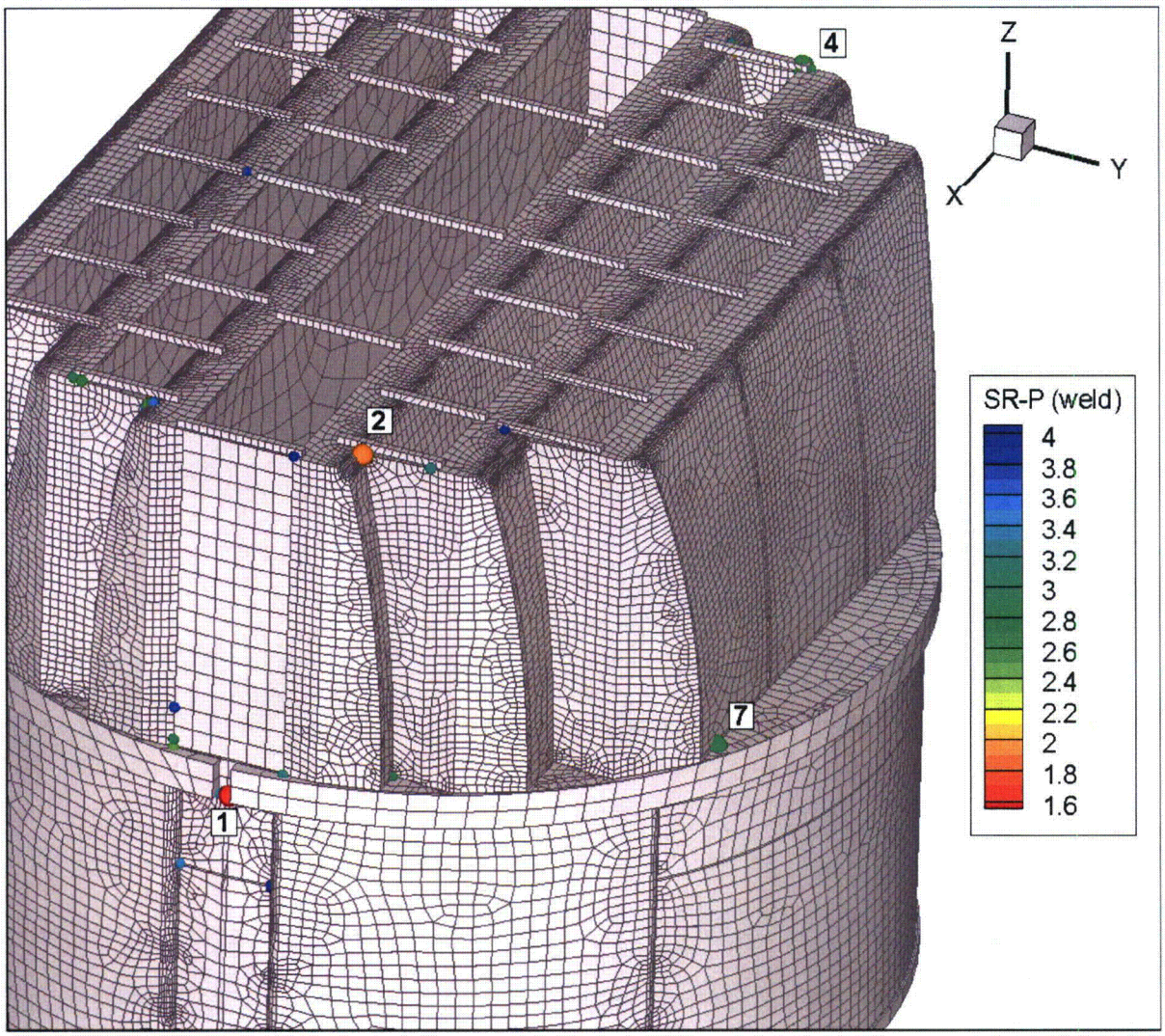

Figure 14b. Locations of minimum stress ratios, SR-P≤4, associated with maximum stress intensities at welds for 115% CLTP operation with frequency shifts. The recorded stress ratio at a node is the minimum value taken over all frequency shifts. Numbers refer to the enumerated locations for SR-P values at welds in Table 9b. This view shows locations 1, 2, 4 and 7.

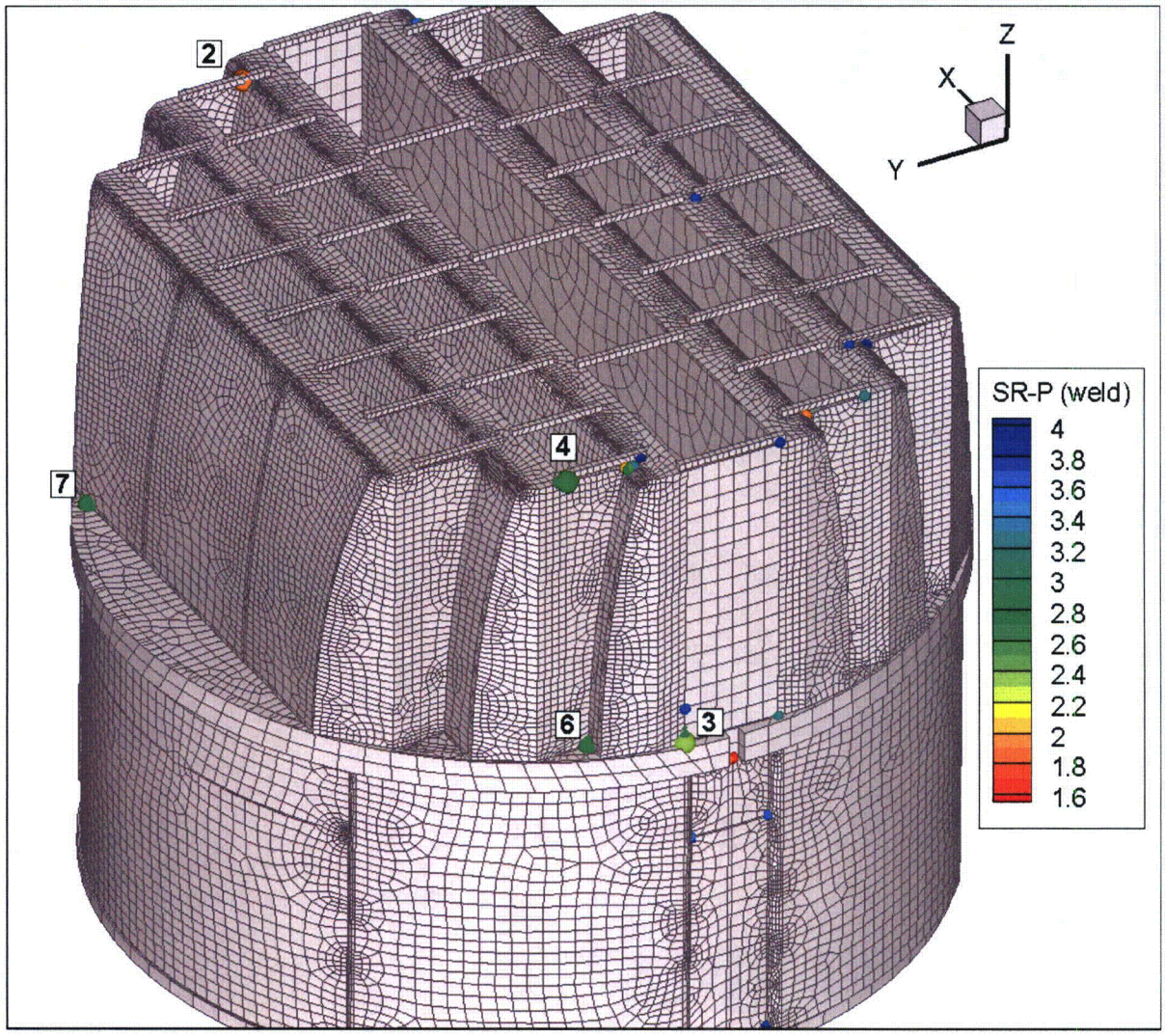

Figure 14c. Locations of minimum stress ratios, SR-P≤4, associated with maximum stress intensities at welds for 115% CLTP operation with frequency shifts. The recorded stress ratio at a node is the minimum value taken over all frequency shifts. Numbers refer to the enumerated locations for SR-P values at welds in Table 9b. This view shows locations 2-4, 6 and 7.

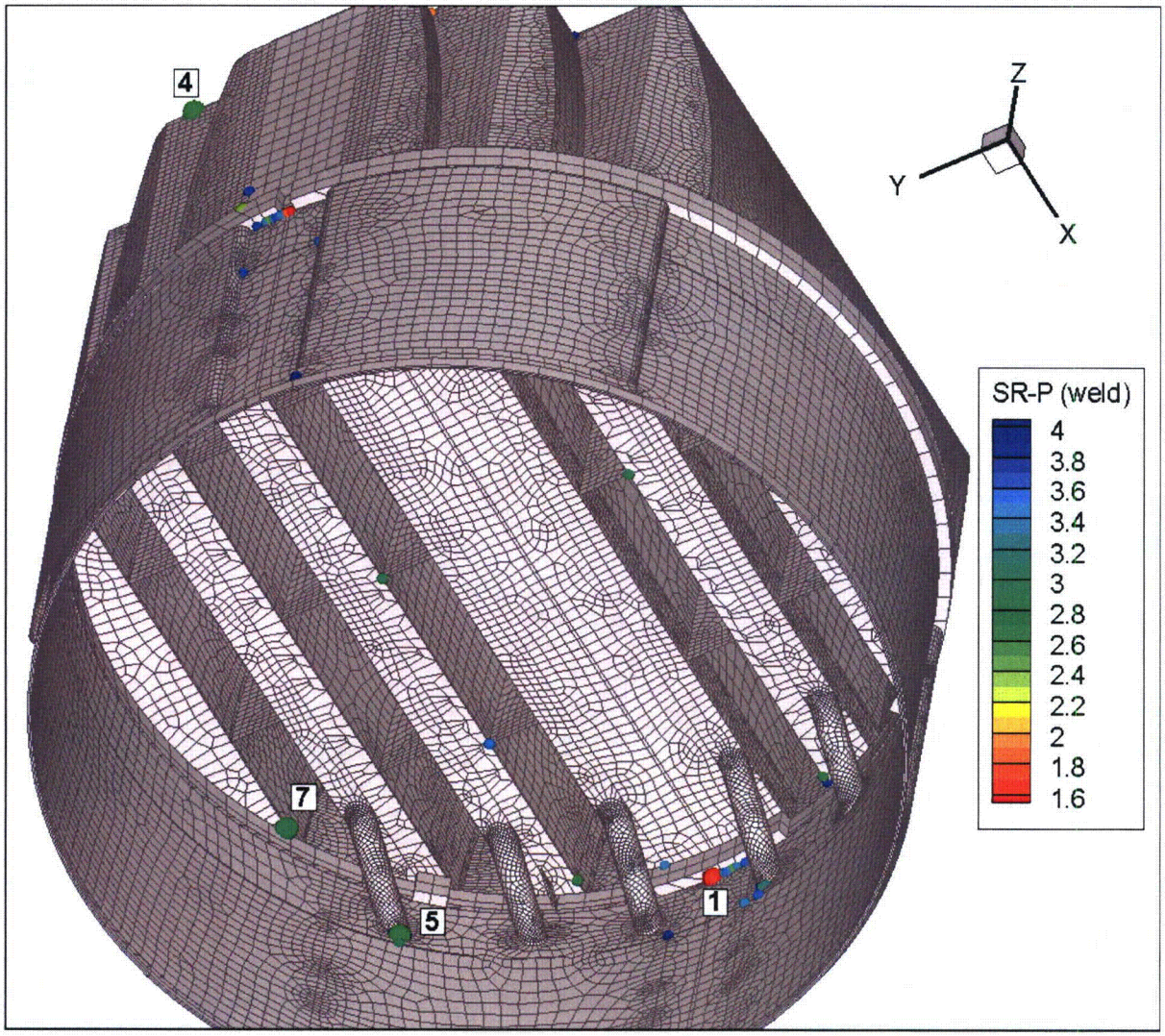

Figure 14d. Locations of minimum stress ratios, SR-P≤4, associated with maximum stress intensities at welds for 115% CLTP operation with frequency shifts. The recorded stress ratio at a node is the minimum value taken over all frequency shifts. This view shows locations 1, 4, 5 and 7.

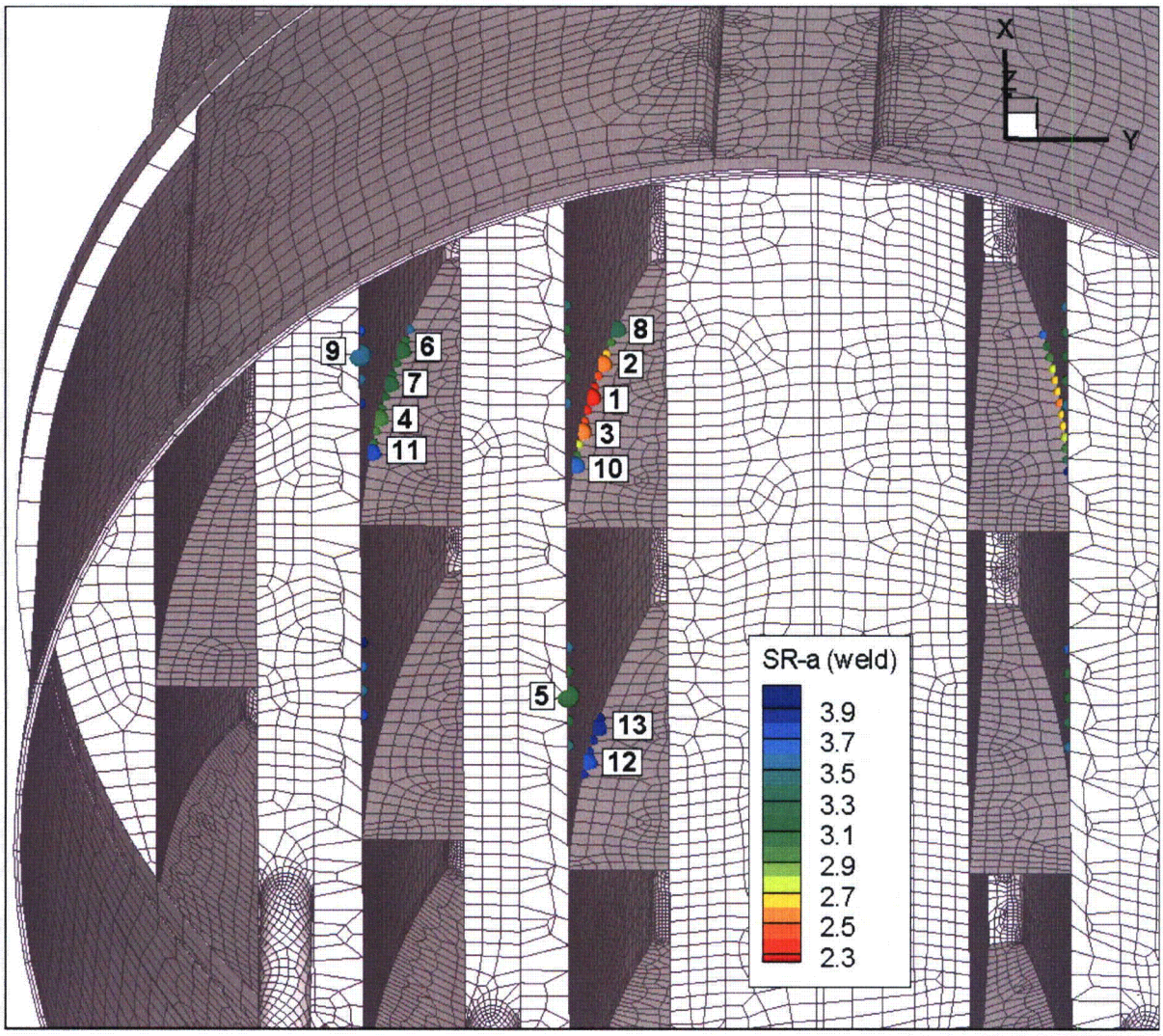

Figure 14e. Locations of minimum alternating stress ratios, SR-a≤4, at welds for 115% CLTP operation with frequency shifts. The recorded stress ratio at a node is the minimum value taken over all frequency shifts. Numbers refer to the enumerated locations for SR-a values at welds in Table 9b. All locations 1-13 are shown.

5.3 Frequency Content and Sensitivity to Frequency Shift of the Stress Signals

The spectral content in the stress response is examined by presenting the PSD and accumulative PSDs of selected nodes and stress components. The accumulative PSDs are computed directly from the Fourier coefficients as

$$\Sigma(\omega_n) = \sqrt{\sum_{k=1}^{n} |\tilde{\sigma}(\omega_k)|^2}$$

where $\tilde{\sigma}(\omega_k)$ is the complex stress harmonic at frequency, ω_k. Accumulative PSD plots are useful for determining the frequency components and frequency ranges that make the largest contributions to the fluctuating stress. Unlike PSD plots, no "binning" or smoothing of frequency components is needed to obtain smooth curves. Steep step-like rises in $\Sigma(\omega)$ indicate the presence of a strong component at a discrete frequency whereas gradual increases in the curve imply significant content over a broader frequency range. From Parsival's theorem, equality between $\Sigma(\omega_N)$ (where N is the total number of frequency components) and the RMS of the stress signal in the time domain is established.

The accumulative PSD and PSDs of the following four nodes are examined:

Nodes 80664 and 80662 - these nodes have the lowest stress ratios; both reside on the inner hood/hood support junction.
Node 90114 – this node lies on the middle hood/hood support junction.
Node79668 – this node lies on the weld joining the backing bar to the inner hood.

In each case, since there are six stress components and up to three different section locations for shells (the top, mid and bottom surfaces), there is a total of 18 stress histories per component. Moreover, at junctions there are at least two components that meet at the junction. The particular stress component that is plotted is chosen as follows. First, the component and section location (top/mid/bottom) is taken as the one that has the highest alternating stress. This narrows the selection to six components. Of these, the component having the highest Root Mean Square (RMS) is selected.

The accumulative PSD and PSD curves are presented in Figure 15. For the two limiting nodes – 80664 and 80662 – there is very little difference between the shifted and non-shifted accumulative PSDs. Both show a strong rise at 41 Hz, and a corresponding peak in the PSD curve. In both cases, this peak does not shift significantly with frequency shift which is indicative of a structural mode being excited by a relatively broad spectrum acoustic loading. Frequency shifting has a more pronounced effect on the third node, 90114, which has a more pronounced change with the -5% frequency shift. However, the peak location, which is now at approximately 46 Hz, also does not shift, but instead increases in amplitude for the -5% shift. Finally the fourth node 79668 is characterized by an increase at 47.5 Hz suggesting that the stress response is driven by a different inner hood mode than the first two nodes.

Further insight into the modal response can be obtained by examining how the maximum and alternating stress intensities of selected nodes vary with frequency shift. This evaluation is made in Figure 16 for the same nodes listed above. To generate these plots the frequency shifts are made in 0.5% increments thus achieving a finer resolution than for the 2.5% increments used to evaluate all the nodes. This is a useful advantage of the harmonic approach since, once the unit solution stresses are computed, the stress response at any shifted frequency can be easily and quickly evaluated thus allowing this higher resolution (in frequency shift) plot to be obtained in a few minutes.

For nodes 80664 and 80662 the curves are qualitatively similar. The highest alternating stress intensity is 3165 psi occurs at the +6% frequency shift which is only 255 psi (or 8.8%) higher than the value at the +7.5% shift. Due to the low static contribution, the maximum and alternating stress intensities differ by approximately 150 psi when frequencies are shifted in the ±10% range. The difference between the lowest and highest alternating stress intensities over the frequency shift range is 1278 psi, which constitutes a 51% variation compared to the nominal (zero shift) value. For the fourth node 79668, the variation in stress intensity with frequency shift is 1400 psi which is 62% of the nominal value.

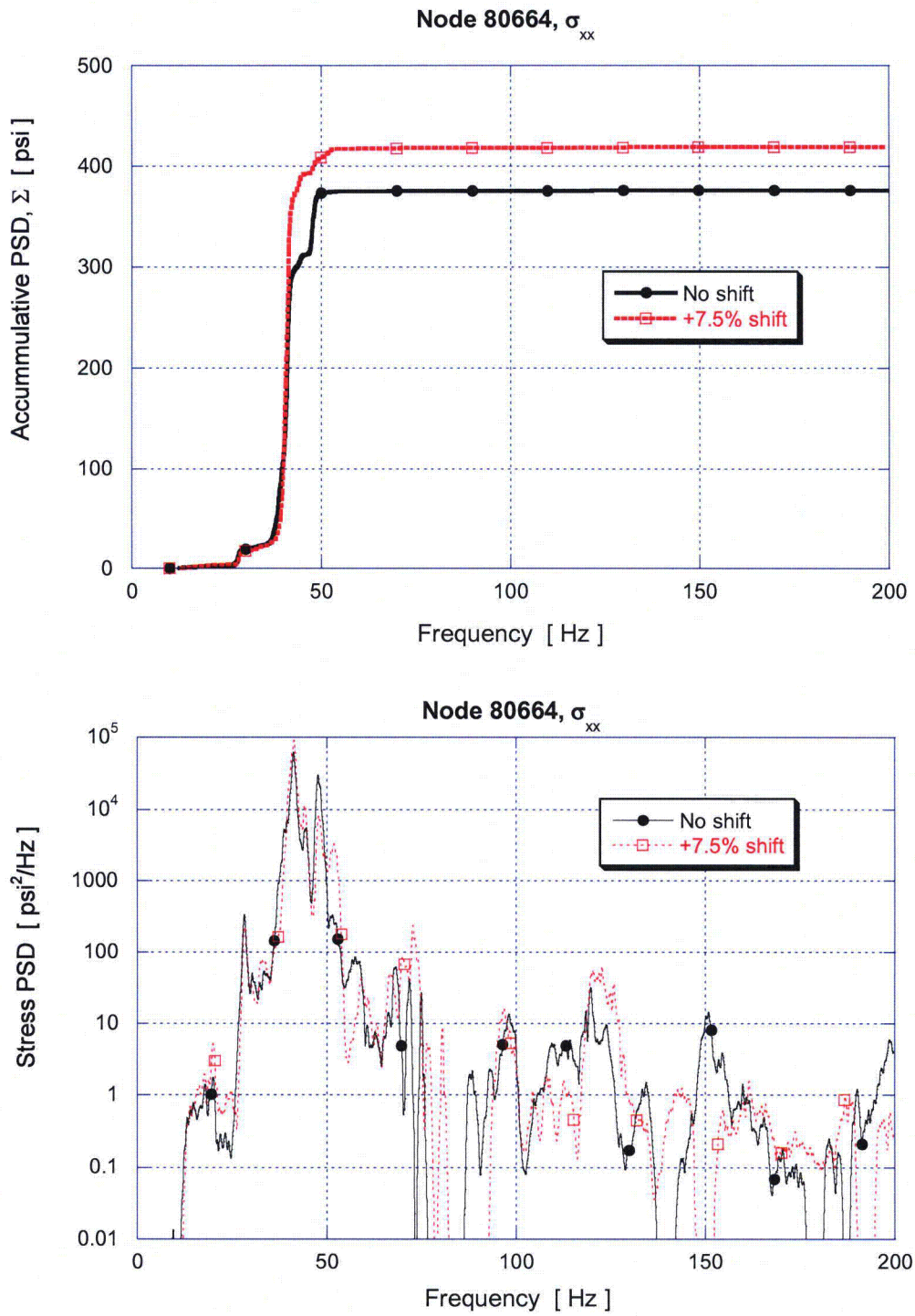

Figure 15a. Accumulative PSD and PSD curves of the σ_{xx} stress response at node 80664 at 115% CLTP operation.

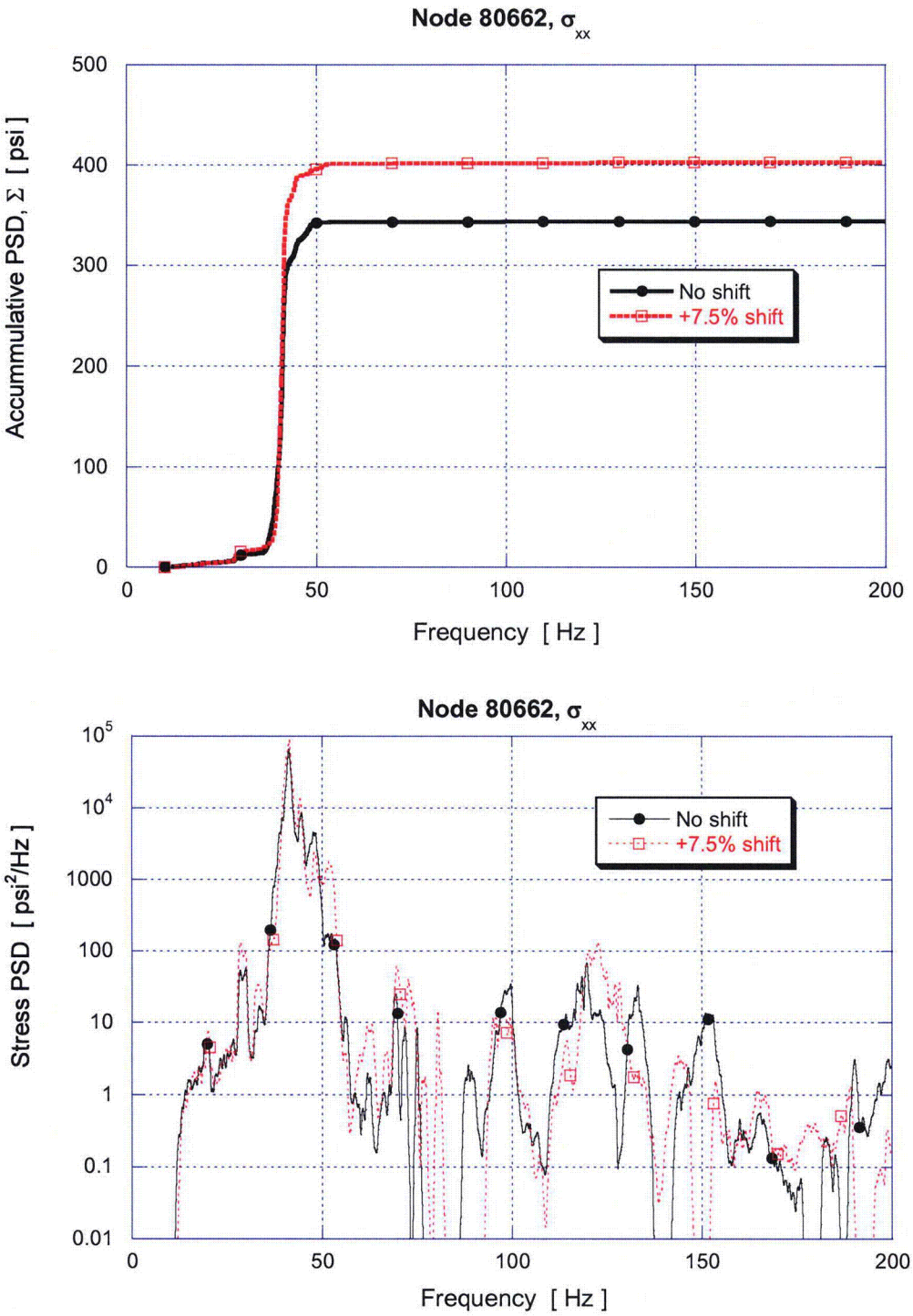

Figure 15b. Accumulative PSD and PSD curves of the σ_{xx} stress response at node 80662 at 115% CLTP operation

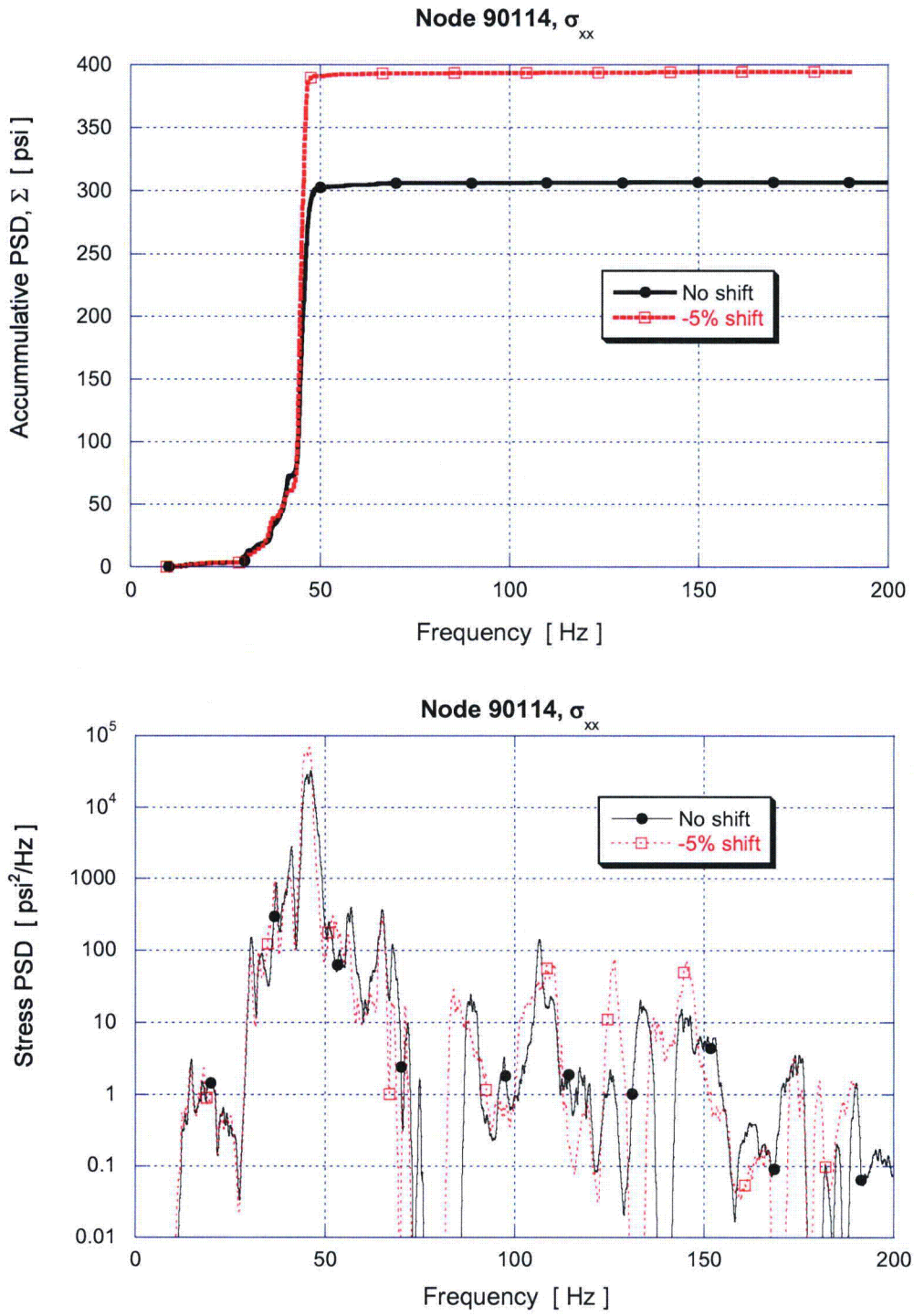

Figure 15c. Accumulative PSD and PSD curves of the σ_{xx} stress response at node 90114 at 115% CLTP operation.

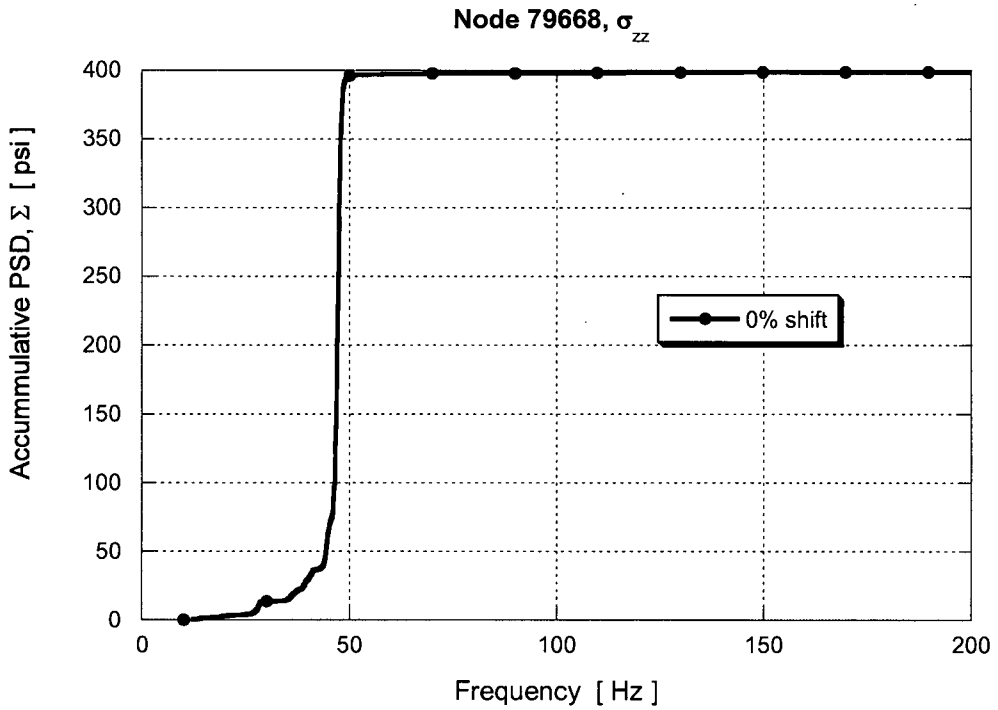

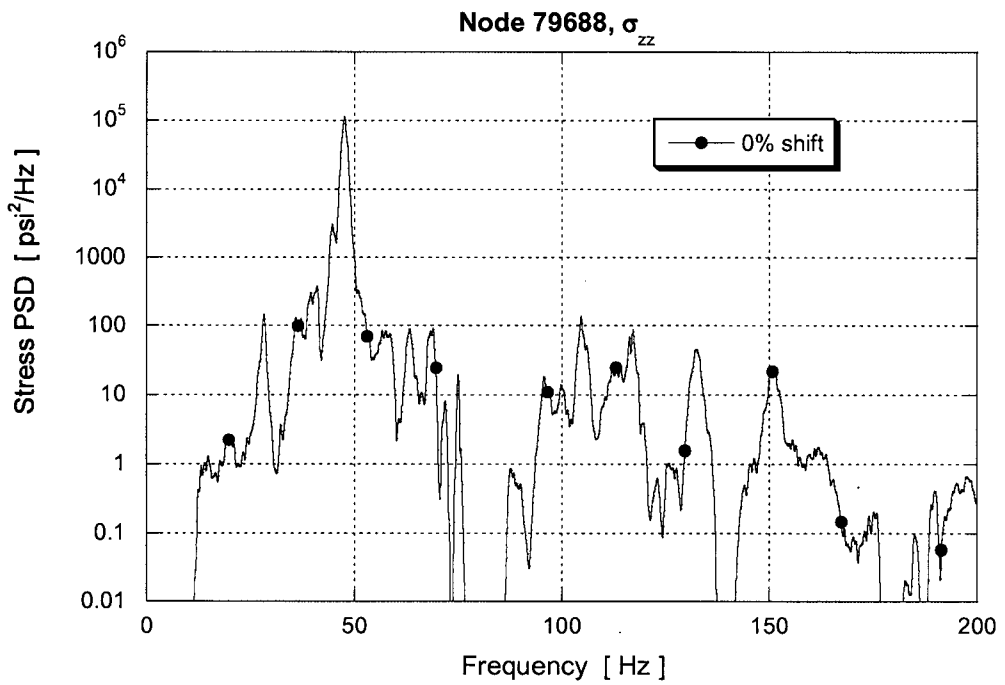

Figure 15d. Accumulative PSD and PSD curves of the σ_{ZZ} stress response at node 79688 at 115% CLTP operation.

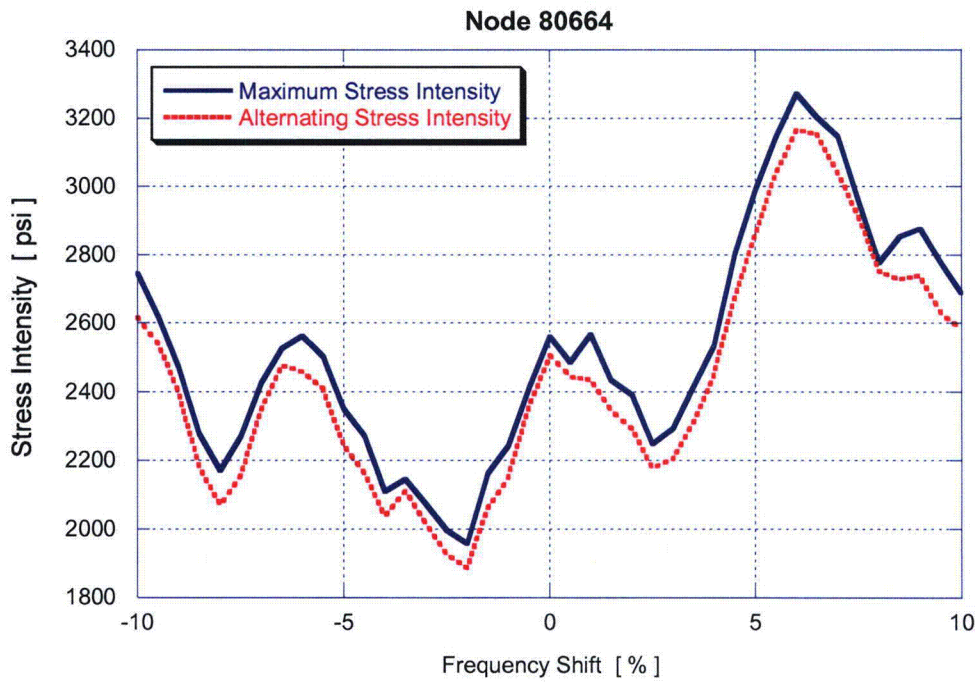

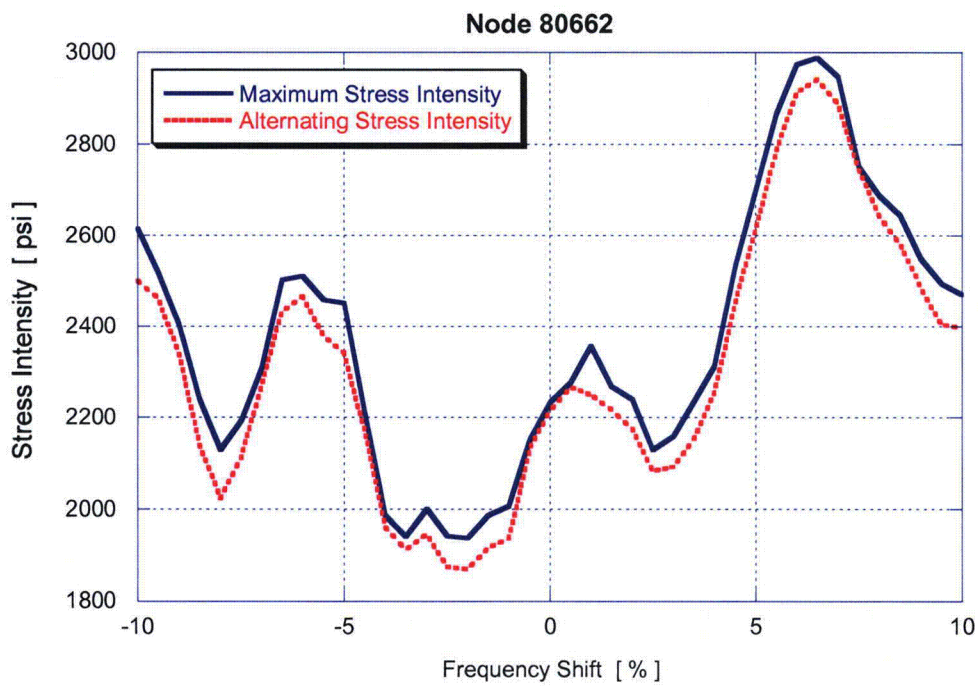

Figure 16a. Variation of maximum and alternating stress intensities with frequency shift for nodes 80664 and 80662.

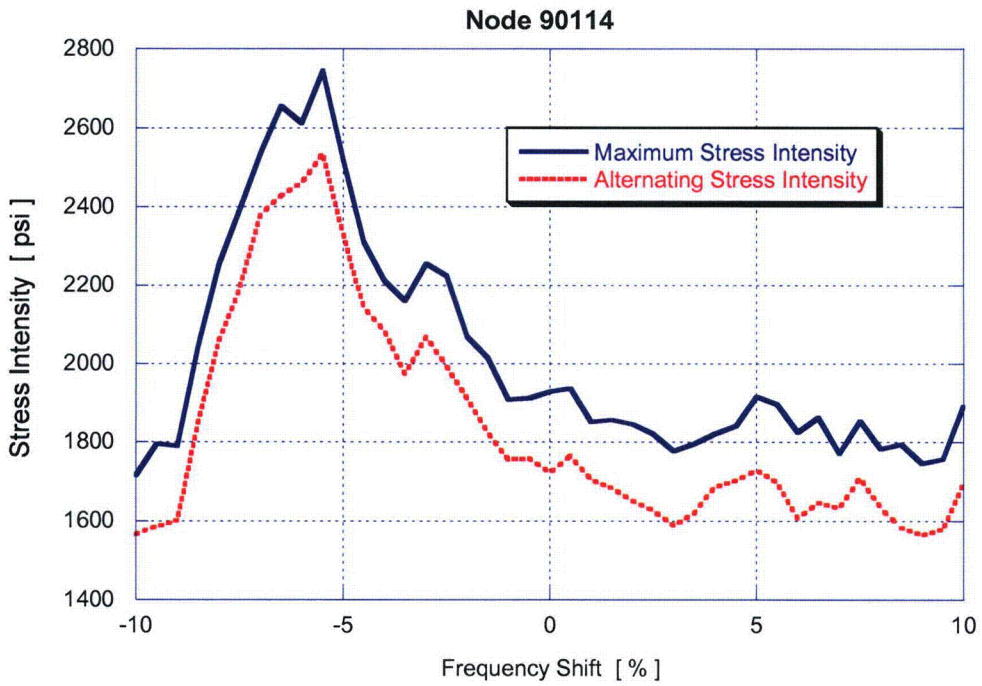

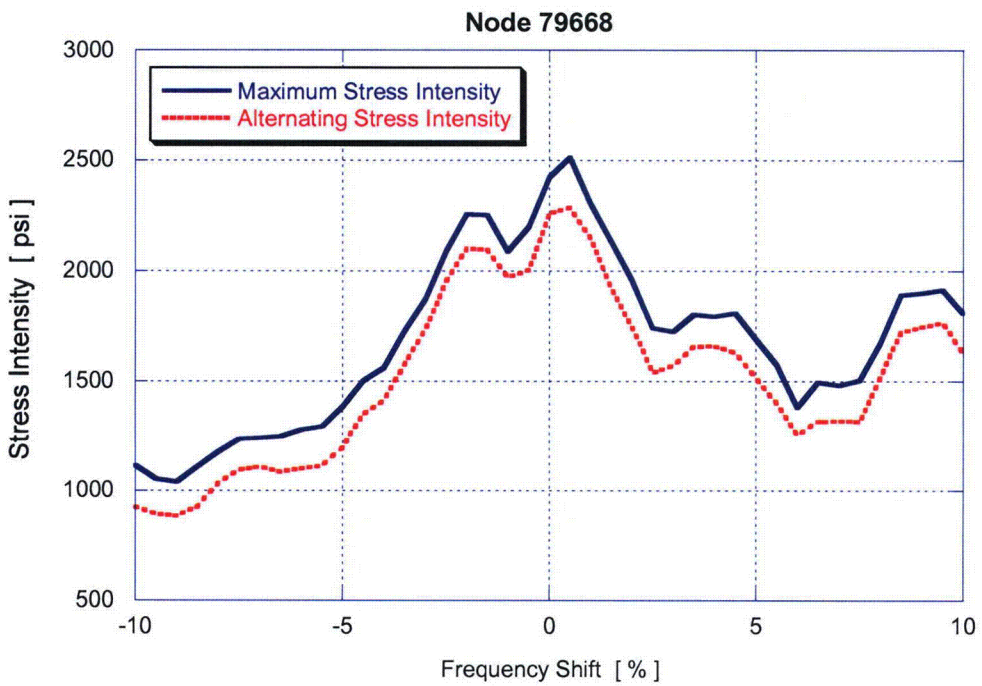

Figure 16b. Variation of maximum and alternating stress intensities with frequency shift for nodes 90114 and 79668.

6. Conclusions

A harmonic steam dryer stress analysis has been used to calculate high stress locations and calculated / allowable stress ratios for the HC1 steam dryer at 115% CLTP load conditions using plant measurement data. A detailed description of the harmonic methodology and the finite element model for the HC1 steam dryer is presented. The CLTP loads obtained in a separate acoustic circuit model [5], including end-to-end bias and uncertainty [4,5], were applied to a finite element model of the steam dryer consisting mainly of the ANSYS Shell 63 elements and brick continuum elements. The resulting stress histories were analyzed to obtain alternating and maximum stresses at all nodes for comparison against allowable levels. These results are tabulated in Table 9 of this report. The minimum alternating stress ratio (SR-a) at the nominal frequency case is 2.74 whereas the minimum SR-a at any frequency shift is 2.36. The most limiting maximum stress intensity stress ratio (SR-P) at the nominal frequency case is 1.51. It decreases slightly to 1.50 when all frequency shifts are taken. These results account for all end to end biases and uncertainties and reflect the elimination of non-acoustic signals based on the 1000# data [7] in the 75-85 Hz frequency range.

On the basis of these 115% CLTP plant loads, the dynamic analysis of the steam dryer shows that the combined acoustic, hydrodynamic, and gravity loads produce the following minimum stress ratios:

Frequency Shift	Minimum Stress Ratio	
	Max. Stress, SR-P	Alternating Stress, SR-a
0% (nominal)	1.51	2.74
-10%	1.53	2.63
-7.5%	1.52	3.08
-5%	1.52	2.81
-2.5%	1.51	3.09
+2.5%	1.51	2.96
+5%	1.51	2.40
+7.5%	1.50	2.36
+10%	1.50	2.66
All shifts	1.50 – 1.53	2.36 – 3.09

Given that the biases and uncertainties in the loads (Table 4) and finite element model (Table 5) are already accounted for, these stress ratios qualify the dryer with considerable margin at the 115% CLTP operating condition. The limiting alternating stress intensity without frequency shifting (Salt=2507 psi) is 7.2% higher than the value at 111.5% CLTP (Salt=2338 psi). This concurs with a velocity-squared scaling which would indicate a 7.1% increase. With frequency shifting however, the highest alternating stress intensity (Salt=2910 psi) is 13.9% higher than the corresponding value obtained at 111.5% CLTP (Salt=2554 psi).

7. References

1. Continuum Dynamics, Inc. (2008). "Stress Assessment of Hope Creek Unit 1 Steam Dryer Based on Revision 4 Loads Model, (Rev. 4)," C.D.I. Report 07-17P (Proprietary).

2. Continuum Dynamics, Inc. (2005). "Methodology to Determine Unsteady Pressure Loading on Components in Reactor Steam Domes (Rev. 6)." C.D.I. Report No. 04-09 (Proprietary).

3. ASME Code (2007). ASME B&PV Code, Section III, subsection NG.

4. Continuum Dynamics, Inc. (2007). "Acoustic and Low Frequency Hydrodynamic Loads at CLTP Power Level on Hope Creek Unit 1 Steam Dryer to 200 Hz" C.D.I. Report No. 07-18P (Proprietary)

5. Continuum Dynamics, Inc. (2007). "Methodology to Predict Full Scale Steam Dryer Loads from In-Plant Measurements, with the Inclusion of a Low Frequency Hydrodynamic Contribution (Rev. 0)" C.D.I. Report No. 07-09P (Proprietary).

6. Continuum Dynamics, Inc., "Finite Element Modeling Bias and Uncertainty Estimates Derived From the Hope Creek Unit 2 Dryer Shaker Test," CDI Report 07-27P (rev. 0), Dec. 2007.

7. Structural Integrity Associates, electronic communication of the Hope Creek MSL SG data taken on November 14, 2007 at 17:43 (data file: 20071114174355.zip) with the plant at normal operating pressure and temperature (920 psig and 527 deg F).

8. Continuum Dynamics, Inc. (2008). "Final Stress Assessment of Hope Creek Unit 1 Steam Dryer at 111.5% CLTP Conditions (Rev. 0)," C.D.I. Report 08-29P (Proprietary), August 2008.

9. Structural Integrity Associates (2007). "Hope Creek Main Steam Line Strain Gage Data: MSL Channel Combinations."

10. ANSYS Release 10.0. URL http://www.ansys.com. Documentation: ANSYS 10.0 Complete User's Manual Set

11. Korn, G.A. & Korn, T.M., *Mathematical Handbook for Scientists and Engineers*, 2nd edition, McGraw-Hill Book Co., 1968

12. Continuum Dynamics, Inc. (2008). Response to NRC Request for Additional Information on the Hope Creek Generating Station, Extended Power Uprate, NRC RAI 14.110, January 2008.

13. Press, W. H., S. A. Teukolsky, et al. (1992). *Numerical Recipes*, Cambridge University Press.

14. Continuum Dynamics, Inc. (2007). "Stress Analysis of the Hope Creek Unit 1 Steam Dryer at EPU Conditions Using 1/8th Scale Model Pressure Measurement Data (Rev. 2) " C.D.I. Report No. 06-27 (Proprietary).

15. O'Donnell W.J. (1973). "Effective Elastic Constants For the Bending of Thin Perforated Plates With Triangular and Square Penetration Patterns," ASME Journal of Engineering for Industry, Vol. 95, pp. 121-128.

16. U.S. Nuclear Regulatory Commission, (2007). Regulatory Guide 1.20 "Comprehensive Vibration Assessment Program for Reactor Internals During Preoperational and Initial Startup Testing," March 2007.

17. Continuum Dynamics, Inc. (2008). Response to NRC Request for Additional Information on the Hope Creek Generating Station, Extended Power Uprate, NRC RAI 14.79, January 2008.

18. Structural Integrity Associates, Inc. 2007. Hope Creek Strain Gage Uncertainty Evaluation and Pressure Conversion Factors. SIA Report No. HC-28Q-301 (Rev. 1).

19. Continuum Dynamics, Inc., "Vermont Yankee Instrument Position Uncertainty," Letter Report dated 01 August 2005.

20. Exelon Nuclear Generating LLC, "An Assessment of the Effects of Uncertainty in the Application of Acoustic Circuit Model Predictions to the Calculation of Stresses in the Replacement Quad Cities Units 1 and 2 Steam Dryers (Revision 0)," Document No. AM-21005-008.

21. Continuum Dynamics, Inc. (2008). Response to NRC Request for Additional Information on the Hope Creek Generating Station, Extended Power Uprate, NRC RAI 14.66 (c), January 2008

22. WRC Bulletin 432 (1998). "Fatigue Strength Reduction and Stress Concentration Factors For Welds In Pressure Vessels and Piping," WRC, NY, p.32

23. Pilkey W.D. (1997). *Peterson's Stress Concentration Factors*, 2nd ed., John Wiley, NY, p.139.

24. Lawrence F.V., Ho N.-J., Mazumdar P.K. (1981). "Predicting the Fatigue Resistance of Welds," Ann. Rev. Mater. Sci., vol. 11, pp. 401-425.

25. General Electric (GE) Nuclear Energy (2003). Supplement 1 to Service Information Letter (SIL) 644, "BWR/3 Steam Dryer Failure," September 5, 2003.

26. Tecplot 10 (2004). URL: http://www.tecplot.com. Documentation: *Tecplot* User's Manual Version 10 Tecplot, Inc. Bellevue, Washington October.